Fisheries and Oceans Canada | Pêches et Océans Canada
Ecosystems and Oceans Science | Sciences des écosystèmes et des océans

Canadian Science Advisory Secretariat (CSAS)

Research Document 2023/045

Quebec Region

Chemical and Biological Oceanographic Conditions in the Estuary and Gulf of St. Lawrence during 2021

M. Blais, P. S. Galbraith, S. Plourde, C. Lehoux and L. Devine

Fisheries and Oceans Canada
Maurice Lamontagne Institute
850 route de la Mer, P.O. Box 1000
Mont-Joli, QC, G5H 3Z4

June 2023

Canada

Foreword

This series documents the scientific basis for the evaluation of aquatic resources and ecosystems in Canada. As such, it addresses the issues of the day in the time frames required and the documents it contains are not intended as definitive statements on the subjects addressed but rather as progress reports on ongoing investigations.

Published by:

Fisheries and Oceans Canada
Canadian Science Advisory Secretariat
200 Kent Street
Ottawa ON K1A 0E6

http://www.dfo-mpo.gc.ca/csas-sccs/
csas-sccs@dfo-mpo.gc.ca

ISSN 1919-5044
ISBN 978-0-660-48917-9 Cat. No. Fs70-5/2023-045E-PDF

Correct citation for this publication:

Blais, M., Galbraith, P.S., Plourde, S., Lehoux, C. and Devine, L. 2023. Chemical and Biological Oceanographic Conditions in the Estuary and Gulf of St. Lawrence during 2021. DFO Can. Sci. Advis. Sec. Res. Doc. 2023/045. iv + 74 p.

Aussi disponible en français :

Blais, M., Galbraith, P.S., Plourde, S., Lehoux, C. et Devine, L. 2023. Les conditions océanographiques chimiques et biologiques dans l'estuaire et le golfe du Saint-Laurent en 2021. Secr. can. des avis sci. du MPO. Doc. de rech. 2023/045. iv + 76 p.

TABLE OF CONTENTS

ABSTRACT iv
INTRODUCTION 1
METHODS 1
SAMPLE COLLECTION 1
OXYGEN 3
NUTRIENTS AND PHYTOPLANKTON 3
REMOTE SENSING OF OCEAN COLOUR AND SPRING BLOOM METRICS 4
ZOOPLANKTON INDICES 5
SCORECARDS 6
OBSERVATIONS 7
PHYSICAL ENVIRONMENT 7
DEEP OXYGEN 7
NUTRIENTS AND PHYTOPLANKTON 7
High-frequency monitoring stations 8
Gulf regions 8
Remote sensing of ocean colour and spring bloom metrics 10
ZOOPLANKTON 10
High-frequency monitoring stations 10
Gulf regions 11
Copepod phenology 12
Scorecards 12
DISCUSSION 13
ENVIRONMENTAL CONDITIONS 13
PHYTOPLANKTON 15
ZOOPLANKTON 16
PERSPECTIVES 17
SUMMARY 18
ACKNOWLEDGEMENTS 19
REFERENCES CITED 19
TABLES 22
FIGURES 23
APPENDICES 65

ABSTRACT

An overview of chemical and biological oceanographic conditions in the Gulf of St. Lawrence in 2021 is presented as part of the Atlantic Zone Monitoring Program (AZMP). AZMP data as well as data from regional monitoring programs are analyzed and presented in relation to long-term means in the context of a warming trend that began in 2010. These long-term means are typically calculated using 1999–2020 as a reference period. Oxygen levels at 300 m reached a record-low concentration in the northwest and central Gulf and in Cabot Strait. Nitrate inventories in the surface layer (0–50 m) of the Gulf were either near or below normal, with record-low levels in the Estuary and northwest Gulf. Mid-layer nitrate inventories (50–150 m) were also below normal in these two subregions, but near or above normal in the other regions. In the bottom layer (150 m–bottom), positive anomalies were found in all Gulf regions with record-high inventories everywhere but in the Estuary. Positive deep nitrate anomalies have been observed regularly since 2012 in the Cabot Strait and the central Gulf and are associated with intrusions of warm and salty waters, but they have been less common in the Estuary over the last decade. The recent increase in the nitrate inventory of the bottom layer is mostly associated with negative anomalies of the N:P ratio and positive anomalies of the Si:N ratio. Annual inventories of vertically integrated chlorophyll *a* (chl *a*; 0–100 m) were near normal in all regions except for the Estuary and northwest Gulf, where they were above normal. In these two subregions, the second highest inventories of chl *a* were observed during fall. Most regions have regularly shown above-normal chl *a* inventories during fall since about 2014. In contrast, phytoplankton biomass derived from satellite data mostly showed negative annual and fall anomalies in most of the ocean colour polygons over the last four years, including several record-low values in 2021. Spring bloom metric anomalies indicated that the bloom was generally on time but was slightly less intense than normal. Zooplankton biomass was either near or below normal everywhere in the Gulf, with a record-low level in the Estuary/northwest Gulf region. *Calanus finmarchicus* annual abundance was near normal except at Rimouski station, where it was slightly above normal. *C. hyperboreus* abundance showed widespread negative anomalies, including a record-low level in the northeast Gulf. Small calanoids were at record-high abundances at Rimouski station and in the Estuary/northwest Gulf region, and their abundances were also above normal in the Magdalen Shallows, and at the Shediac Valley station. Abundances of warm-water copepods were also at record-high levels in the Estuary/northwest Gulf region as well as in northeast Gulf and Magdalen Shallows, and abundances were also above normal in other regions. Cold-water copepod abundances were either near normal or above normal, and record-high values were observed at both high-frequency monitoring stations. The characterization of *C. finmarchicus* phenology at Rimouski station indicated that the peak of early copepodite stages (CI–CIII) was the earliest and longest-lasting peak ever recorded.

INTRODUCTION

The Atlantic Zone Monitoring Program (AZMP) was implemented in 1998 (Therriault et al. 1998) with the aim of:

1. increasing Fisheries and Oceans Canada's (DFO) capacity to understand, describe, and forecast the state of the marine ecosystem, and
2. quantifying the changes in the ocean's physical, chemical, and biological properties and the predator-prey relationships of marine resources.

AZMP provides data to support the sound development of ocean activities. A critical element of the AZMP observational program is the annual assessment of the distribution and variability of oxygen, nutrients, and plankton communities.

A description of the spatiotemporal distribution of dissolved oxygen, nutrients (nitrate, silicate, and phosphate), and chlorophyll *a* (chl *a*) concentrations provides important information on water-mass movements and on the location, timing, and magnitude of biological production cycles. A description of the phytoplankton and zooplankton communities and their distribution provide important information on the organisms forming the base of the marine food web. Understanding plankton production cycles is essential for an ecosystem approach to fisheries management.

The AZMP derives its information on the state of the marine ecosystem from a combination of satellite remote sensing and *in situ* data collected at a network of sampling locations (high-frequency monitoring stations, cross-shelf sections) in each DFO region (Québec, Gulf, Maritimes, Newfoundland and Labrador; see Figure 1 for station locations in the St. Lawrence Gulf and Estuary) occupied at a frequency of weekly to once annually. The sampling design provides valuable information on the natural variability in physical, chemical, and biological properties of the northwest Atlantic continental shelf: cross-shelf sections provide a broadscale overview of the conditions but are limited in their seasonal coverage while strategically located high-frequency monitoring stations complement the sampling by providing more detailed information on seasonal-scale changes in ecosystem properties. In recent years, Viking oceanographic buoy sensors have also complemented the core observations with high temporal resolution data.

In this document, we review the chemical and biological oceanographic (lower trophic levels) conditions in the Gulf of St. Lawrence in 2021. Physical oceanographic conditions that prevailed in the Gulf in 2021 are described in Galbraith et al. (2022).

METHODS

SAMPLE COLLECTION

All sample collection and processing steps meet the standards of the AZMP protocol (Mitchell et al. 2002). Field measurements included in this report were made along seven oceanographic sections as well as stations located between these sections during dedicated AZMP surveys carried out in winter, early summer, and fall (generally in March, June, and October) of each year and at two high-frequency monitoring stations (Figure 1). Field measurements made during multidisciplinary surveys (August and September; hereafter referred to as late summer surveys) and during the mackerel egg survey (June; zooplankton samples only) have been included in recent reports for all years (2006–2021) for which these data are available. In this document,

the seven AZMP sections as well as additional stations were grouped into four main regions for which biochemical indices are presented (Figure 2):

1. Estuary and northwestern Gulf: this region is generally deep (> 200 m) and cold in summer. It is strongly influenced by freshwater runoff from the St. Lawrence River, and by cold and dense waters from the Laurentian Channel;
2. Northeastern Gulf: this region, with deep channels and a relatively wide shelf (< 100 m), is characterized by high surface salinity and is influenced by the intrusion of water from the Labrador Shelf through the Strait of Belle Isle;
3. Central Gulf and Cabot Strait: this region is generally deep (> 200 m) and is directly influenced by deep waters that mix at the continental slope (warm north Atlantic Central Water that has a Gulf Stream signature and cold Labrador Current water) and enter the Gulf through Cabot Strait;
4. Magdalen Shallows: this region is shallow (< 100 m) and warm at the surface in summer. It is largely influenced by the Gaspé Current.

These regions are slightly different than those used in previous reports (2019 and earlier) and are meant to match the regions used in the Gulf for the newly implemented DFO Ecosystem Approach to Fisheries Management. When sufficient data are available, biochemical indices are sometimes presented for region subdivisions (Figure 1, hereafter referred to as subregions) to provide more details about spatial patterns. Since there are few biochemical data collected in Mecatina, Northumberland and Laurentian Hermitage (Figure 1), indices will not be reported for those regions.

Table 1 provides details about the 2021 sampling surveys and Figures 2 and 3 summarize the sampling effort during the seasonal surveys and at the high-frequency monitoring stations, respectively. Rimouski station (depth 320 m) has been sampled since 1991—about weekly throughout the summer, once or twice a month in early spring and late fall, and rarely in winter (except during the winter survey) due to the presence of sea ice. It has been included in AZMP's annual review of environmental conditions since 2004 to represent conditions in the Estuary and northwestern Gulf. Since the beginning of AZMP, Shediac Valley station (depth: 84 m) was meant to represent conditions on the Magdalen Shallows and the Estuary outflow. However, sampling frequency at Shediac Valley station in good years is closer to monthly between May and November and decreases from January through April. Shediac Valley station was occupied on nine occasions in 2021, but four of those occupations occurred within a two-day period in September. In addition to the occupations at the high-frequency monitoring stations, Viking oceanographic buoys equipped with temperature, salinity, and fluorescence surface sensors (data collected every 30 minutes) have been deployed at the high-frequency stations since 2002 and 2004 at Rimouski and Shediac Valley stations, respectively. Since 2018 (Rimouski) and 2019 (Shediac Valley), the buoys are also equipped with automatic profilers. In 2021, they carried out 246 full depth casts at Shediac Valley station and 114 casts down to 320 m at Rimouski station. Deployment of the Viking buoys typically occurs in late April or early May and the recovery of the buoy is usually done in late October or early November.

Sampling on the oceanographic sections and at the high-frequency monitoring stations includes a CTD profile (temperature, salinity, fluorescence, dissolved oxygen) as well as water sampling using Niskin bottles (surface, 5 m, 15 m, 25 m, 50 m, 100 m, 200 m, 300 m, 400 m, bottom). Water from the Niskin bottles is collected for the analysis of dissolved oxygen (Winkler method), nutrients (Seal Analytical AutoAnalyzer 3 or Alpkem AutoAnalyzer), chl *a* (fluorometer), and phytoplankton enumeration (inverted microscopy) (Mitchell et al. 2002). Finally, mesozooplankton (< 1 cm) is collected with bottom-to-surface vertical ring net tows (75 cm

diameter, 200 µm mesh) for most of the surveys. During the mackerel egg survey, however, zooplankton sampling differs: the water column (surface to a maximum of 50 m) is sampled with 333 µm mesh bongo nets (61 cm diameter) using double oblique tows for a minimum of 10 min while cruising at ~2.5 kts (Ouellet 1987; Grégoire et al. 2014). A correction that accounts for the vertical distribution of mesozooplankton in the whole water column allows the estimation of their abundance in waters deeper than 50 m (Lehoux et al. 2020). However, validation with independent samples suggests that the correction for waters deeper than 50 m does not perform well for stations deeper than 200 m (C. Lehoux, DFO, Mont-Joli, QC; unpublished data). Consequently, stations deeper than 200 m (about 5 or 6 stations every year) were removed from the analysis. Taxonomists are responsible for the identification, counts, and bulk biomass measurements of zooplankton samples collected during regular AZMP surveys (early summer and fall surveys) whereas samples collected during the late summer multidisciplinary survey and during the mackerel egg survey are analyzed using a semi-automated procedure developed with the ZooImage 5.5.2 software package (Grosjean et al. 2018) following the methodology described in Plourde et al. (2019). The flat-bed scanners used for zooplankton counts and identification were changed in early 2022. To provide a time series that is comparable among years, estimates of *Temora/Eurytemora* abundance from samples analyzed with the new scanner were multiplied by 2 and 1.5 for the late summer multidisciplinary and mackerel egg survey respectively (the detailed intercalibration procedure is described in Appendix 1). Since methods are different, and considering the larger size of net mesh used during the mackerel egg survey, large calanoid taxa indices developed with the ZooImage analysis only include copepodite stages CIV–CVI, and these data are not included in the annual anomaly estimates.

OXYGEN

Oxygen concentration at 300 m is used as an indicator of hypoxic conditions in the Gulf. Oxygen concentration was measured using an oxygen probe (Sea-Bird SBE43) mounted on the CTD; the probe was calibrated against collected seawater samples and analyzed by Winkler titration on every cast (for the calibration procedure, see Sea-Bird application notes 61-1, -2, -3). Here, we present the mean annual distribution of deep oxygen in the Gulf derived from the CTD-mounted probe along with time series of annual concentrations of deep oxygen based on gridded (2 km^2) inverse-distance-weighted interpolation. In the last report (Blais et al. 2021b), temporal series were inverted between central Gulf and Cabot Strait; they have been corrected in this report.

NUTRIENTS AND PHYTOPLANKTON

Nutrient and chl *a* concentrations collected along the AZMP sections and at the high-frequency monitoring stations were integrated over various depth intervals (i.e., 0–100 m for chl *a*; 0–50 m, 50–150 m, and 150 m–bottom for nutrients) using trapezoidal numerical integration. In 2016 and 2017, winter vertical profiles of nutrients performed all over the Gulf revealed that nitrate concentrations were relatively homogeneous in the upper 50 m of the water column during that season. Thus, for years when vertical nutrient profiles were not available, including 2021, integrated nitrate values for the winter survey were calculated using surface concentrations (2 m) × 50 m, assuming homogeneity of nitrate concentrations in the winter mixed layer.

In this document, detailed descriptions of the seasonal and interannual patterns are provided for different nutrient and phytoplankton indices. Chlorophyll *a* is used as a proxy for phytoplankton biomass. For the high-frequency monitoring stations, we present vertical and seasonal nitrate and chl *a* distribution, as well as seasonal phytoplankton abundance and composition in terms of main taxa. Phytoplankton taxonomic identification is performed for the high-frequency

monitoring stations only. The ratio between diatoms and flagellates, or between diatoms and dinoflagellates, is used to provide information on the phytoplankton community size structure. For the Gulf regions described above, time series of annual and/or seasonal inventories of nitrate, nutrient ratios (N:P and Si:N), and chl *a* integrated over different depth layers as well as their spatial distributions are presented. Spring nutrient drawdown was estimated using the difference between the March and June nitrate inventories (0–50 m) and is used as a proxy for phytoplankton spring production since the early summer sampling occurs after the spring bloom. Anomalies were computed for these indices (see Scorecards section below) for both the high-frequency monitoring stations and the Gulf subregions.

REMOTE SENSING OF OCEAN COLOUR AND SPRING BLOOM METRICS

Satellite ocean colour data provide large-scale images of surface phytoplankton biomass (chl *a*) over the northwest Atlantic. We used daily satellite composite images within four ocean-colour polygons (northwest Gulf, northeast Gulf, Magdalen Shallows, and Cabot Strait; see Figure 4 for locations) to supplement our ship-based observations, especially regarding the spring bloom phenology, and to provide seasonal coverage and a large-scale context over which to interpret our survey data. However, since ocean colour imagery does not provide information on the dynamics that take place below the surface of the water column, it should be used as complementary information to the field data.

It should be noted that the ocean-colour polygons have been revised in this report compared to older reports (2019 and earlier) to reduce the possible bias in chl *a* retrievals associated with coastal waters and freshwater input. All ocean-colour polygons are located outside of the St. Lawrence River plume because satellite-based chl *a* estimates in such areas are unreliable due to contamination by river inputs loaded with coloured matter of terrestrial origin; polygons are not directly adjacent to the coast for the same reason. This also explains why spring bloom metrics in the Estuary cannot be derived from ocean color data. Moreover, in the Estuary, the significance of the spring bloom for the food web remains to be determined considering that primary production is generally maintained throughout summer and early fall due to frequent mixing episodes, in contrast with other regions where spring bloom represents the main food pulse for zooplankton. For these reasons, we do not provide estimates of spring bloom metrics for the Estuary. However, high-temporal-resolution information on the phytoplankton dynamics at the surface of the Estuary is available from the surface fluorescence sensor on the oceanographic Viking buoy located near Rimouski station and is presented in this document. To increase the accuracy of daily chl *a* estimates, data from the buoy sensor are calibrated against chl *a* concentrations measured in the water samples collected weekly at Rimouski station.

Near-surface phytoplankton biomass was estimated from ocean colour data collected by the Moderate Resolution Imaging Spectroradiometer (MODIS) “Aqua” sensor launched by NASA in July 2002 (4 km spatial resolution). In this report, MODIS data from 2003–2021 are used to construct a continuous time series of surface chl *a* in the four ocean-colour polygons (Figure 4). The continued calibration and data reprocessing done by NASA ensure data quality over the whole MODIS time series (Xiong et al. 2020). Previous reports (before 2019) used a combination of sensors (SeaWiFS, MODIS, VIIRS) to construct a time series starting in 1998. However, since the consistency between chl *a* estimates using these three sensors has not been assessed in the waters of the Gulf, it was decided that only one sensor should be used to avoid sensor bias over the time series.

Composite satellite images of remote sensing reflectance sourced from NASA’s Goddard Space Flight Center were converted to chl *a* using an algorithm based on empirical orthogonal function (EOF) analysis (Laliberté et al. 2018). Daily chl *a* concentrations were averaged over each ocean-colour polygon and were extracted using the PhytoFit application v1.0.0 (Clay and Layton

2020). The timing (start and duration) of the spring phytoplankton bloom was defined using a symmetric shifted Gaussian function of time in days (Zhai et al. 2011) that was smoothed using a LOESS function (locally estimated scatterplot smoothing) over days with a minimal polygon coverage of 20%. While the start (day when 20% of the bloom amplitude is reached) and duration of the spring bloom were derived from the smoothed Gaussian curve, the amplitude (maximum chl *a*) and magnitude (the integral of chl *a* concentration under the Gaussian curve) of the spring bloom were calculated from the daily satellite-derived chl *a* within the spring bloom period rather than from the Gaussian curve. In addition, seasonal mean chl *a* biomass during spring (March to May), summer (June to August), and fall (September to November) as well as the annual average (March to November) were computed. For each of these metrics, we computed normalized annual anomalies (see Scorecards section below) to describe temporal trends for each ocean-colour polygon and for Rimouski station. Note that ocean colour data from January, February, and December were discarded due to lack of data (cloud, sea-ice cover, and low sun angles).

ZOOPLANKTON INDICES

We provide a detailed description of the seasonal patterns for different zooplankton indices. For the high-frequency monitoring stations, we present total mesozooplankton biomass (dry weight), total copepod abundance, and the relative abundances of the copepod species making up 95% of the total abundance. In addition, we include *Pseudocalanus* spp. (Rimouski station only) and *Calanus finmarchicus* abundances and stage composition. Because of its importance to the total zooplankton biomass in the Gulf, a detailed description of *Calanus hyperboreus* is provided for Rimouski and Shediac Valley stations. We also present the early summer and fall distributions and time series of total zooplankton biomass and total abundances of *C. finmarchicus*, *C. hyperboreus*, and *Pseudocalanus* spp. for the Gulf regions as well as similar indices (*C. finmarchicus*, *C. hyperboreus*, large calanoids and small calanoids) from the egg mackerel survey and the late summer survey (ZooImage). Since zooplankton samples are collected over the entire water column, zooplankton indices represent depth-integrated metrics.

We used the time series at Rimouski station to describe *C. finmarchicus* phenology and its changes through time because adequate sampling and stage identification started there more than 25 years ago (1994). However, sampling methodology has changed over time: from 1994 to 2004, prior to the use of AZMP standard nets (i.e., 75 cm diameter, 200 µm mesh bottom-to-surface ring net tows; Mitchell et al. 2002), *C. finmarchicus* copepodite stage abundance was determined using samples collected with 333 µm (CIV–CVI) and 73 µm (CI–III) mesh nets, towed from bottom to surface and from 50 m to surface, respectively. The 73 µm mesh nets were analyzed for only six years (1994, 1996–2000) of the time series (see Plourde et al. 2009 for details). In other years before 2004 for which 73 µm samples were not analyzed, the abundance of CI–III in the 333 µm samples was adjusted based on a comparison performed with a 158 µm mesh net (S. Plourde, DFO, Mont-Joli, QC; unpublished data). The phenology of *C. finmarchicus* was described using the following steps:

1. Stage-relative abundances were normalized (proportion of a copepodite stage/maximum proportion for the stage) within each year for CI–III, CIV, CV, and CVI (male and female); and
2. Stage proportions were smoothed using a LOESS function.

Finally, annual anomalies were computed for zooplankton biomass and for the abundances of several zooplankton indices that reflect either key copepod taxa, different functional groups, or groups of species indicative of cold- or warm-water intrusions and/or local temperature conditions specific to the Gulf (see Scorecards section below) for both the high-frequency

monitoring stations and the Gulf regions. Only samples collected during regular AZMP surveys (early summer and fall) and analyzed by taxonomists were included in the calculation of regional zooplankton annual anomalies. A detailed list of species included in each large copepod index is presented in Appendix 2. Since 2018, when taxonomists cannot distinguish *C. finmarchicus* from *C. glacialis,* we use the results of a genetic study based on prosome length to properly identify them (Parent et al. 2011).

SCORECARDS

Normalized anomalies for the chemical and biological indices presented in scorecards were computed for the high-frequency monitoring station and oceanographic regions and subregions. These anomalies are calculated as the difference between the variable's average for the season or for the complete year and the variable's average for the climatology (usually 1999–2020 unless otherwise noted); this number is then divided by the standard deviation over the climatological period. Due to the COVID-19 pandemic, there was no early summer oceanographic survey in the Gulf during 2020 so the climatology for the early summer time series is 1999–2019.

Anomalies are presented as scorecards with positive anomalies depicted as shades of red, negatives as blues, and anomalies within ± 0.5 SD as white (considered as normal conditions, i.e., similar to the climatology). A standard set of indices representing anomalies of nitrate inventories, phytoplankton biomass and bloom dynamics, mesozooplankton biomass, and the abundance of dominant mesozooplankton species and groups (*C. finmarchicus, Pseudocalanus* spp., total copepods, and total non copepods) are produced for each AZMP region (Casault et al. 2022; Maillet et al. 2022). To visualize Northwest Atlantic shelf-scale patterns of environmental variation, a zonal scorecard including observations from all AZMP regions is presented in DFO 2022.

Annual nutrient, phytoplankton, and zooplankton index anomalies are based on the mean annual concentration (mmol m^{-2} for nutrients and mg chl *a* m^{-2} for phytoplankton biomass) or density (cells L^{-1} for phytoplankton abundance and ind m^{-2} for zooplankton abundance) estimated at each high-frequency monitoring station and each Gulf region/subregion. These annual estimates are derived from general linear models (GLM) of the form:

$$\log_{10}(Density + 1) = \alpha + \beta_{YEAR} + \delta_{MONTH} + \varepsilon$$

for the high-frequency monitoring stations, and

$$\log_{10}(Density + 1) = \alpha + \beta_{YEAR} + \delta_{STATION} + \gamma_{SEASON} + \varepsilon$$

for the regions and subregions, where α is the intercept, and ε is the error. The GLM is applied to each region/subregion separately. For the high-frequency monitoring stations, β and δ are the categorical effects for year and month, respectively. For the regions/subregions, β, δ, and γ are the categorical effects of year, station, and season, respectively. Results of the GLM (significance of each factor and adjusted R squared of the regression) are presented in Appendices 3 to 7. Four seasons (winter, early summer, late summer, and fall) are included in the GLM estimating the annual average of surface nutrient inventories; three seasons are used to estimate the annual average of deeper nutrient inventories and phytoplankton indices (sample collection during the winter helicopter survey is limited to the collection of surface nutrient samples); and two seasons are used to calculate annual estimates of zooplankton indices (samples analyzed via ZooImage are presented separately). An estimate of the least-squares means based on type III sums of squares is used as the measure of the overall year effect. We log-transformed concentrations and density values before computing anomalies

to compensate for the skewed distribution of observations. We added one unit to *density* terms for the abundance indices to include observations with values of zero.

OBSERVATIONS

PHYSICAL ENVIRONMENT

Water column temperature, salinity and sea ice conditions in 2021 are described in detail in Galbraith et al. (2022). The sea ice seasonal maximum volume was just shy of the series low record of 2010 and the winter mixed layer volume was second lowest of the 1996–2021 time series for waters colder than -1°C and lowest for waters colder than 0°C. The cold intermediate layer (CIL) seasonally averaged minimum temperature index was the highest since 1980. The May–November average sea-surface temperature for the Gulf was 3rd highest of the time series. Since 2009, deep-water temperatures (> 150 m) have been increasing overall in the Gulf, and new record highs were set at 150 m, 200 m, 250 m, and 300 m in 2021.

Stratification is one of the key physical parameters controlling primary production. For this reason, we present the upper water column stratification at the high-frequency monitoring stations (Figure 5). The weak freshwater discharge into the Estuary during springtime (Galbraith et al. 2022) led to weaker-than-normal stratification from May to July at Rimouski station. Stratification was only stronger than normal during December. At Shediac Valley station, stratification stayed close to normal the whole year except for a strong positive anomaly in March.

DEEP OXYGEN

In the Gulf, a dissolved oxygen value of 100 µM corresponds to approximately 30% saturation, below which the water is considered to be hypoxic and can reduce the survival of some species such as Atlantic cod (Plante et al. 1998). The lowest levels of dissolved oxygen (below 20% saturation in recent years) have been found in the deep waters at the head of the Laurentian Channel in the Estuary (Figure 6). In 2021, concentrations of dissolved oxygen at 200 m, 250 m and 300 m were again well below normal everywhere along the Laurentian Channel, and the strongest negative anomalies were observed at 200 m in the Cabot Strait subregion (Figure 6). At 300 m, dissolved oxygen concentrations reached record-low values in the northwest Gulf, central Gulf, and Cabot Strait (Figure 7). At Rimouski station and in the Estuary, deep dissolved oxygen concentrations were the second lowest of the time series, slightly above the 2020 record-low values (Figure 7). The combination of AZMP data with the time series published in Gilbert et al. (2005) indicates that the deep waters of the Estuary have consistently been hypoxic since 1984. The dissolved oxygen concentration was 46 µM in 2021, corresponding to ca., 15% saturation (Figure 7).

NUTRIENTS AND PHYTOPLANKTON

Distributions of dissolved inorganic nutrients (nitrate, silicate, phosphate) strongly co-vary in space and time (Brickman and Petrie 2003). For this reason and because nitrogen availability controls phytoplankton growth in coastal waters of the Gulf, emphasis in this document is given to the variability in nitrate concentrations and inventories, even though the distributions of other nutrients are also briefly discussed. In this document, we use the terms “nitrate” or “total nitrate” to refer to the sum of nitrate and nitrite (NO_3^- + NO_2^-).

High-frequency monitoring stations

The two high-frequency monitoring stations typically exhibit a biologically-mediated reduction in surface nitrate inventories in spring/summer, a minimum during summer, and a subsequent increase during fall/winter once water column mixing intensifies due to cooling processes and wind forcing (Figures 8a, b). However, chl *a* displays different seasonal patterns at each station: it reaches its maximum during early summer at Rimouski station (Figure 8c) while the maximum is reached in early spring before diminishing rapidly and staying stable for the remainder of the year at Shediac Valley station (Figure 8d). Following the spring bloom, nitrate and chl *a* inventories are typically two to three times higher at Rimouski station than at Shediac Valley station (Figure 8).

In 2021, Rimouski station nitrate inventories in the surface layer were generally close to normal until June and well below normal afterwards; they were associated with chl *a* inventories that were generally close to normal, with the exception of a few samples showing high phytoplankton biomass (Figures 8a, c). Overall, the mean annual nitrate inventory set a new record low in the upper layer, while it was slightly below normal and normal in the mid and deep layers, respectively (Figure 8 scorecard). The annual average chl *a* inventory was above normal (Figure 8 scorecard). Most of the phytoplankton biomass was in the upper 15 m of the water column from May to November, where nitrate inventories were depleted (Figure 9). A strong vertical export of phytoplankton biomass to the deeper layers was observed in June and July. Replenishment of nitrate in the surface layer only started in December, while it typically starts during late summer/early fall (Figures 8a, 9). At Shediac Valley in 2021, both surface nitrate and chl *a* inventories were generally close to or below normal (Figures 8b, 8d, 10), except for nitrate inventories measured in September that were mostly above normal (Figure 8b). Annual averages were below normal for chl *a* and deep nitrate inventories, and near normal for surface nitrate inventories (Figure 8 scorecard).

Phytoplankton abundances at Rimouski station were generally below normal during spring and summer, except for two samples collected in June and September that showed very high abundances, and near normal during fall (Figure 11a). The seasonal phytoplankton community composition had a lower contribution of diatoms compared to the climatology from April until November, and their contribution only started rising in mid-May, while it typically does so in mid-March. However, their contribution was about 10 times higher than the climatology in November and December (Figures 11b, c). Overall, the annual average diatom abundance showed a slightly positive anomaly while all other phytoplankton taxonomic indices were near normal. Negative anomalies for dinoflagellates and positive anomalies of the diatom:dinoflagellate ratio have often been observed at Rimouski station since 2014 (Figure 12). At Shediac Valley, phytoplankton abundances were either below normal or near normal, and contribution of diatoms was reduced during June and July compared to the climatology (Figure 13). This main departure from the climatology was reflected in the annual anomaly scorecard, with a record-low abundance of diatoms in 2021. Ciliates showed a small positive anomaly while the abundances of the other groups were normal (Figure 12).

Gulf regions

The distribution of nitrate in the surface layer during winter 2021 was slightly different from the climatology, with lower-than-normal inventories in northern Gulf and higher-than-normal inventories on the northern side of Prince Edwards Island, in the southern Gulf (Figure 14). The suggested nitrate drawdown during spring was generally close to or below normal, except for the same areas that showed positive nitrate anomalies in winter (Figure 14). During early summer, nitrate inventories were near or below normal in the surface layer, and generally near or above normal in deeper layers, except in the Estuary and the westernmost area of northwest

Gulf subregion where negative anomalies were recorded in the deeper layers (Figure 15). Nitrate inventories during late summer and fall also follow this general pattern with the exception of positive anomalies in the surface layer of the Magdalen Shallows and central Gulf during late summer (Figures 16, 17).

Overall, 2021 nitrate anomalies in the surface layer were negative in the Estuary, northwest and northeast Gulf, and near normal in the other regions, with record-low values in the Estuary and northwest Gulf. Linear regressions of the surface layer nitrate annual average by year suggest a significant ($p < 0.05$) decrease of 15 to 35% of the nutrient content in all regions but the northwest Gulf over the past 20 years. Interestingly, the N:P ratio in the surface layer has diminished in the same regions over the time series, but its decrease is only significant during late summer and fall (linear regression; $p < 0.05$).

In deeper layers, nitrate anomalies were generally positive, except in the mid-layer of the Estuary and northwest Gulf region, where they stayed below normal (Figure 18). The nitrate inventory was a record high in the deep layer of northeast Gulf. Since 2012, deep nitrate inventories have regularly shown positive annual anomalies in Cabot Strait and the central Gulf. The Redfield-Brzezinski C:Si:N:P ratio, which presumes equilibrium between phytoplankton composition and the deep-ocean nutrient inventory, is 106:15:16:1 (Redfield, 1958; Brzezinski, 1985). In the deep waters of the Gulf, the N:P ratio is lower and typically ranges from 9.5 to 13.5 (Figure 19) while the Si:N ratio tends to be higher, ranging between 0.8 and 2.2 (Figure 20). In 2021, the N:P ratios in all layers and regions were either close to or below normal, including record lows in the Estuary and northwest Gulf, except for the positive anomalies recorded in the mid-layers of the central Gulf, Cabot Strait, and Magdalen Shallows (Figure 19). The Si:N ratio showed a contrasting pattern, with near-normal or positive anomalies in all layers and regions but the surface layer of the central Gulf (Figure 20). Interestingly, the N:P ratio has mostly shown negative anomalies in the deep layer (150 m–bottom) over the last six years, while the Si:N ratio anomalies have mostly been positive. Moreover, there has been a decrease in the climatological deep N:P ratio and an increase in the climatological deep Si:N ratio as water progresses up the deep channel from Cabot Strait through the Central Gulf and northwest Gulf to the Estuary (Figures 19, 20).

In 2021, the seasonal phytoplankton biomass distribution was similar to that of the climatology during early summer, showed generally lower phytoplankton biomass in most Gulf regions during late summer, and was associated with mixed anomalies during fall—positive anomalies in the westernmost and easternmost areas and neutral to negative anomalies in between (Figure 21). These patterns are reflected in seasonal time series anomalies (Figure 22). During early summer, anomalies were either close to normal or positive while they were mostly negative during late summer. They also suggest the occurrence of a strong fall bloom in the Estuary for a fourth consecutive year and in the northwest Gulf, where chl *a* inventories were at a record high during fall (Figure 22). The overall annual average was near normal except in the Estuary and northwest Gulf, where it was higher than the climatology owing to the strong fall bloom in this region, even setting a new record high for phytoplankton biomass in northwest Gulf (Figure 22). Removing the effect of the fall AZMP survey timing by selecting only field data collected within a two week period (27 Oct–6 Nov), linear regressions suggest that the increase in phytoplankton biomass during fall is significant over the time series in the Estuary ($p < 0.01$), the Magdalen Shallows ($p = 0.02$), and the central Gulf/Cabot Strait ($p < 0.001$), and almost significant in the northeast Gulf ($p = 0.075$). In these regions/subregion, it corresponds to an average increase of fall phytoplankton biomass of roughly 60% when comparing the beginning and the end of the time series.

These broad spatial patterns were somewhat mirrored by local conditions encountered at the high-frequency monitoring stations, with below normal nitrate inventories in the surface layer

and above-normal chl *a* inventories at Rimouski station and in the Estuary, and near-normal nitrate inventories in the surface layer at Shediac Valley station and in the Magdalen Shallows (Figure 8).

Remote sensing of ocean colour and spring bloom metrics

Satellite imagery suggests that the spring phytoplankton bloom started in early April and peaked in the second half of April in most ocean-colour polygons (Figures 23, 24). Maximum chl *a* concentrations in the surface layer during spring averaged ca., 2 mg chl *a* m^{-3} over the Gulf and were close to the climatology (Figure 23). In the Estuary, as represented by Rimouski station, surface phytoplankton biomass is typically maintained around 4 mg chl *a* m^{-3} from April to September (Figure 23). In 2021, surface phytoplankton biomass was either close to or below this value at Rimouski station (Figure 23). A look at surface chl *a* distribution during fall suggests that negative anomalies were widely distributed over the Gulf except for the fall bloom that was somewhat visible at the surface in some small areas of the northwest Gulf in November (Figure 25). This fall bloom was also detected at the surface of the Estuary, as suggested by above-normal concentrations of chl *a* in October and November at Rimouski station (Figure 23).

Spring bloom metrics (Figure 26) were mostly close to normal in all polygons or showed relatively small negative anomalies, with the exception of the slightly later-than-normal start of the bloom in the Magdalen Shallows (positive anomaly). Thus, overall, the timing of the bloom was similar to the climatology and the bloom was less intense than normal in terms of both magnitude and amplitude. The third and fourth lowest bloom magnitudes of their time series were recorded in the Northwest Gulf and Magdalen Shallows ocean-colour polygons (Figure 26). Phytoplankton biomass in the surface layer reached record-low in all ocean-colour polygons, especially during summer and fall (Figure 26).

To a certain extent, remote sensing surface chl *a* concentrations are consistent with *in situ* observations, considering that many polygons/regions showed negative chl *a* anomalies over the year, particularly during late summer (Figure 22). However, the main contrast occurs during fall, when field data suggest a large fall bloom in the northwest Gulf and moderate fall bloom in Cabot Strait. These diverging patterns could be explained by the vertical structure of phytoplankton in the water column and suggest that the fall bloom mostly occurred below the top few meters of the surface layer. Moreover, the seasonal anomalies derived from satellites are calculated for three-month periods in each ocean-colour polygon while our *in situ* sampling in each Gulf region is generally completed within a few days (timing of sampling of each dedicated AZMP surveys is indicated in Figure 23). Thus, these different time scales might also explain divergences between in situ and remote sensing data. In addition, bias in remote sensing data during fall due to higher cloud cover as well as the influence that field sampling timing can have on the annual anomalies of phytoplankton indices could also account for some of the discrepancies between satellite and field data.

ZOOPLANKTON

High-frequency monitoring stations

In 2021, the zooplankton biomass at Rimouski station followed the monthly climatology, with mostly near-normal values during spring and summer, except for two high biomass values in June and below-normal values during fall (Figure 27a). At Shediac Valley, zooplankton biomass was also mostly close to normal apart from the lower-than-normal value recorded in May (Figure 27b).

At Rimouski station, the total copepod abundance was close to normal during spring and early summer and then increased to values well above normal from late summer until late fall (Figure 28a). In summer, the relative abundance of *Microcalanus* spp. and *Metridia longa* were higher than normal at the expense of *C. hyperboreus* whose relative abundance was much lower than usual from June onward. The sudden copepod abundance increase in late summer was associated with a large proportion (ca., 20%) of *Temora longicornis*, which is not among the climatology's 95% dominant copepod taxa at this station (Figures 28b, c). *Oithona similis* also showed a proportion about twice as large as that of the climatology during October (Figures 28b, c).

Copepod abundance at Shediac Valley was normal in May and then oscillated between above- and below-normal values during the few occupations (Figures 29a). Community composition was also relatively similar to the climatology during May despite the presence of *C. glacialis,* which represented about 5% of the copepod community whereas it is not included in the climatology 95% dominant taxa. In June and July, *Oithona similis* and *Pseudocalanus* spp. respectively indicated larger-than-usual proportions while the relative abundance of *Temora longicornis* in October was more than twice its normal value. From June, the relative abundance of large *Calanus* was lower than normal (Figures 29b, c).

There was a shift in the *C. finmarchicus* abundance from near-normal levels from April to June to higher-than-normal levels from July onward at Rimouski station in 2021 (Figure 30a). This sharp increase followed the peak of early-stage copepodites in June and was accompanied by a larger-than-normal contribution of CIV and CV to the population (Figures 30b, c). By November, the *C. finmarchicus* population was almost exclusively composed of pre-adult stage (CV) with a small proportion of adults (CVI). At Shediac Valley, the abundance of *C. finmarchicus* was either near or slightly below normal. Beside the absence of early copepodite stage in July, the stage composition was relatively similar to normal, with the early stage peak (CI–CIII) proportion being slightly higher than normal in May and October (Figures 30e, f).

Abundances of *C. hyperboreus* were generally below normal at Rimouski station except for two higher-than-normal abundances in June (Figure 31a). The peak in early stage copepodites occurred at normal time and was larger than for the climatology (Figures 31b, c). At Shediac Valley, both the abundance and stage composition were similar to the climatology in 2021 (Figures 31d, e, f). *Pseudocalanus* spp. abundances were generally near normal except during fall, when they were higher than normal at both high-frequency monitoring stations in 2021 (Figures 32a, d). At Rimouski station, the spring maximum contribution of *Pseudocalanus* spp. early stages occurred earlier in 2021 than normal (April instead of May), and an unusual and even larger second peak was also observed during fall (Figures 32b, c).

Gulf regions

During early summer and fall 2021, zooplankton biomass was largely concentrated in the deep channels of the Estuary and Gulf, where higher abundances of *C. hyperboreus* generally occur; zooplankton biomass is very low on coastal portions of sections and is also generally low in the Magdalen Shallows (Figure 33). Zooplankton biomass was mostly below normal during both seasons, except for near-normal biomasses in the northeast Gulf and Magdalen Shallows during fall (Figure 33). In the Estuary/northwest Gulf region, zooplankton biomass showed record-low values during both seasons, slightly below 2017 levels. Over the time series, the decrease of zooplankton biomass is significant ($p = 0.02$), and represents a biomass loss of about 15–20% in the northwestern and northeastern Gulf and nearly 40% on the Magdalen Shallows and in the central Gulf/Cabot Strait.

The highest abundances of *C. finmarchicus* were found during early summer around the Gaspé Peninsula and near Shediac Valley, and abundances were close to normal during both seasons and in all regions (Figure 34).The abundance of *C. hyperboreus* followed the same anomaly patterns as observed for zooplankton biomass, and it was the lowest recorded over the time series during early summer in the northeast Gulf and the central Gulf/Cabot Strait regions (Figure 35). The abundance of *Pseudocalanus* spp. was generally near or slightly below normal during both seasons, except for the Estuary/northwest Gulf region during fall and the Magdalen Shallows region during early summer, when a massive abundance of *Pseudocalanus* spp. was detected on the western side of Cabot Strait (the western side of Cabot Strait is included in the Magdalen Shallows region; Figure 36).

Time series of zooplankton indices from the mackerel egg survey on the Magdalen Shallows and from the northern Gulf late-summer survey (ZooImage) both suggest that *C. finmarchicus* abundance was higher than normal while that of *C. hyperboreus* was lower. On average, the large calanoid index was close to or slightly below normal during these two seasons. Small calanoids were slightly more abundant than normal on the Magdalen Shallows during the mackerel egg survey and were near normal, although slightly below normal in the northern Gulf during late summer (Figure 37). These results are generally consistent with the observations made during the AZMP surveys.

Copepod phenology

Changes in the timing of zooplankton development were described using the detailed seasonal pattern of the copepodite stage relative abundances of *C. finmarchicus* at Rimouski station from 1994 to 2021 (Figure 38). A scorecard showing the anomaly of the first and last days when the normalized proportion of CI–CIII copepodite stages was higher than 0.3 (visually defining early stage peaks in most cases) was also added to provide an objective tool to describe *C. finmarchicus* phenology. Overall, there is a trend towards earlier population development, with negative anomalies in the “first day” index strengthening in recent years. This trend was reinforced by the record low in 2021. However, the early copepodite stage main peak in late June and the phenology of the other copepodite stages were relatively similar to what has been observed over the past decade. The abundance of CI–CIII copepodite stages stayed relatively high until fall and the “last day” index showed a record-high value. Conversely to this unique and long-lasting pulse, the positive anomalies of the “last day” index from 2010 to 2014 were associated with a second distinct pulse of early stages in late summer. In recent years, the negative anomalies of this index are mostly associated with single presence of CI–CIII copepodite stages in substantial abundance (Figure 38).

Scorecards

The time series of annual zooplankton biomass anomalies highlight recent major changes in the community, with mostly negative anomalies across the Gulf since 2009 (Figure 39). In 2021, zooplankton biomass anomalies were strongly negative in most of the Gulf regions, except at Rimouski station and the Magdalen Shallows (including Shediac Valley station). It was the lowest biomass recorded over the time series in the Estuary/northwest Gulf region and the second lowest in the northeast Gulf and central Gulf/Cabot Strait regions (Figure 39). Zooplankton biomass is strongly influenced by the abundance of large *Calanus* spp. While *C. finmarchicus* annual abundances were near-normal everywhere in the Gulf and only above normal at Rimouski station (Figure 40), *C. hyperboreus* mostly showed strong negative anomalies, including unprecedented low abundances in the northeast Gulf (Figure 41). As a consequence, the large calanoid index showed important spatial variability with a positive

anomaly at Rimouski station, a negative anomaly in the northeast Gulf and central Gulf/Cabot Strait region, and near normal elsewhere (Figure 41).

The general decrease in zooplankton biomass over time is consistent with increases in *Pseudocalanus* spp., total copepod, non-copepod, and small calanoid abundances, for which positive anomalies have been regularly observed over the last decade or so (Figures 40, 41; see Appendix 2 for a detailed list of the species included in each of these indices). These groups all presented similar anomaly patterns in 2021. Their anomalies were positive or slightly positive in the Estuary/northwest Gulf (including Rimouski station) and the Magdalen Shallows (including Shediac Valley station), and they were negative (near normal for the non-copepod and small calanoid indices) in the northeast Gulf and central Gulf/Cabot Strait region (Figure 40). In the latter region, total copepod abundance reached a record-low value, which is in agreement with the low zooplankton biomass measured there. At Rimouski station and in the Estuary/northwest Gulf, small calanoids were at their highest level ever recorded. Cyclopoids also followed a similar pattern in 2021, but they showed near-normal anomalies for the Magdalen Shallows and Shediac Valley station (Figure 41).

The abundance of warm-water copepods has also increased since about 2010. This was observed again in 2021, with positive anomalies over the whole Gulf, including several record-high abundances (Estuary/northwest Gulf, Northeast Gulf, Magdalen Shallows). The abundance of *Centropages* spp. in those regions also reached record-high levels over the time series (not shown). Cold-water copepods showed either near-normal or positive anomalies with record-high abundance observed at both high-frequency monitoring stations (Figure 41). A detailed list of species included in each of these indices is presented in Appendix 2.

In general, annual anomalies were coherent among the high-frequency monitoring stations and their associated Gulf region (Figures 39, 40, 41). This suggests a high reliability of our annual estimates throughout the Gulf even though data collection is limited to early summer and fall surveys for zooplankton indices.

DISCUSSION

ENVIRONMENTAL CONDITIONS

The timing of the onset and extent of water column stratification plays a role in defining spring bloom phenology, phytoplankton production, species succession, and trophic interactions over the complete growth season (Levasseur et al. 1984). In 2021, the timing of upper water column stratification was similar to the climatology at both high-frequency monitoring stations, but the strength of spring stratification of the upper water column was much below normal due to reduced freshwater inflows from the St. Lawrence River (Galbraith et al. 2022). In addition to the effect of water column stratification on phytoplankton dynamics, thermal properties of the surface, intermediate, and deep water masses play a role in defining zooplankton dynamics (Plourde et al. 2002). Galbraith et al. (2022) reported on the physical conditions that prevailed in the Gulf during 2021, showing warmer-than-normal conditions for most indices. This document reports on the chemical and biological conditions in the Gulf in the context of these conditions.

Changes in dissolved oxygen of the deep waters entering the Gulf at the continental shelf are related to the varying proportions of Labrador Current water (cold/fresh, high dissolved oxygen levels) and slope water (warm/salty, low dissolved oxygen levels), which together form the source of Gulf deep waters (McLellan 1957; Lauzier and Trites 1958; Gilbert et al. 2005). In recent years, the contribution of slope water to the deep Gulf waters has increased (Gilbert et al. 2005; Galbraith et al. 2021). Given the inherent properties of Gulf source waters (North Atlantic Central Water versus Labrador Current water; Gilbert et al. 2005), changes in their mixing ratio

at Cabot Strait imply that a decrease of 1.46 µM might be expected for each 0.1°C temperature increase. However, today's deep oxygen concentrations at Cabot Strait represent a drop of ca.,70 µM compared with their concentrations in the early 1970s (ca., 190 µM; Blais et al. 2021a), for a 1.85°C increase in temperature over the same period (Figure 46 in Galbraith et al. 2022). These deep waters travel from the mouth of the Laurentian Channel to the Estuary in roughly three to four years (Gilbert 2004), decreasing in dissolved oxygen content in response to *in situ* respiration and oxidation of organic material by microbes as they progress to the channel heads. The inflow of warmer waters to the Estuary is expected to exacerbate the hypoxic conditions since these waters are typically poor in dissolved oxygen (McLellan 1957; Lauzier and Trites 1958; Gilbert et al. 2005). Deep-water temperature has increased by 1.82°C at 300 m between the early 1970s and 2021 (Figure 46 in Galbraith et al. 2022) while oxygen concentration has decreased from ca., 105 µM (Blais et al. 2021a) to 46.2 µM over the same period. This is over twice as much as what could be expected from temperature only according to the mixing ratio of source waters. Thus, warming of bottom water and changes in the mixing ratio of source waters are not the only factors contributing to the decrease in oxygen concentrations in the Gulf. Other factors that can cause variability in oxygen concentration include interannual changes in the vertical flux of organic matter and microbial metabolic processes of the bottom waters.

Winter mixing is a critical process for bringing nutrient-rich deep water to the surface. In the Gulf, winter convection is partly driven by buoyancy loss of surface waters attributable to cooling and reduced freshwater runoff, brine rejection associated with sea-ice formation, and wind-driven mixing prior to ice formation (Galbraith 2006). Warmer-than-normal surface waters throughout the winter, minimal sea-ice formation and reduced volume of winter mixed-layer can be associated with low winter convection and may reduce the amount of nutrients available for spring primary production. The CIL represents the winter surface mixed layer that has been insulated from the atmosphere by near-surface stratification and whose nutrient inventory will supply primary producers during the growth season through vertical mixing. In 2021, the CIL temperature and winter mixed-layer volume suggest reduced winter convection, and the mean annual nitrate inventory showed negative anomalies in many regions, including record lows in the surface layer of the Estuary and northwest Gulf. The freshwater inflow, which accounts for up to 35% of nutrient input to the Estuary (Lavoie et al. 2021), was also largely reduced in 2021 and probably emphasized the effect of a reduced winter convection. Negative nitrate anomalies in the surface layer have been regularly encountered in the Gulf since 2010, a period over which several temperature and ice-cover indices have shown clear warming of the Gulf (Galbraith et al. 2022), and they resulted in a significant decrease of the nitrate content of the surface layer over the time series. Thus, low winter convection and strengthening of the stratification in association with global warming could have limited the nutrient flux to the surface layer, but the significant change in the N:P ratio during late summer and fall suggests that a change in biological activity likely accounts in part for the reduced nitrate content during these seasons.

Positive anomalies in deep-water (300 m) nitrates have regularly been observed since 2012 in the central Gulf and Cabot Strait in association with high temperature/high salinity water intrusions into the Gulf from Cabot Strait (Galbraith et al. 2022). These higher-than-average deep inventories are associated with a water mass composition that has a greater contribution of slope water than Labrador Shelf water (Gilbert et al. 2005; Galbraith et al. 2022). Moreover, a reduction of exchanges between the upper and bottom layers due to a shallower thermocline (generally increased stratification due to global warming) might further increase the deep nutrient pool. A positive deep nitrate anomaly was also observed in the Estuary for a second consecutive year. This could indicate that waters with a larger proportion of slope water have reached the Estuary, as suggested by increased bottom water temperature in the Estuary (Galbraith et al. 2022). The year 2021 marks the fifth consecutive year of rather strong nutrient

ratio anomalies in deep waters of the Estuary and northwest Gulf and of the northeast Gulf (negative anomalies for N:P and positive anomalies for Si:N). This suggests that despite a rise in nitrate content in the deep layer, the regeneration of nitrate does not occur at the same pace as other nutrients in these regions. The change in nutrient ratio as water progresses from Cabot Strait to the Estuary also supports this hypothesis of differential nutrient regeneration time. This could be the result of changes in the nitrogen cycle due to microbial activity, such as decreased nitrification or increased denitrification associated with low oxygen concentrations. Nitrification was recently identified as a key process in the accurate modeling of nitrogen fluxes in the Gulf (Lavoie et al. 2021). Moreover, the routine measurement of NH_4 concentrations has recently been added to AZMP sampling in the Gulf and will eventually be helpful in verifying the latter hypothesis.

PHYTOPLANKTON

Except at Rimouski station, where sampling regularly covers the spring bloom period, phytoplankton production during the spring bloom must be inferred either from indirect indices, such as the difference in the nutrient inventory of the surface mixed layer between the winter and the early summer surveys, or from satellite observations. The estimate of nutrient drawdown during spring suggests that bloom production in 2021 was generally near, or slightly below normal, in agreement with satellite observations. Furthermore, satellite observations suggest that the timing nearly matched the climatology, being slightly early in northern Gulf and slightly late in the Magdalen Shallows. The intensity (magnitude) of the spring bloom is a combined index of its duration and amplitude (maximum chl *a* concentration reached). While duration tends to be negatively correlated with the start of the spring bloom, which depends on the onset of the water column stratification, the amplitude is mostly determined by the availability of nitrogen. Thus, weak winter convection and low nitrate availability likely played a key role in preventing a strong spring bloom.

No distinct trends in spring bloom metrics can be identified over the time series. Under global warming scenarios, an earlier onset of stratification is expected to trigger an early spring bloom. However, the expected concomitant large freshet (due to an increase in precipitation) may prevent the accumulation of phytoplankton biomass in the water column in regions under the influence of freshwater, which may instead delay detection of the bloom start in these regions. Densities of overwintering copepods, which were generally low in the Gulf for 2016–2018 and 2021 (low annual biomass), also impact spring bloom intensity and other bloom metrics through grazing (Sommer and Lengfellner 2008). Along with winter convection and nutrient availability, they largely influence bloom metrics and likely account for the large interannual variability seen in these metrics.

For all seasons but spring, ocean colour data is complemented by field data. These two data sources have regularly offered different conclusions in terms of anomalies in the seasonal phytoplankton biomass. Although these two sources of observations both suggest that phytoplankton biomass was below normal during late summer 2021, a major contradiction occurred during fall and is among the recurrent differences between the methods. Over the last four years, ocean colour data often suggested below-normal chl *a* concentrations in the thin surface layer during fall while field data have regularly suggested positive phytoplankton biomass anomalies in recent years, including 2021. Field data actually suggest a significant increase of phytoplankton biomass during fall over the time series in several regions. Possible causes of discrepancies between the methods were presented in the results (Remote sensing section). Data collected at Rimouski station (occupations of the station and Viking buoy) agree with data from the fall AZMP dedicated survey on the occurrence of a late summer/fall bloom in the Estuary in 2021. Indeed, there was a large withdrawal of nitrate in the surface layer during

late summer at Rimouski station despite near-normal chl *a* concentrations. The late summer increase in the abundance of *C. finmarchicus* at Rimouski station possibly maintained phytoplankton biomass at near-normal levels. An increased occurrence of fall storms, as observed during 2019 and 2020 (Galbraith et al. 2020, 2021), may favour ideal growth conditions for phytoplankton, especially if combined with a reduction of grazing pressure due to the diminution of grazer biomass.

ZOOPLANKTON

Zooplankton biomass has generally been below normal in recent years, with several record-low levels in 2016–2017 and in 2021, resulting in a significant decreasing trend in all regions. Lower biomass is typically associated with a decrease in the abundance of large zooplankton species. The mean weight of large calanoids (e.g., *C. hyperboreus*: 3.5 mg per adult female) is between one and two orders of magnitude greater than that of small calanoids (e.g., *Pseudocalanus* spp.: 0.02 mg per adult female; Conover and Huntley 1991; Plourde et al. 2003). Thus, the decrease in large calanoid abundance has a greater impact on zooplankton biomass than, for instance, the increase of *Pseudocalanus* spp. abundance that has been regularly recorded over recent years. The increase in small calanoids seems to be coupled with an increase in non-copepod abundance, mostly larvae of benthic organisms. Suitability of environmental conditions, competition for food, the availability of large versus small phytoplankton cells, and/or differential predation pressure might favour the dominance of either one of these communities, i.e., one dominated by large calanoids versus one dominated by a combination of small calanoids and non-copepods (Hall et al. 1976; Daewel et al. 2014), with potential implications for the pelagic food web and pelago-benthic coupling.

In 2021, there was again a major decrease in zooplankton biomass and in the abundance of the large *C. hyperboreus* in all regions where deep channels are a dominant bathymetric feature. Warm conditions throughout the water column all year round and the relatively weak spring bloom possibly reduced the survival of *C. hyperboreus* early copepodite stages. While the interannual variations in the abundance of *C. hyperboreus* and its overwintering stage structure is known to be mostly influenced by spring conditions (Plourde et al. 2003), the phenology of *C. finmarchicus* is influenced by fall environmental conditions. Under favorable conditions, and quite often since 2010, *C. finmarchicus* sometimes produces a second cohort that typically occurs in late summer. There are several field observations indicating strong fall bloom conditions in 2021 in the Estuary, where the abundance of *C. finmarchicus* suddenly increases during late summer. It is likely that the bloom actually started during late summer, as suggested by an observation of very high phytoplankton biomass in August at Rimouski station. However, high grazing pressure would have limited phytoplankton biomass accumulation until it diminished later in fall. The late summer/fall bloom in the Estuary might also have played a key role in the second pulse of early copepodite stage for *Pseudocalanus* spp. observed at Rimouski station.

Life cycle strategies vary among large copepod species, and so do the environmental drivers influencing their phenology. For instance, while the phenology of *C. hyperboreus* is correlated with the timing of sea-ice retreat, temperature strongly influences *C. finmarchicus* (Lehoux et al. 2022). Moreover, the timing of reproduction relative to the freshet—considering its influence on water-mass circulation and transport in regions that are under the influence of freshwater—could explain dissimilarities in the distribution patterns of these species (Runge et al. 1999). However, anomalies in 2021 were largely coherent among regions under the influence of freshwater (northwestern Gulf and Magdalen Shallows). Yet, deep water mass transport from northwest Gulf could explain the early occurrence of CI–CIII copepodites in April 2021 at Rimouski station. The northeastern Gulf and the central Gulf/Cabot Strait regions are less

influenced by freshwater: their anomaly patterns in the small copepods/non-copepods community largely contrasted with that from freshwater-influenced regions in 2021. Environmental conditions modifying the zooplankton community in these regions might instead include CIL conditions or the mixing ratio of source waters that enters the deep Laurentian Chanel through Cabot Strait. Differences in these environmental drivers might explain why these two regions often show distinct anomaly patterns for the zooplankton assemblage compared to what is observed elsewhere.

PERSPECTIVES

Questions that may arise from these indications of changes in nutrient inventories, phytoplankton biomass, and zooplankton community composition and size structure are related to the underlying explanatory drivers and how they are expected to change in the near future. While the roles of predation and of changing predator stocks in the observed trends have yet to be determined, it is possible to get some insight regarding the effect of environmental variables using a simple correlation matrix (Figure 42). Among other things, this matrix shows that a cold CIL—which would imply higher winter convection and a later onset of stratification—promotes a late bloom start and high nitrate inventories. Interestingly, high nitrate inventories in the surface layer are well correlated with higher zooplankton biomass. The latter is strongly positively correlated to a community dominated by large copepods and inversely correlated with small calanoids and non-copepods as would be expected. While nutrients likely have little direct effect on the zooplankton community composition, thermal properties of the CIL and spring bloom—especially its timing—could be major drivers of zooplankton assemblage. Indeed, it seems that a cold CIL favours high zooplankton biomass (dry weight; negative correlation) while it reduces the abundance of non-copepods (positive correlation). Phytoplankton community composition and changes in species successions may also be important drivers for the zooplankton assemblage, but they were not included in this correlation matrix since information is only available at the high-frequency monitoring stations. These environmental drivers may also trigger changes in the developmental timing of zooplankton taxa (not illustrated on the figure), such as the earlier development of *C. finmarchicus* at Rimouski station in recent years. Overall, these preliminary analyses highlight the importance of bottom-up controls in shaping zooplankton communities, although the relative importance of these processes is not yet well understood.

SUMMARY

This document reports on the chemical and biological (plankton) conditions in the Gulf of St. Lawrence in 2021 in the context of a strong warming event initiated in 2010.

- Concentrations of dissolved oxygen at 300 m reached record-low levels in the northwestern Gulf, central Gulf, and Cabot Strait. In the Estuary and at Rimouski station, deep dissolved oxygen concentrations were the second lowest of the time series, slightly above the 2020 record-low levels.
- Nitrate inventories were generally near or below normal in the surface layer of the Gulf, and near or above normal in the mid and deep layers. Positive deep nitrate anomalies have been frequently observed since 2012 in Cabot Strait and the central Gulf, and these are associated with intrusions of warm and saline water entering the Gulf through Cabot Strait.
- The recent rise in nitrate content of the bottom layer is mostly associated with near-normal or negative anomalies of the N:P ratio and near-normal or positive anomalies of the Si:N ratio.
- Annual averages of the in situ chl *a* inventory over the Gulf were normal except in the Estuary and northwest Gulf, where they were above normal and at record-high levels. Strong blooms occurred during fall in the Estuary and northwest Gulf.
- Ocean colour data showed negative annual surface chl *a* anomalies in most ocean-colour boxes over the last four years including 2021, during which record-low levels were set in all boxes but Cabot Strait.
- Spring bloom metrics indicated normal onset but the magnitude (intensity) was below normal in the northwest Gulf and Magdalen Shallows, and near-normal in the other ocean colour boxes.
- The phytoplankton community was similar to the climatology community at Rimouski station, but dinoflagellate abundances have declined since 2014. At Shediac Valley, there is instead a decline in the abundance of diatoms since 2010 reaching record-low abundance in 2021.
- Zooplankton biomass was the lowest recorded in the Estuary/northwest Gulf region, and second lowest in the northeast Gulf and central Gulf/Cabot Strait regions. This coincided with very low abundances of *C. hyperboreus* everywhere in the Gulf, but especially in the northeast Gulf where record-low abundance was observed.
- The community size-structure shift towards a higher proportion of small copepods continued in 2021 with several positive anomalies for *Pseudocalanus* spp., small calanoids, and non-copepods in the regions under the influence of freshwater (i.e., Estuary/northwest Gulf, Magdalen Shallows, and the Shediac Valley high-frequency station).
- Warm-water copepod abundances were above normal across the Gulf in 2021 following the trend observed since 2010. Their abundances were at their highest levels of the time series in the Estuary/northwest Gulf, northeast Gulf, and Magdalen Shallows.

ACKNOWLEDGEMENTS

We thank Jean-Yves Couture, Marie-France Beaulieu, Caroline Lebel, Isabelle St-Pierre, and Caroline Lafleur for preparation and standardization of the phytoplankton and zooplankton data. The data used in this report would not be available without the work of François Villeneuve and his AZMP team (Félix St-Pierre, Caroline Lafleur, Anthony Ouellet, Nicolas Coulombe, Michel Rousseau, David Leblanc, and Marie-Noëlle Bourassa) in organizing and carrying out AZMP surveys, analyzing samples, and ensuring quality control of the data. We thank Jeff Spry and Kevin Pauley for providing data from Shediac Valley station. We also thank Emmanuel Devred and Stephanie Clay for their large contribution and support in providing ocean colour data. We are grateful to Benoit Casault and David Bélanger for their critical reviews.

REFERENCES CITED

Blais, M., Galbraith, P.S., Plourde, S., Devine, L. and Lehoux, C. 2021a. Chemical and Biological Oceanographic Conditions in the Estuary and Gulf of St. Lawrence during 2019. DFO Can. Sci. Advis. Sec. Res. Doc. 2021/002. iv + 66 p.

Blais, M., Galbraith, P.S., Plourde, S., Devred, E., Clay, S., Lehoux, C. and Devine, L. 2021b. Chemical and Biological Oceanographic Conditions in the Estuary and Gulf of St. Lawrence during 2020. DFO Can. Sci. Advis. Sec. Res. Doc. 2021/060. iv + 67 p.

Brickman, D. and Petrie, B. 2003. Nitrate, silicate and phosphate atlas for the Gulf of St. Lawrence. Can. Tech. Rep. Hydrogr. Ocean Sci. 231. xi + 152 p.

Brzezinski, M.A. 1985. The Si:C:N ratio of marine diatoms: interspecific variability and the effect of some environmental variables. J. Phycol. 21:347–357.

Casault, B., Johnson, C., Devred, E., Head, E., Beazley, L. and Spry, J. 2022. Optical, Chemical, and Biological Oceanographic Conditions on the Scotian Shelf and in the eastern Gulf of Maine during 2020. DFO Can. Sci. Advis. Sec. Res. Doc. 2022/018. v + 82 p.

Clay, S. and Layton, C. 2020. BIO-RSG/PhytoFit: First release (Version 1.0.0).

Conover, R.J. and Huntley, M. 1991. Copepods in ice-covered seas – Distribution, adaptations to seasonally limited food, metabolism, growth patterns and life cycle strategies in polar seas. J. Mar. Syst. 2:1–41.

Daewel, U., Hjøllo, S.S., Huret, M., Ji, R., Maar, M., Niiranen, S., Travers-Trolet, M., Peck, M.A. and van de Wolfshaar, K.E. 2014. Predation control of zooplankton dynamics: a review of observations and models. ICES J. Mar. Sci. 71(2):254–271.

DFO. 2022. Oceanographic conditions in the Atlantic zone in 2021. DFO Can. Sci. Advis. Sec. Sci. Advis. Rep. 2022/025. 32 p.

Galbraith, P.S. 2006. Winter water masses in the Gulf of St. Lawrence. J. Geophys. Res. 111:C06022. doi:10.1029/2005JC003159

Galbraith, P.S., Desmarais, R., Pigeon, R. and Cantin, S. 2006. Ten years of monitoring winter water masses in the Gulf of St. Lawrence by helicopter. AZMP Bulletin PMZA. 5:32–35.

Galbraith, P.S., Chassé, J., Shaw, J.-L., Dumas, J., Caverhill, C., Lefaivre, D. and Lafleur, C. 2020. Physical Oceanographic Conditions in the Gulf of St. Lawrence during 2019. DFO Can. Sci. Advis. Sec. Res. Doc. 2020/030. iv + 84 p.

Galbraith, P.S., Chassé, J., Shaw, J.-L., Dumas, J., Caverhill, C., Lefaivre, D. and Lafleur, C. 2021. Physical Oceanographic Conditions in the Gulf of St. Lawrence during 2020. DFO Can. Sci. Advis. Sec. Res. Doc. 2021/045. iv + 81 p.

Galbraith, P.S., Chassé, J., Shaw, J.-L., Dumas, J., Caverhill, C., Lefaivre, D. and Lafleur, C. 2022. Physical oceanographic conditions in the Gulf of St. Lawrence during 2021. DFO Can. Sci. Advis. Sec. Res. Doc. 2022/034. iv + 81 p.

Gilbert, D. 2004. Propagation of temperature signals from the northwest Atlantic continental shelf edge into the Laurentian Channel. ICES CM. 2004/N:07. 12 p.

Gilbert, D., Sundby, B., Gobeil, C., Mucci, A. and Tremblay, G.-H. 2005. A seventy-two-year record of diminishing deep-water oxygen in the St. Lawrence estuary: The Northwest Atlantic connection. Limnol. Oceanogr. 50(5):1654–1666.

Grégoire, F., Girard, L. and Boudreau, M. 2014. Résultats des relevés du programme de monitorage zonal atlantique (PMZA)-maquereau bleu (*Scomber scombrus* L.) réalisés dans le sud du golfe du Saint-Laurent en 2012 et 2013. Secr. can. de consult. sci. du MPO. Doc. de rech. 2014/075. v + 82 p.

Grosjean, P., Denis K. and Wacquet G. 2018. ZooImage: Analysis of numerical plankton images. R package version 5.5.2.

Hall, D.J., Threlkeld, S.T., Burns, C.W. and Crowley, P.H. 1976. The size-efficiency hypothesis and the size structure of zooplankton communities. Annu. Rev. Ecol. Evol. Syst. 7:177–208.

Laliberté, J., Larouche, P., Devred, E. and Craig, S. 2018. Chlorophyll-a concentration retrieval in the optically complex waters of the St. Lawrence Estuary and Gulf using principal component analysis. Remote Sens. 10(2):265. doi:10.3390/rs10020265

Lavoie, D., Lambert, N., Starr, M., Chassé, J., Riche, O., Le Clainche, Y., Azetsu-Scott, K., Béjaoui, B., Christian, J.R. and Gilbert, D. 2021 The Gulf of St. Lawrence biogeochemical model: A modelling tool for Fisheries and Ocean management. Front. Mar. Sci. 8:732269. doi:10.3389/fmars.2021.732269

Lauzier, L.M. and Trites, R.W. 1958. The deep waters of the Laurentian Channel. J. Fish. Res. Board Can. 15:1247–1257.

Lehoux, C., Plourde S. and Lesage, V. 2020. Significance of dominant zooplankton species to the North Atlantic Right Whale potential foraging habitats in the Gulf of St. Lawrence: a bio-energetic approach. DFO Can. Sci. Advis. Sec. Res. Doc. 2020/033. iv + 44 p.

Lehoux, C., Plourde, S., Chamberland, J.-M. and Benoît, H. 2022. Linking interannual variations of capelin abundance indices in the Gulf of St. Lawrence to environmental proxies of bottom-up regulation of cohort strength. DFO Can. Sci. Advis. Sec. Res. Doc. 2021/068. iv + 51 p.

Levasseur, M., Therriault, J.-C. and Legendre, L. 1984. Hierarchical control of phytoplankton succession by physical factors. Mar. Ecol. Prog. Ser. 19:211–222.

Maillet, G., Bélanger, D., Doyle, G., Robar, A., Rastin, S., Ramsay, D. and Pepin, P. 2022. Optical, Chemical, and Biological Oceanographic Conditions on the Newfoundland and Labrador Shelf during 2018. DFO Can. Sci. Advis. Sec. Res. Doc. 2022/075. viii + 53 p.

McLellan, H.J. 1957. On the distinctness and origin of the slope water off the Scotian Shelf and its easterly flow south of the Grand Banks. J. Fish. Res. Board Can. 14:213–239.

Mitchell, M.R., Harrison, G., Pauley, K., Gagné, A., Maillet, G. and Strain, P. 2002. Atlantic Zonal Monitoring Program sampling protocol. Can. Tech. Rep. Hydrogr. Ocean Sci. 223: iv + 23 p.

Ouellet, P. 1987. Distribution automnale des stades larvaires de capelan (*Mallotus villosus*) et de hareng (*Clupea harengus*) dans le nord du golfe Saint-Laurent en Octobre 1985. Rapp. tech. Can. sci. halieut. aquat. 1583. 27 p.

Parent, G.J., Plourde, S. and Turgeon, J. 2011. Overlapping size ranges of *Calanus* spp. off the Canadian Arctic and Atlantic coasts: impact on species' abundances. J. Plankton Res. 33:1654–1665.

Plante, S., Chabot, D. and Dutil, J.-D. 1998. Hypoxia tolerance in Atlantic Cod. J. Fish Biol. 53:1342–1356.

Plourde, S., Dodson, J.J., Runge, J.A. and Therriault, J.-C. 2002. Spatial and temporal variations in copepod community structure in the lower St. Lawrence Estuary, Canada. Mar. Ecol. Prog. Ser. 230:221–224.

Plourde, S., Joly, P., Runge, J.A., Dodson, J. and Zakardjian, B. 2003. Life cycle of *Calanus hyperboreus* in the lower St. Lawrence Estuary and its relationship to local environmental conditions. Mar. Ecol. Prog. Ser. 255:219–233.

Plourde, S., Maps, F. and Joly, P. 2009. Mortality and survival in early stages control recruitment in *Calanus finmarchicus*. J. Plankton Res. 31(4):371–388.

Plourde, S., Lehoux, C., Johnson, C.L., Perrin, G. and Lesage, V. 2019. North Atlantic right whale (*Eubalaena glacialis*) and its food: (I) a spatial climatology of *Calanus* biomass and potential foraging habitats in Canadian waters. J. Plankton Res. 41(5):667–685.

Redfield, A.C. 1958. The biological control of chemical factors in the environment. Am. Sci. 46:205–221.

Runge, J.A., Castonguay, M., de Lafontaine, Y., Ringuette, M. and Beaulieu, J.L. 1999. Covariation of climate, zooplankton biomass and mackerel recruitment in the southern Gulf of St. Lawrence. Fish. Oceanogr. 8(2):139–149.

Sommer, U. and Lengfellner, K. 2008. Climate change and the timing, magnitude, and composition of the phytoplankton spring bloom. Glob. Chan. Biol. 14:1199–1208.

Therriault, J.-C., Petrie, B., Pépin, P., Gagnon, J., Gregory, D., Helbig, J., Herman, A., Lefaivre, D., Mitchell, M., Pelchat, B., Runge, J. and Sameoto, D. 1998. Proposal for a Northwest Atlantic zonal monitoring program. Can. Tech. Rep. Hydrogr. Ocean Sci. 194: vii + 57 p.

Xiong, X., Angal, A., Chang, T., Chiang, K., Lei, N., Li, Y., Sun, J., Twedt, K. and Wu, A. 2020. MODIS and VIIRS calibration and characterization in support of producing long-term high-quality data products. Remote Sens. 12:3167. doi:10.3390/rs12193167

Zhai, L., Platt, T., Tang, C., Sathyendranath, S. and Hernández Walls, R. 2011. Phytoplankton phenology on the Scotian Shelf. ICES J. Mar. Sci. 68:781–791. doi:10.1093/icesjms/fsq175

TABLES

Table 1. List of oceanographic surveys with locations, dates, and sampling activities for 2021 in each Gulf region. See Figure 1 for section and station locations. While numbers of CTD/bottle are indicated for each subregion, numbers of nets are only indicated for main regions (see region versus subregion in Figure 1).

High Frequency monitoring

Dates (2021)	Vessel	Station	CTD/bottle	Net
Mar. 3–Dec.16	*Beluga II* (+ others)	Rimouski	29	25
Mar. 6–Oct. 14	Multiple	Shediac Valley	9	4

Surveys

Survey	Dates (2021)	Vessel	Region/subregion	CTD/bottle	Net
Winter	Mar. 3–10	GC-945 Helicopter	Estuary	5	0
			Northwest Gulf	12	
			Northeast Gulf	21	0
			Central Gulf	8	0
			Cabot Strait	7	
			Magdalen Shallows	24	0
			Total	**77**	**0**
Early summer	Jun. 2–28	*Teleost*	Estuary	12	17
			Northwest Gulf	13	
			Northeast Gulf	13	4
			Central Gulf	9	9
			Cabot Strait	4	
			Magdalen Shallows	37	12
			Total	**88**	**42**
Late summer	Jul. 27–Sept. 29	*Teleost*	Estuary	13	24
			Northwest Gulf	8	
			Northeast Gulf	10	21
			Central Gulf	17	9
			Cabot Strait	7	
			Magdalen Shallows	103	1
			Total	**158**	**55**
Fall	Oct. 11–26	*Hudson*	Estuary	15	18
			Northwest Gulf	14	
			Northeast Gulf	14	7
			Central Gulf	10	9
			Cabot Strait	5	
			Magdalen Shallows	18	12
			Total	**76**	**46**

FIGURES

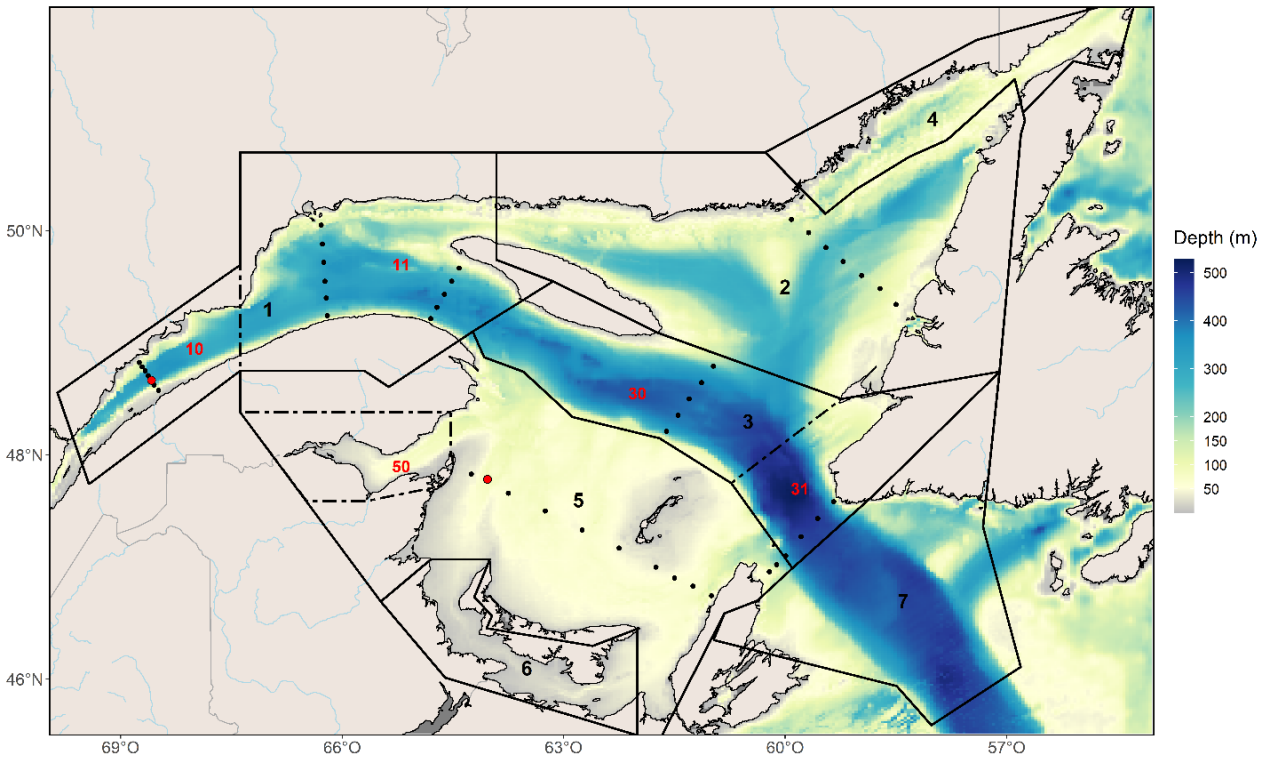

Figure 1. Bathymetric map of the Estuary and Gulf of St. Lawrence showing regular core AZMP sampling stations on the different sections (dots) and high-frequency Rimouski and Shediac Valley stations (red circles). Region 1: Estuary (subregion 10) and northwest Gulf (subregion 11); Region 2: northeast Gulf; Region 3: central Gulf (subregion 30) and Cabot Strait (subregion 31); Region 4: Mecatina; Region 5: Magdalen Shallows; Region 6: Northumberland; Region 7: Laurentian Hermitage. Region numbers are in black and subregion numbers in red.

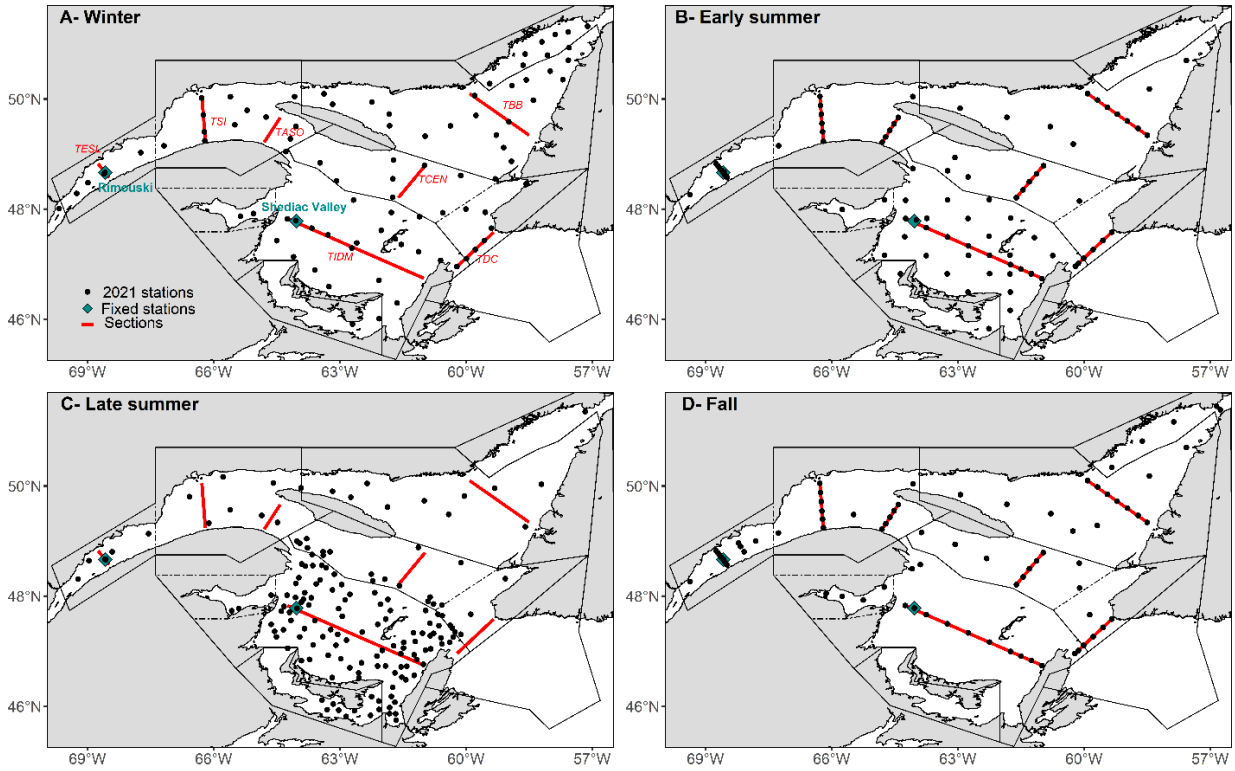

Figure 2. Locations of stations sampled (complete CTD/bottle profile) during winter (A), early summer (B), late summer (C),and fall (D) 2021 (see Figure 1 caption for region and subregion descriptions).

Figure 3. Sampling frequencies at Rimouski and Shediac Valley stations through 2021. Sampling included CTD/bottle as well as plankton net tows most of the time (weather permitting). In September 2021, there were four occupations of the Shediac Valley station within a two-days period.

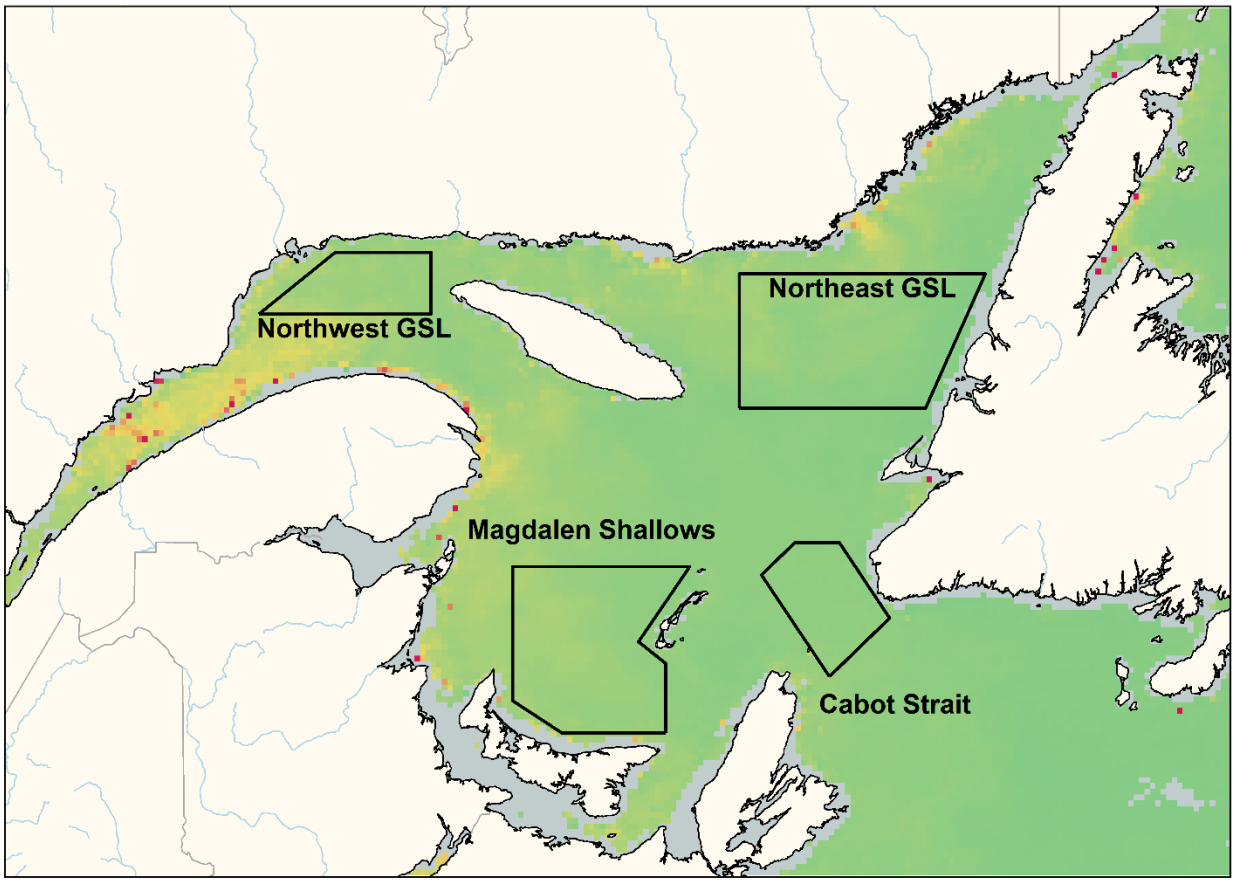

Figure 4. Statistical polygons in the Gulf identified for the spatial/temporal analysis of satellite ocean colour data. The figure is a MODIS composite image showing chlorophyll a from 1–15 June 2021. Grey areas indicate no data (near-shore regions in this case).

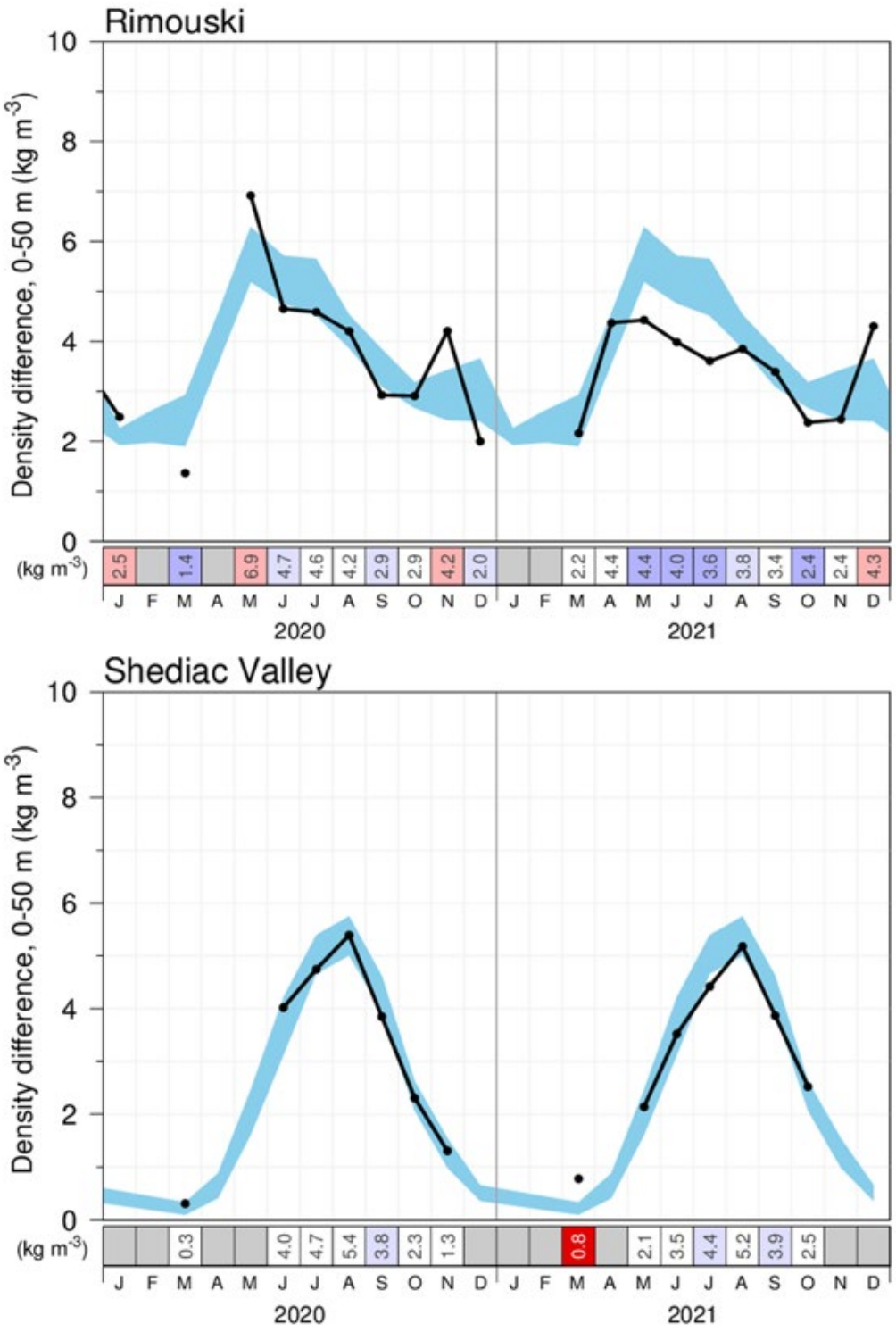

Figure 5. Seasonal stratification index (calculated as the density difference between 50 m and the surface; solid black lines) during 2020 and 2021 at Rimouski station (upper panel) and at Shediac Valley station (lower panel). The blue area represents the climatological monthly mean ± 0.5 SD (1999–2020). Numbers in the scorecard are monthly density differences in kg m^{-3}. The positive anomalies are shown in red and correspond to stratification stronger than normal; negative anomalies are shown in blue and correspond to stratification weaker than normal. White represents near-normal stratification conditions.

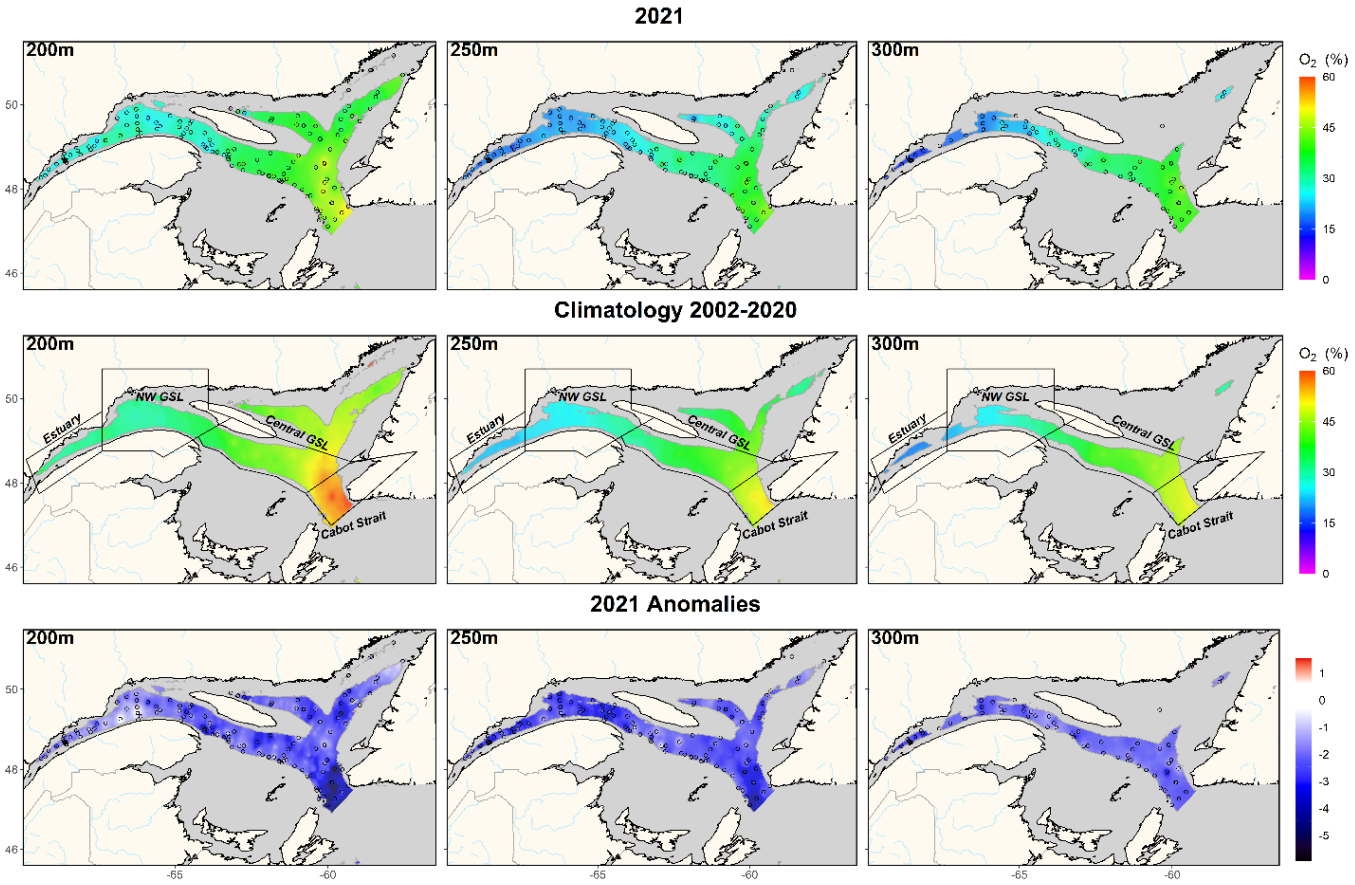

Figure 6. Annual average distribution of dissolved oxygen saturation at depths of 200 m, 250 m, and 300 m in the Estuary and Gulf of St. Lawrence during 2021 (upper panel). The climatology (2002–2020; middle panel) and anomalies (lower panel) are also shown. Blue colours indicate below-normal levels (negative anomaly), reds are above-normal levels (positive anomaly), and white represents normal levels. Open circles represent station locations in 2021.

Dissolved oxygen concentrations (µM) at 300m

	2002	2003	2004	2005	2006	2007	2008	2009	2010	2011	2012	2013	2014	2015	2016	2017	2018	2019	2020	2021	Mean	SD
Rimouski	62.7	57	62.1	61.7	68.3	64.5	62.4	64.7	59.3	66.2	63.8	64.5	58.3	56.4	54.6	53.3	55.7	50.5	44.2	46.2	59.5	6
Estuary	64.4	57.9	61.5	64	66.8	65.1	62.8	65.9	60.2	67.1	64.7	66.7	61.7	58.2	56.6	56.1	57.1	51.5	45.9	46.8	60.8	5.7
Northwest Gulf	90.2	78.4	87	88.7	90.9	91.7	80.2	84.7	90.3	105.1	93.6	89.9	80.8	90.9	71.5	77.3	71.3	69.6	68.1	65.6	84.2	9.8
Central Gulf	134.1	112.8	127.3	131.6	137.8	129.1	124.4	136.1	132.3	139.7	136.9	134	131.2	128.9	114.8	110.1	105.2	102.8	107.3	102.3	125.1	12.1
Cabot Strait	154.6	141.9	150.6	166.9	153.3	162.6	157.7	152.4	155.5	165.4	151.5	155.4	144.3	141.5	129.4	127.1	125.2	120.4	122.8	117.6	146.2	14.8

Figure 7. Time series of deep-layer dissolved oxygen concentrations (µM) at 300 m. The numbers on the right are the 2002–2020 climatological means and standard deviations, and the numbers in the boxes are the oxygen concentrations. Cell colour represents the anomaly: blue colours indicate below-normal levels (negative anomaly), reds are above-normal levels (positive anomaly), and white represents normal levels.

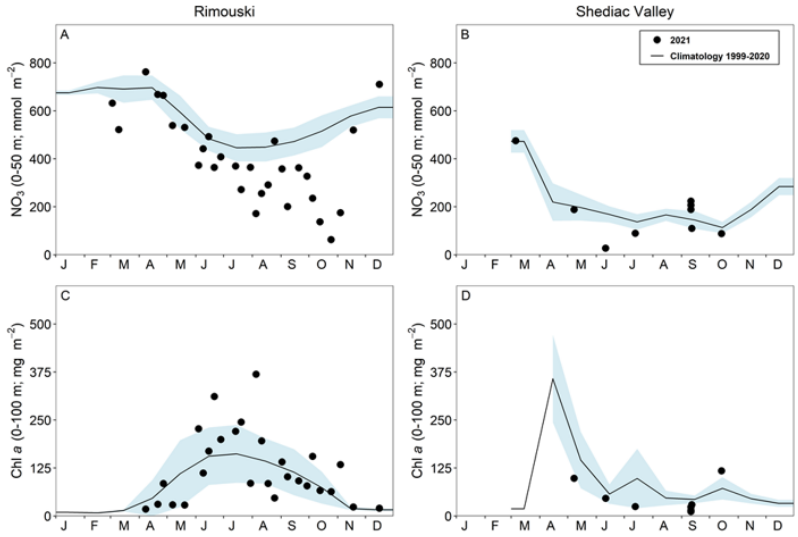

Rimouski

	1999	2000	2001	2002	2003	2004	2005	2006	2007	2008	2009	2010	2011	2012	2013	2014	2015	2016	2017	2018	2019	2020	2021	Mean	SD
Chl *a* 0-100m	2.44	-0.79	0.73	-0.12	0.75	-1.58	-1.04	-1	0.62	-2.21	-0.33	-0.07	-0.09	0.35	-0.52	1.27	0.17	0.63	-0.4	0.41	0.76	0.02	0.94	34.4	17.2
NO_3 0-50m	-0.23	1.07	0.48	1.88	-0.3	1.37	-0.25	0	-0.41	0.76	-1.62	-2.16	-0.84	-0.57	0.43	0.78	0.7	-1.28	0.25	-1.16	0.47	0.63	-2.84	571.7	73.9
NO_3 50-150m	-1.32	-0.44	0.95	1.31	-0.61	-0.15	-0.37	1.11	1.31	-0.38	0.2	-1.67	-1.22	0.22	-0.65	0.99	0.59	0.33	-0.29	-2.02	1.36	0.76	-0.66	1434.9	106.4
NO_3 150-320m	2.72	-0.68	-1.02	0.5	0.16	0.12	1.18	1.56	0.48	-1.17	0.2	-1.52	-0.55	-0.23	-0.24	0.69	0.46	-0.81	-0.89	-1.21	0.06	0.2	0.37	3851.6	134.4

Shediac Valley

	1999	2000	2001	2002	2003	2004	2005	2006	2007	2008	2009	2010	2011	2012	2013	2014	2015	2016	2017	2018	2019	2020	2021	Mean	SD
Chl *a* 0-100m	-1.03	-1.43	-0.13	2.47	0.17	-0.34	-0.67	-0.03	1.57	1.52	-0.04	-0.7	-1.18	0.36	0.54	-0.31	-0.38	-0.96	1.26	-0.55	-0.15		-1.11	50	15.9
NO_3 0-50m	0.81	1.72	-0.04	0.59	0.7	0.75	-0.88	0.68	-2.01	-0.1	1.14	-1.96	-1.12	0.05	0.19	0.54	0	-0.15	0.96	-1.33	-0.55		-0.22	172.6	42.9
NO_3 50-84m	-0.21	0.21	0.7	0.38	0.39	1.45	-2.04	0.82	-1.72	-0.16	-0.29	-0.48	-0.26	0.57	0.61	-0.84	0.95	0.44	0.74	-2.21	0.95		-1.57	230.5	43.8
	1999	2000	2001	2002	2003	2004	2005	2006	2007	2008	2009	2010	2011	2012	2013	2014	2015	2016	2017	2018	2019	2020	2021	Mean	SD

Figure 8. Nitrate inventories (0–50 m; top panels) and chlorophyll a inventory (0–100 m for Rimouski and 0–84 m for Shediac Valley; bottom panels) in 2021 (black circles) with monthly mean conditions (± 0.5 SD) for the 1999–2020 climatology (black line with blue shading) at Rimouski and Shediac Valley stations. Time series of normalized annual anomalies for nitrate inventories (mmol m^{-2}) and chlorophyll a (mg chl a m^{-2}) are also presented with the variable means and standard deviations for the 1999–2020 climatology to the right of the scorecard. Blue colours indicate below-normal levels (negative anomaly), reds are above-normal levels (positive anomaly), and white represents normal levels.

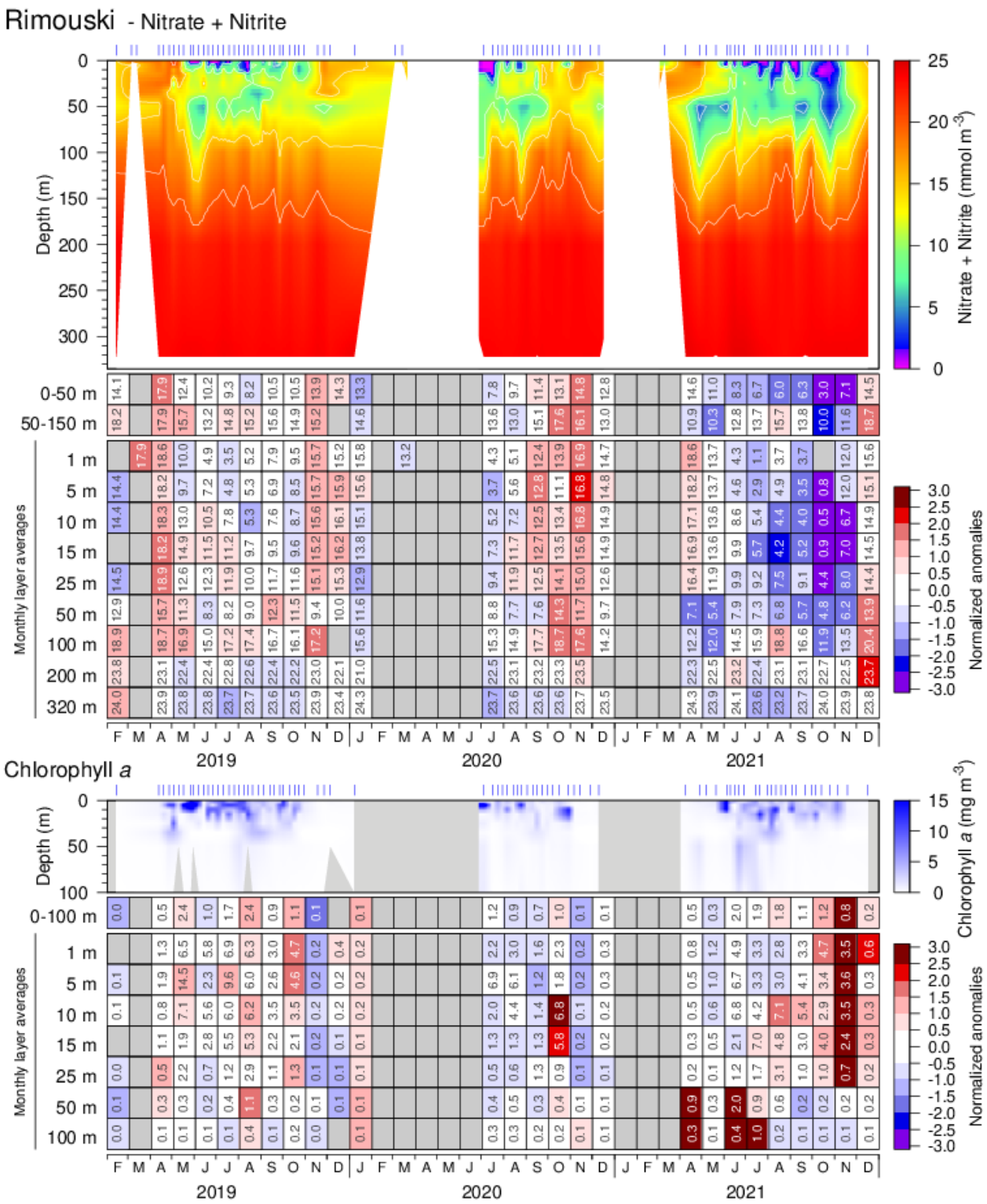

Figure 9. Nitrate (top) and chlorophyll a *(bottom) concentrations at Rimouski station during the 2019 to 2021 sampling seasons. Contour plots use data from individual sampling events while monthly means are shown in the tables below the graphics (nitrates: mmol m^{-3}; chl* a*: mg m^{-3}). Cell colours indicate normalized anomalies based on the 1999–2020 climatology: blue colours indicate below-normal levels (negative anomaly), reds are above-normal levels (positive anomaly), and white represents normal levels. During March, the integrated (0–50) monthly average and the depth-specific average for nitrate for the climatology do not include the same amount of data, and this might result in inconsistent anomalies between integrated and depth-specific values.*

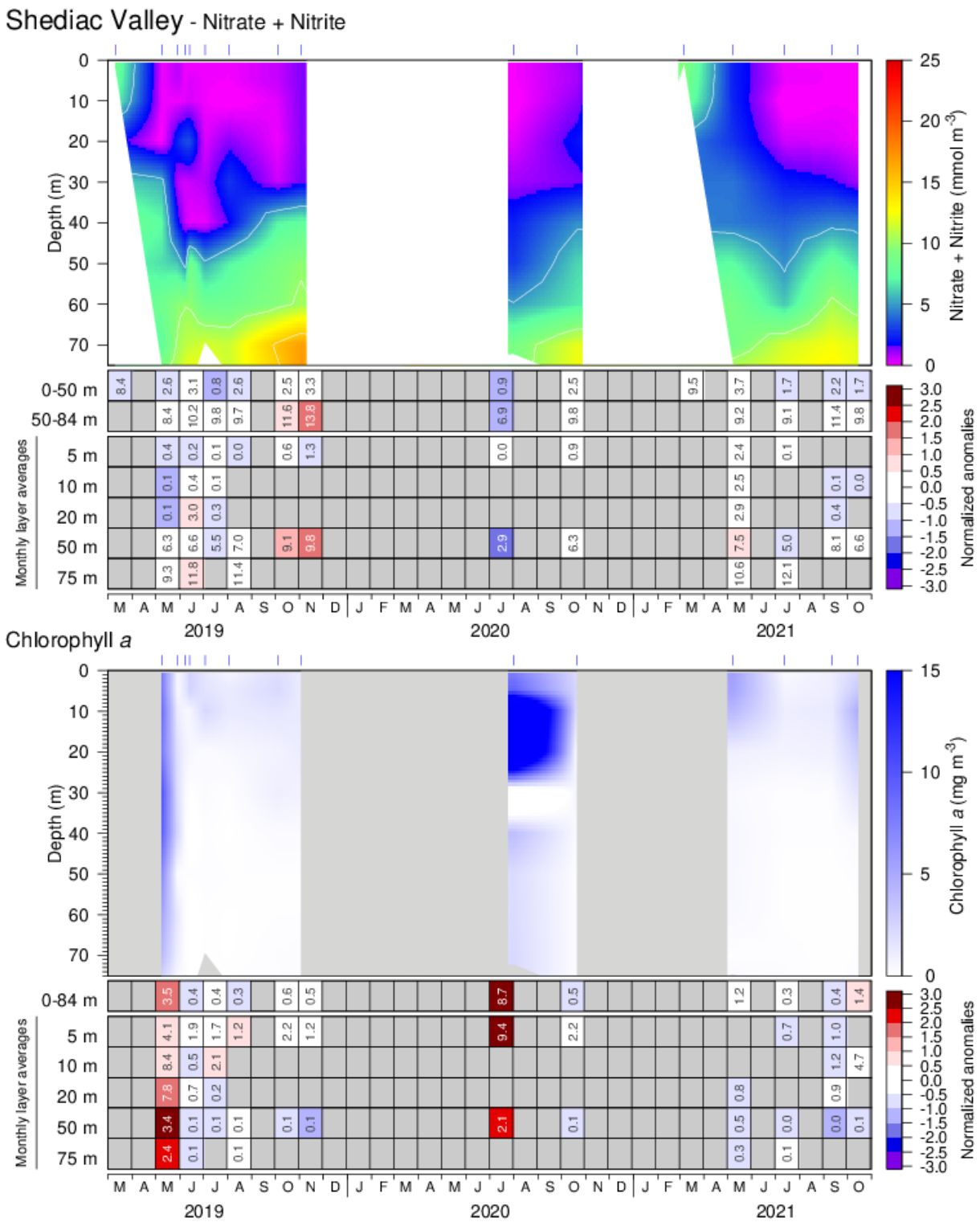

Figure 10. Nitrate (top) and chlorophyll a *(bottom) concentrations at Shediac Valley station during the 2019 to 2021 sampling seasons. Contour plots use data from individual sampling events while monthly means are shown in the tables below the graphics (nitrates: mmol m^{-3}; chl* a*: mg m^{-3}). Cell colours indicate normalized anomalies based on the 1999–2020 climatology: blue colours indicate below-normal levels (negative anomaly), reds are above-normal levels (positive anomaly), and white represents normal levels. During March, the integrated (0–50) monthly average and the depth-specific average for nitrate for the climatology do not include the same amount of data, and this might result in inconsistent anomalies between integrated and depth-specific values.*

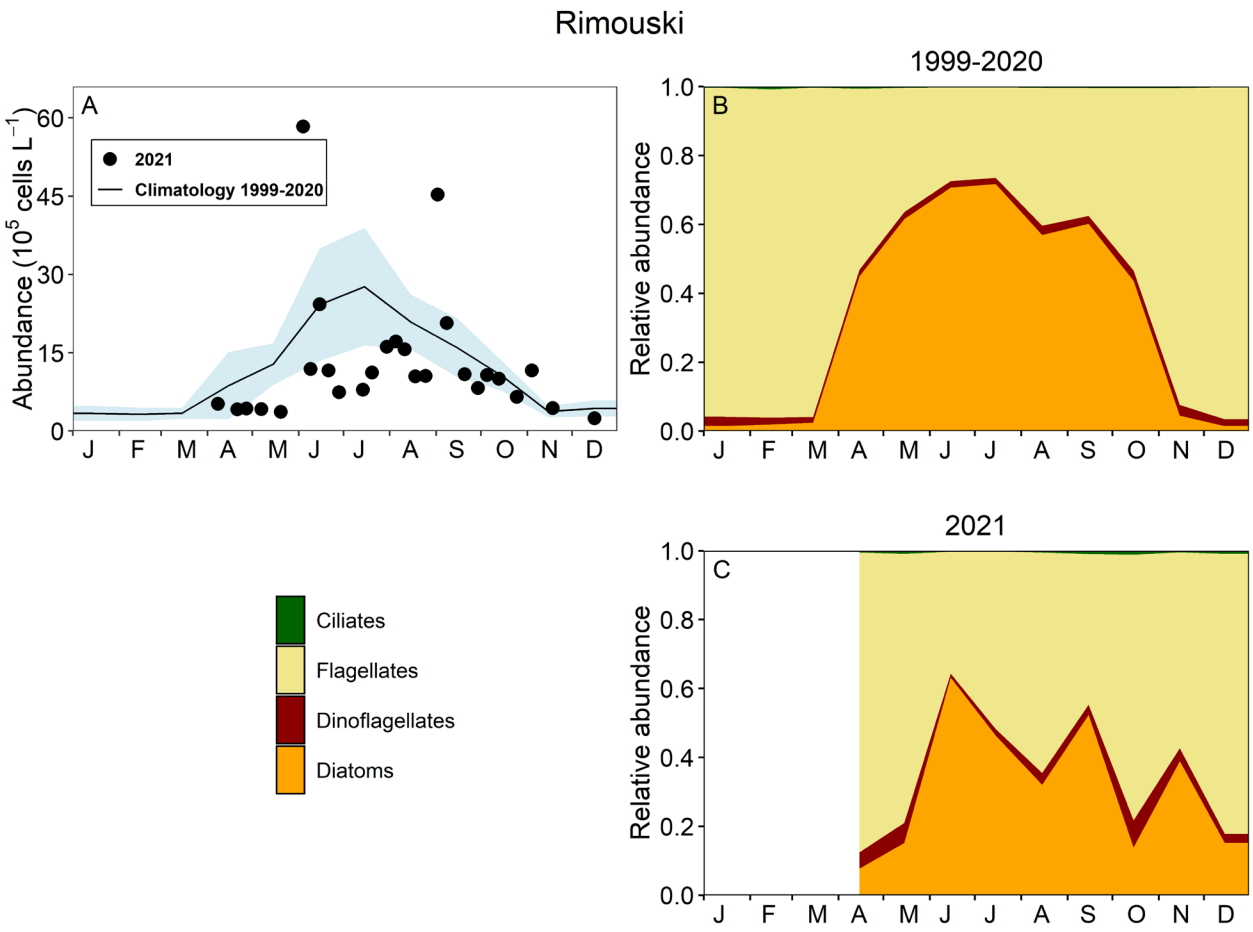

Figure 11. Phytoplankton abundance (A) and community composition at Rimouski station for the 1999–2020 climatology (B; no data in 2010) and for 2021 (C). Blue shading on panel (A) represents ± 0.5 SD of the monthly mean phytoplankton abundance for the climatology. While ciliate abundances were included in the graphics, they are not visible because they represents < 1% of phytoplankton cells each month for the climatology. This was also the case in 2021.

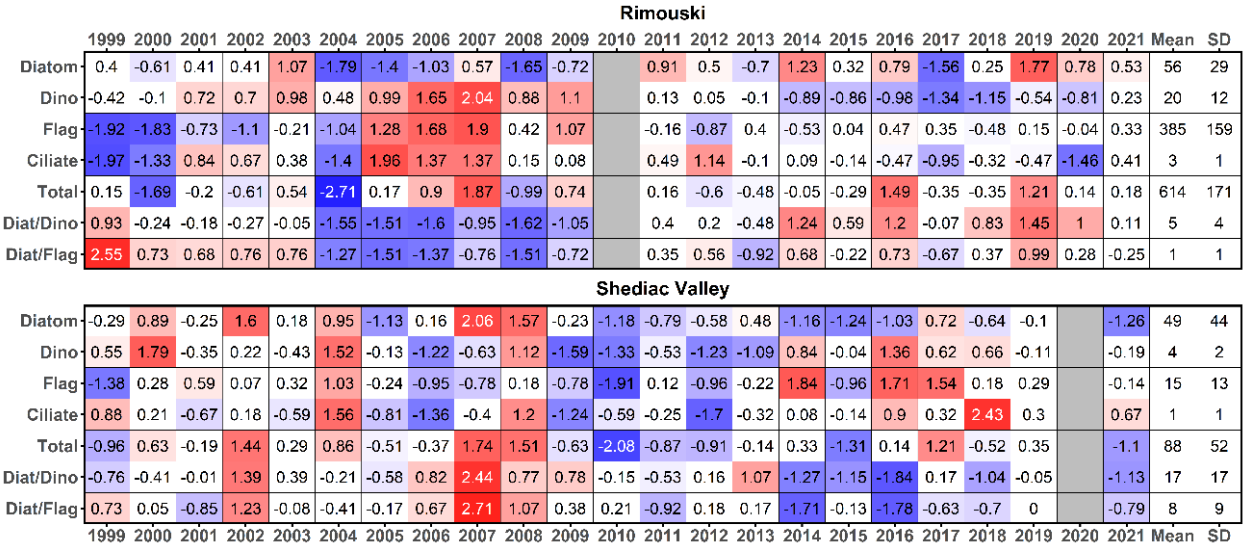

Figure 12. Time series of normalized annual (April–December) anomalies for abundance (10^3 cells L^{-1}) of the main phytoplankton taxonomic groups (diatoms, dinoflagellates, flagellates, ciliates) and total phytoplankton abundance, and for the diatom/dinoflagellate and diatom/flagellate ratios at Rimouski and Shediac Valley stations (calculated using GLM). Variable means and standard deviations for the 1999–2020 climatology are shown to the right of the scorecard. Blue colours indicate below-normal levels (negative anomaly), reds are above-normal levels (positive anomaly), and white represents normal levels. No data are available for 2010 at Rimouski station, and there were not enough samples collected at Shediac Valley in 2020 to calculate an anomaly.

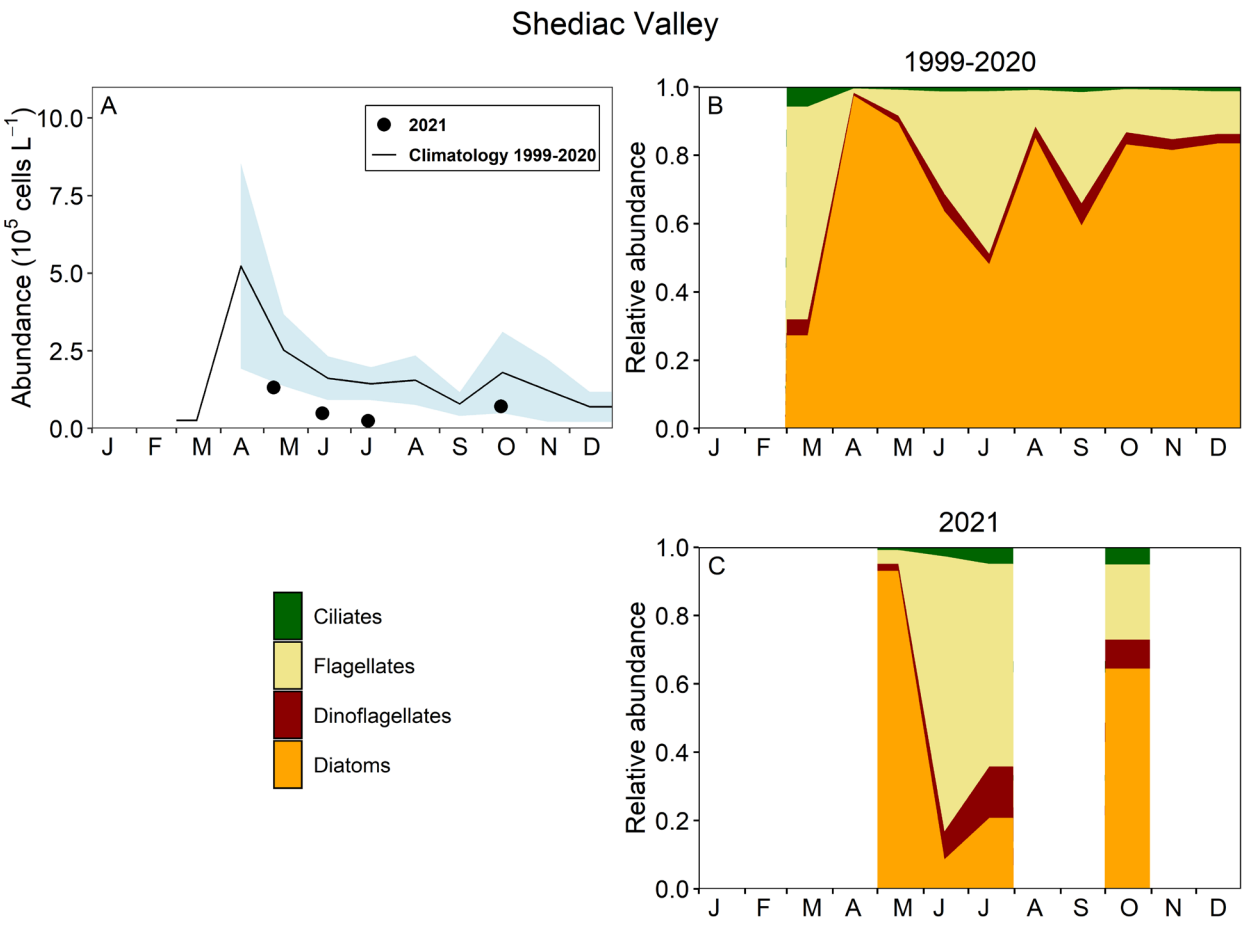

Figure 13. Phytoplankton abundance (A) and community composition at Shediac Valley station for the 1999–2020 climatology (B) and for 2021 (C). Blue shading on panel (A) represents ± 0.5 SD of the monthly mean phytoplankton abundance for the climatology.

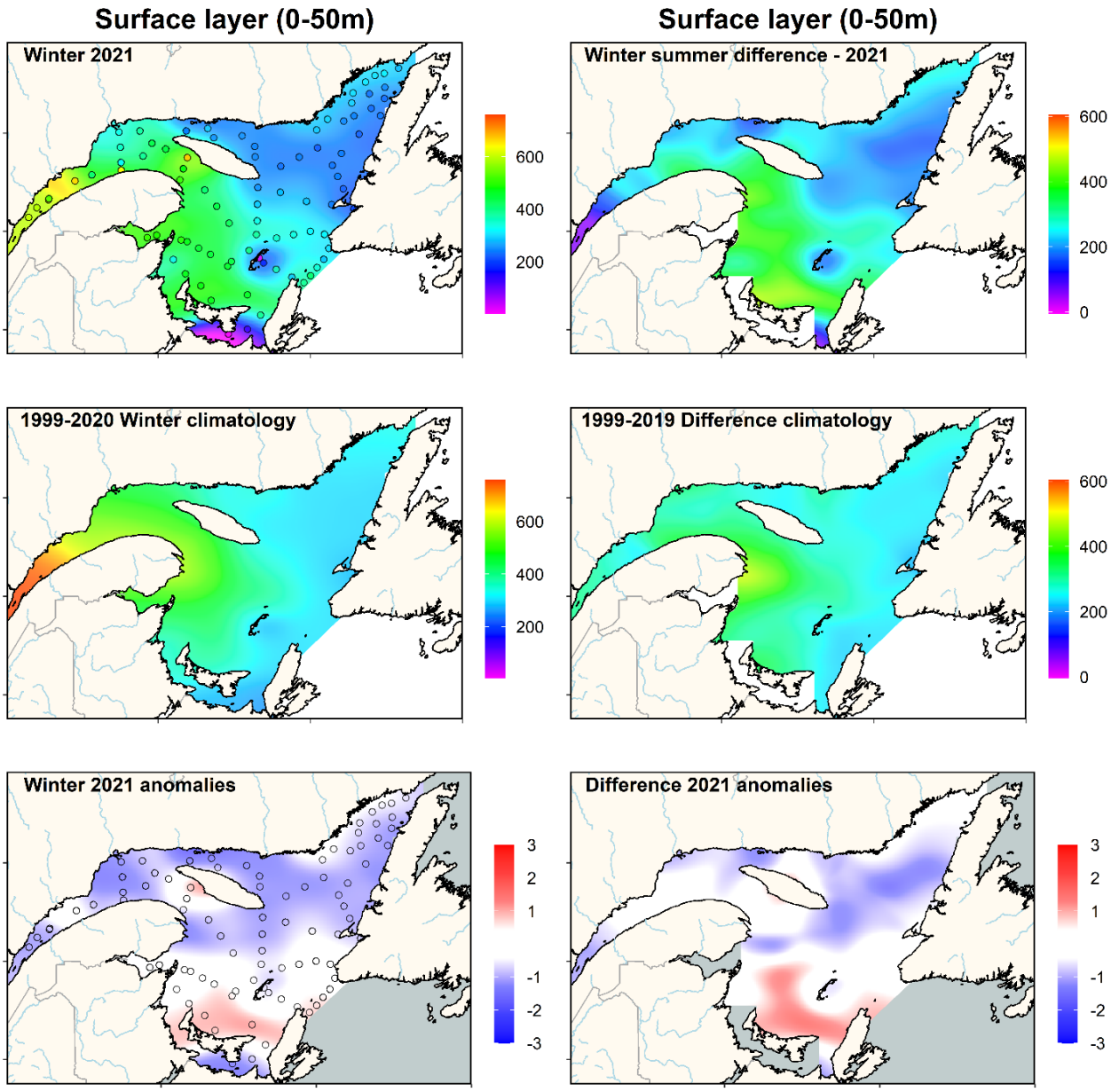

Figure 14. Total nitrate (NO_3^- + NO_2^-) inventories (mmol m^{-2}) in the surface layer (0–50 m) of the Estuary and Gulf of St. Lawrence during early March 2021 (upper left panel). Difference in total nitrate inventories (mmol m^{-2}) in the surface layer of the Estuary and Gulf of St. Lawrence between winter and early summer (upper right panel). The climatology (1999–2020 for winter, 1999–2019 for difference; middle panels) and anomalies (lower panels) are shown. Blue colours indicate below-normal levels (negative anomaly), reds are above-normal levels (positive anomaly), and white represents normal levels.

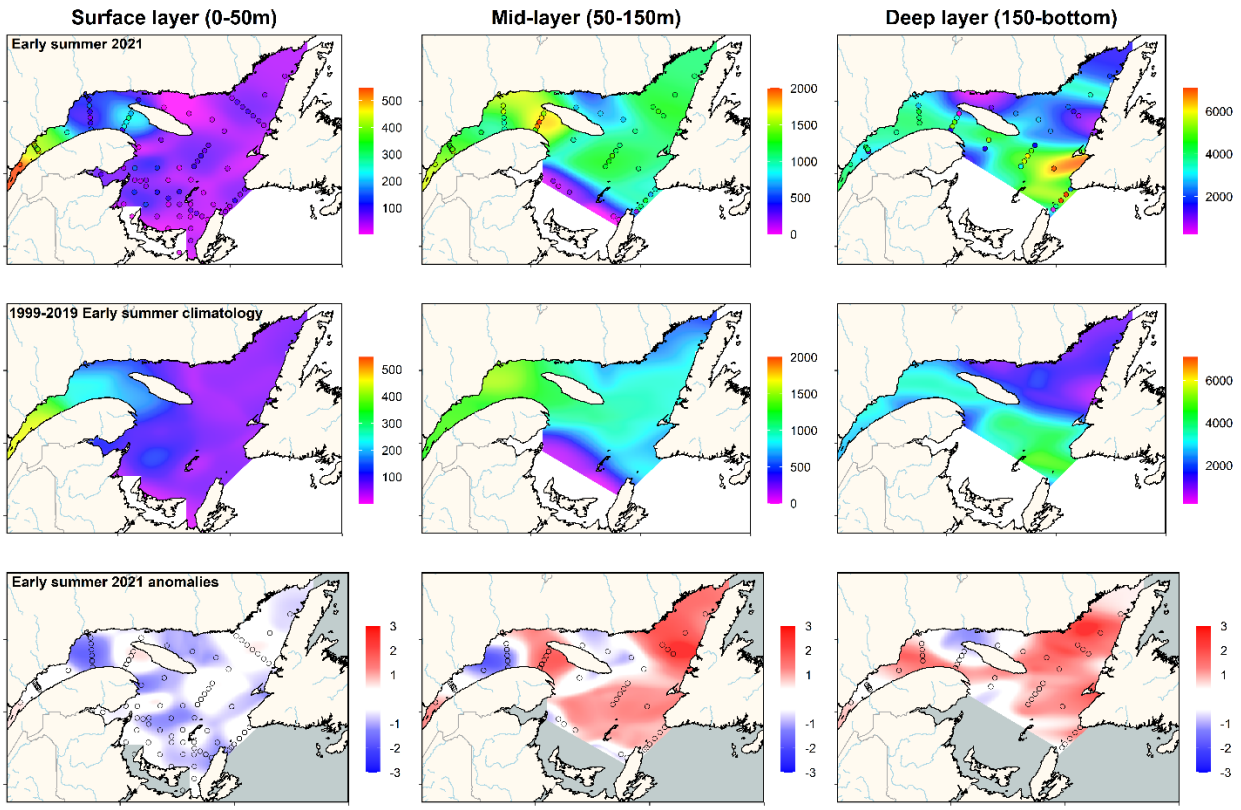

Figure 15. Total nitrate (NO_3^- + NO_2^-) inventories (mmol m^{-2}) in the surface (left panels), mid (middle panels), and deep (right panels) layers of the Estuary and Gulf of St. Lawrence during early summer 2021 (upper panels). The climatology (1999–2019; middle panels) and anomalies (lower panels) are shown for each layer. Blue colours indicate below-normal levels (negative anomaly), reds are above-normal levels (positive anomaly), and white represents normal levels.

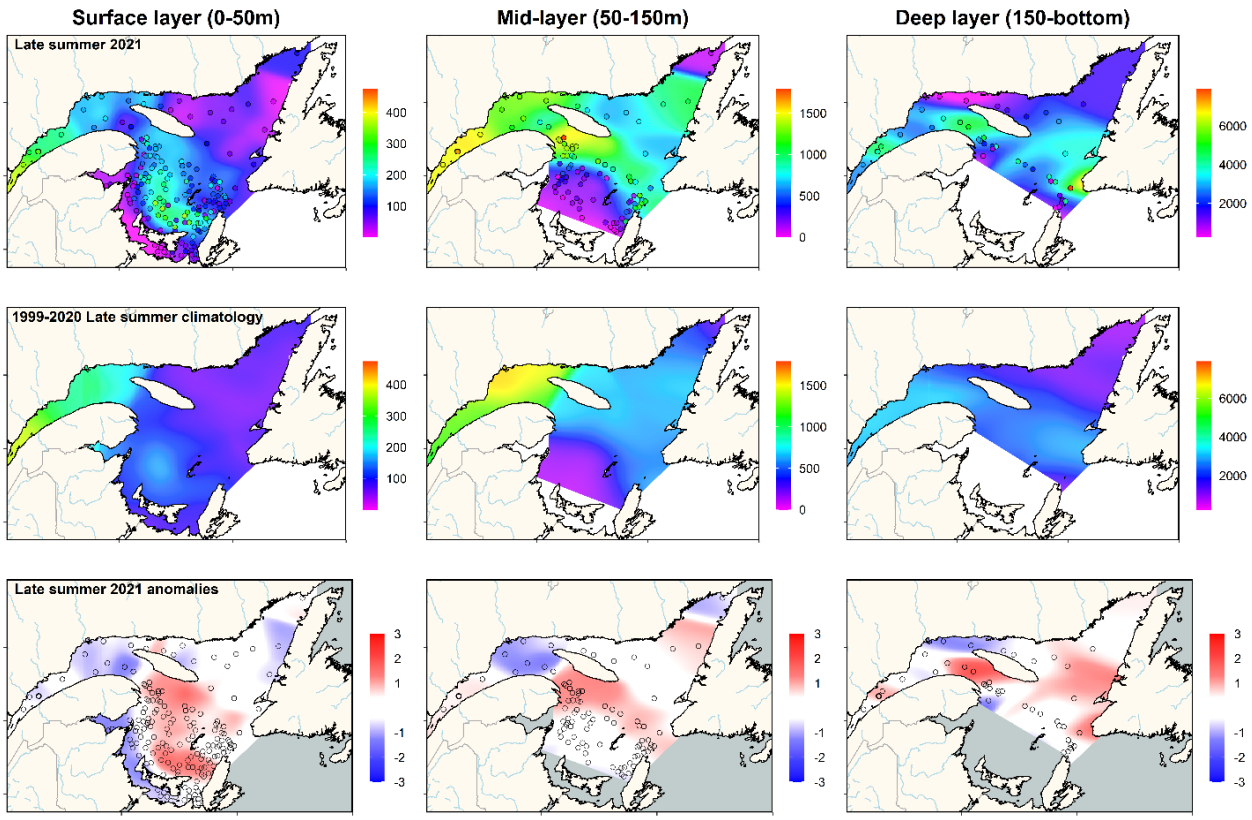

Figure 16. Total nitrate (NO_3^- + NO_2^-) inventories (mmol m^{-2}) in the surface (left panels), mid (middle panels), and deep (right panels) layers of the Estuary and Gulf of St. Lawrence during late summer 2021 (upper panels). The climatology (1999–2020; middle panels) and anomalies (lower panels) are shown for each layer. Blue colours indicate below-normal levels (negative anomaly), reds are above-normal levels (positive anomaly), and white represents normal levels.

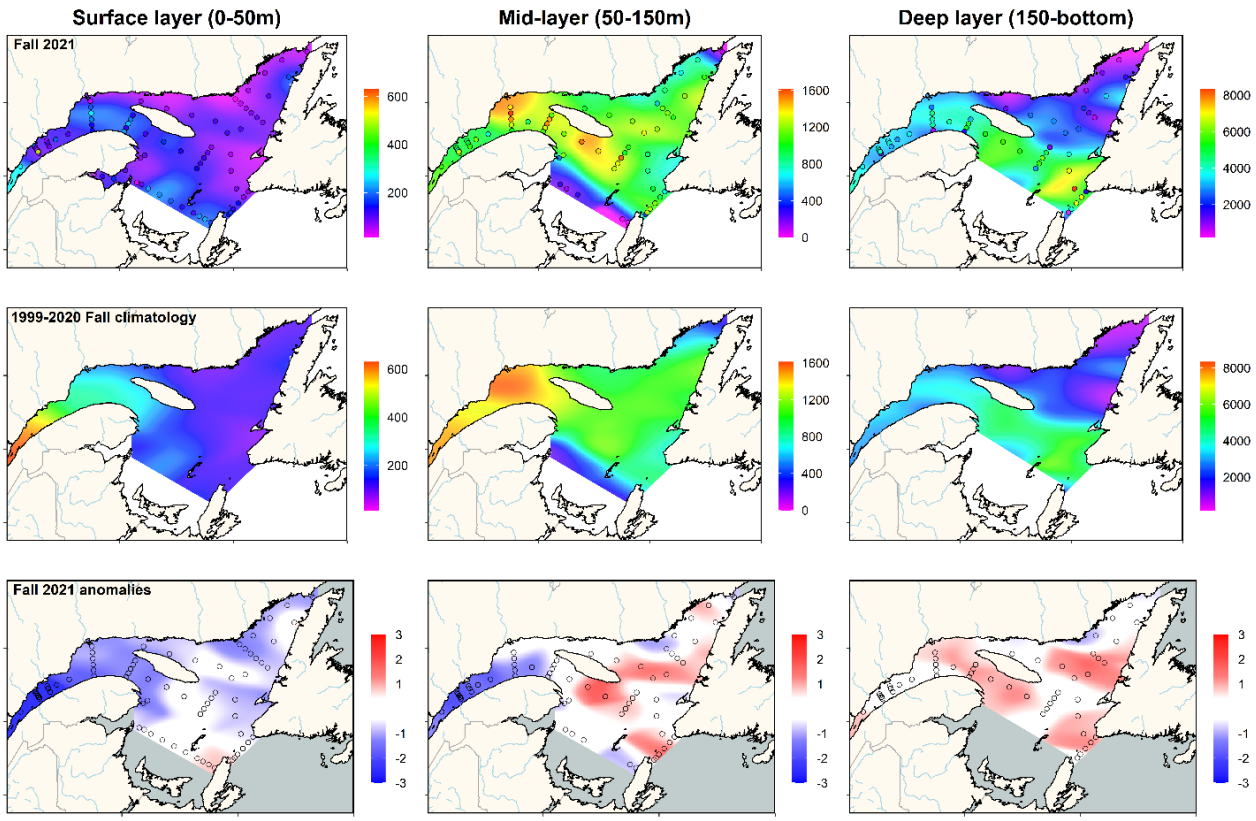

Figure 17. Total nitrate (NO_3^- + NO_2^-) inventories (mmol m^{-2}) in the surface (left panels), mid (middle panels), and deep (right panels) layers of the Estuary and Gulf of St. Lawrence during fall 2021 (upper panels). The climatology (1999–2020; middle panels) and anomalies (lower panels) are shown for each layer. Blue colours indicate below-normal levels (negative anomaly), reds are above-normal levels (positive anomaly), and white represents normal levels.

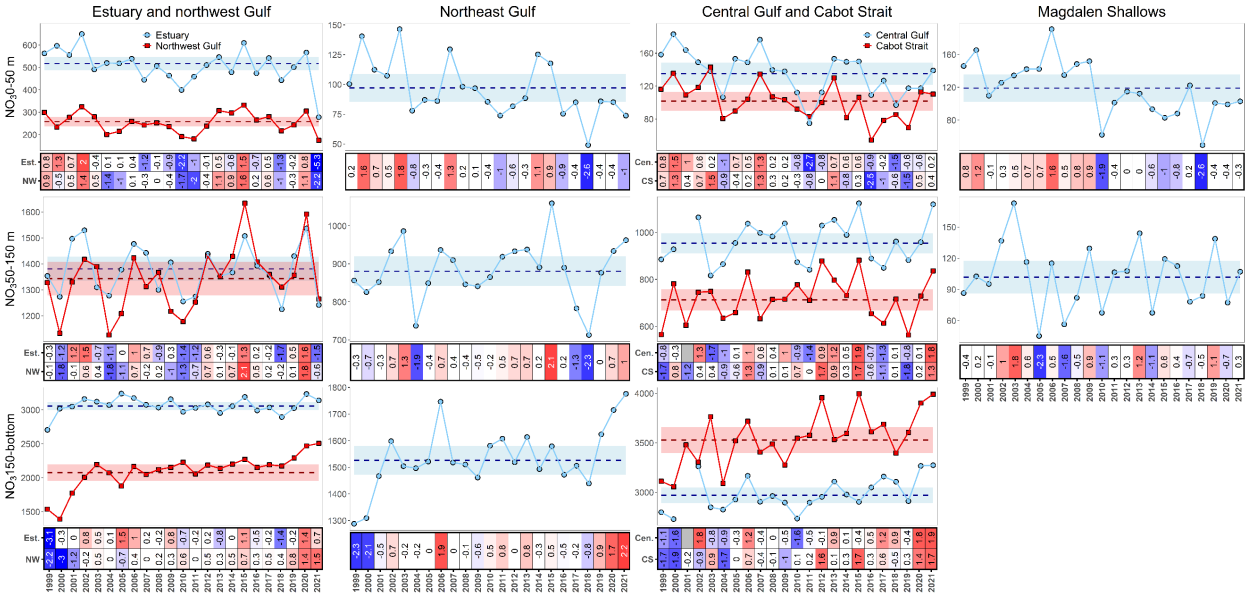

Figure 18. Time series of annual averages (lines) and normalized annual anomalies (scorecards) for nitrate (mmol m^{-2}) in the surface, mid and bottom layers for Gulf regions/subregions. Means (horizontal dashed lines) and standard deviations (blue or red shading) for the 1999–2020 climatology are shown for each region/subregion and water column layer. In the scorecards, blue colours indicate below-normal levels (negative anomaly), reds are above-normal levels (positive anomaly), and white represents normal levels.

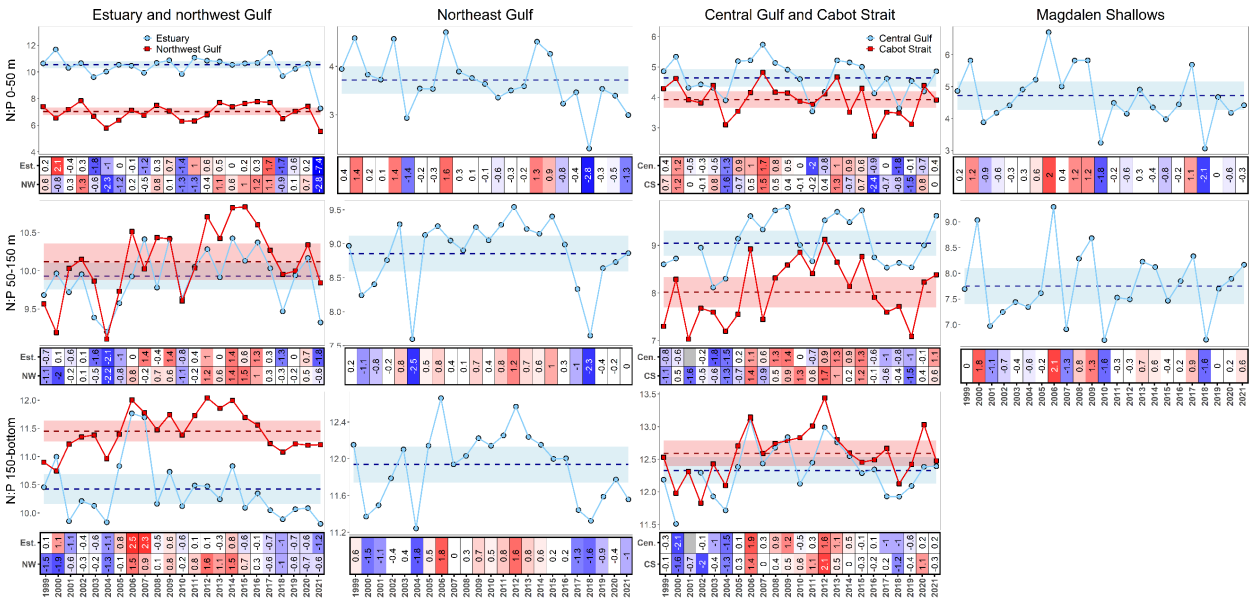

Figure 19. Time series of annual averages (lines) and normalized annual anomalies (scorecards) for the N:P ratio in the surface, mid and bottom layers for Gulf regions/subregions. Means (horizontal dashed lines) and standard deviations (blue or red shading) for the 1999–2020 climatology are shown for each region/subregion and water column layer. In the scorecards, blue colours indicate below-normal levels (negative anomaly), reds are above-normal levels (positive anomaly), and white represents normal levels.

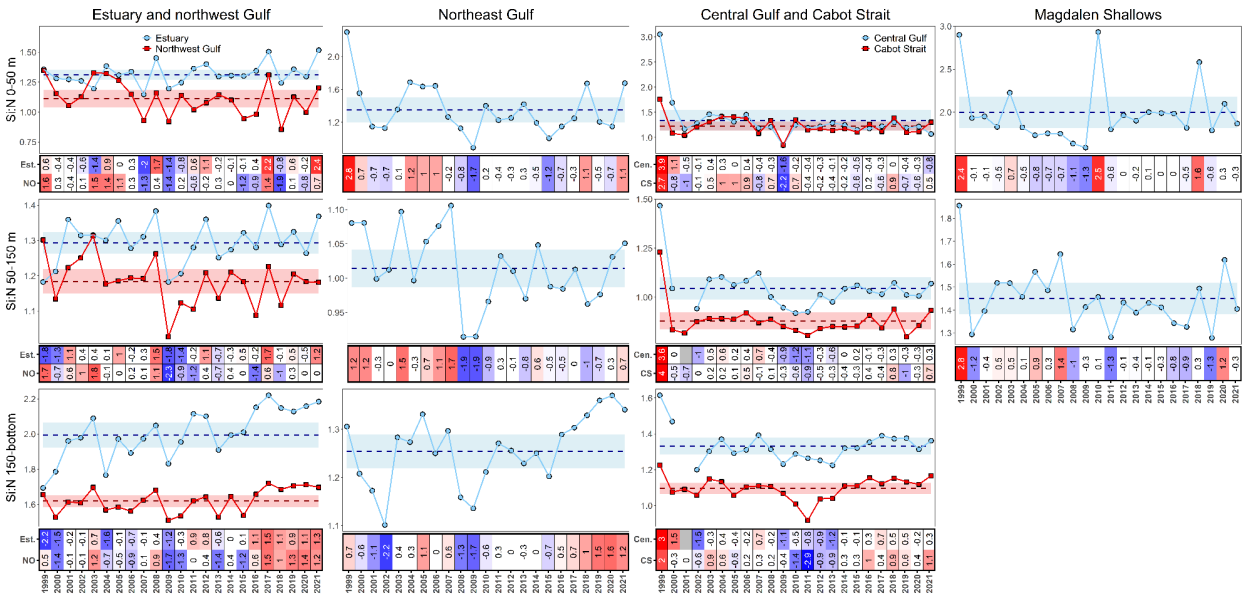

Figure 20. Time series of annual averages (lines) and normalized annual anomalies (scorecards) for the Si:N ratio in the surface, mid and bottom layers for Gulf regions/subregions. Means (horizontal dashed lines) and standard deviations (blue or red shading) for the 1999–2020 climatology are shown for each region/subregion and water column layer. In the scorecards, blue colours indicate below-normal levels (negative anomaly), reds are above-normal levels (positive anomaly), and white represents normal levels.

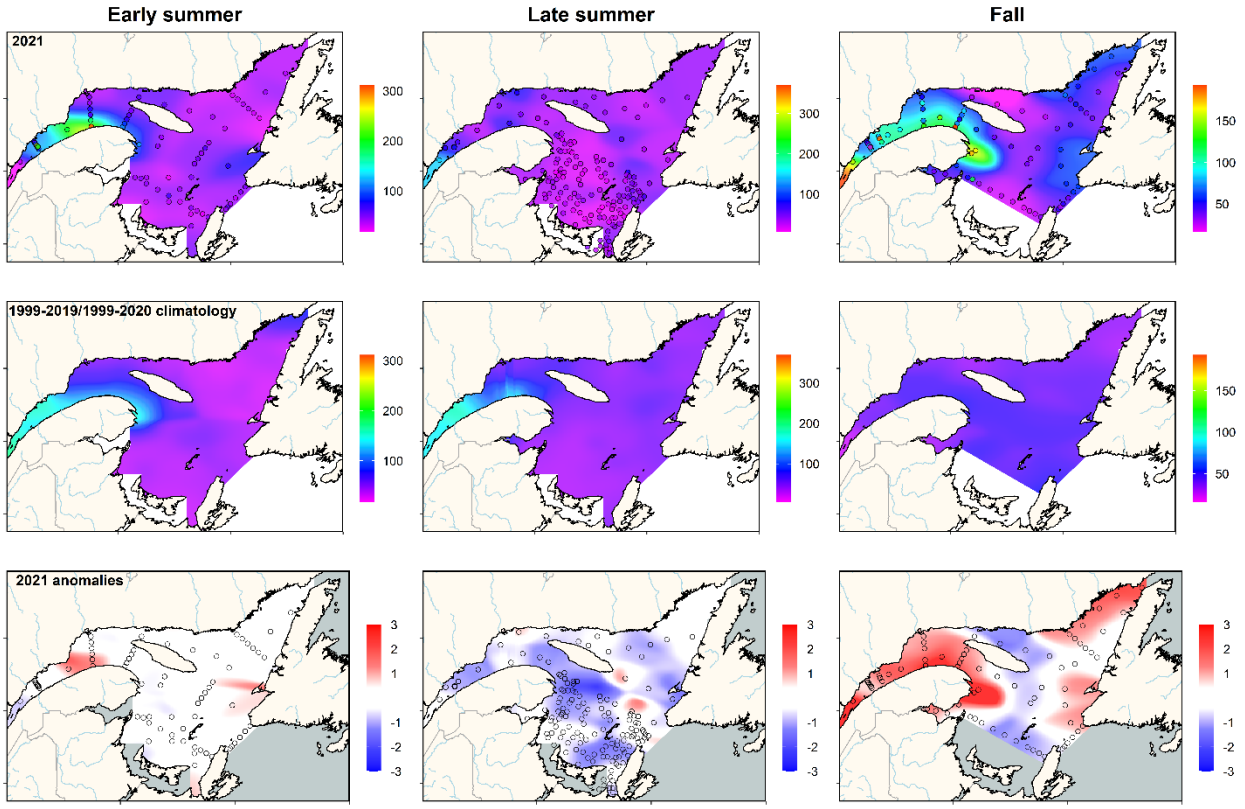

Figure 21. Vertically integrated (0–100 m) chlorophyll a inventory (mg m^{-2}) in the Estuary and Gulf of St. Lawrence during early summer (left panels), late summer (middle panels), and fall (right panels) 2021. The climatology (1999–2019 for early summer and 1999–2020 for other seasons; middle panels) and anomalies (lower panels) are shown for each season. Blue colours indicate below-normal levels (negative anomaly), reds are above-normal levels (positive anomaly), and white represents normal levels.

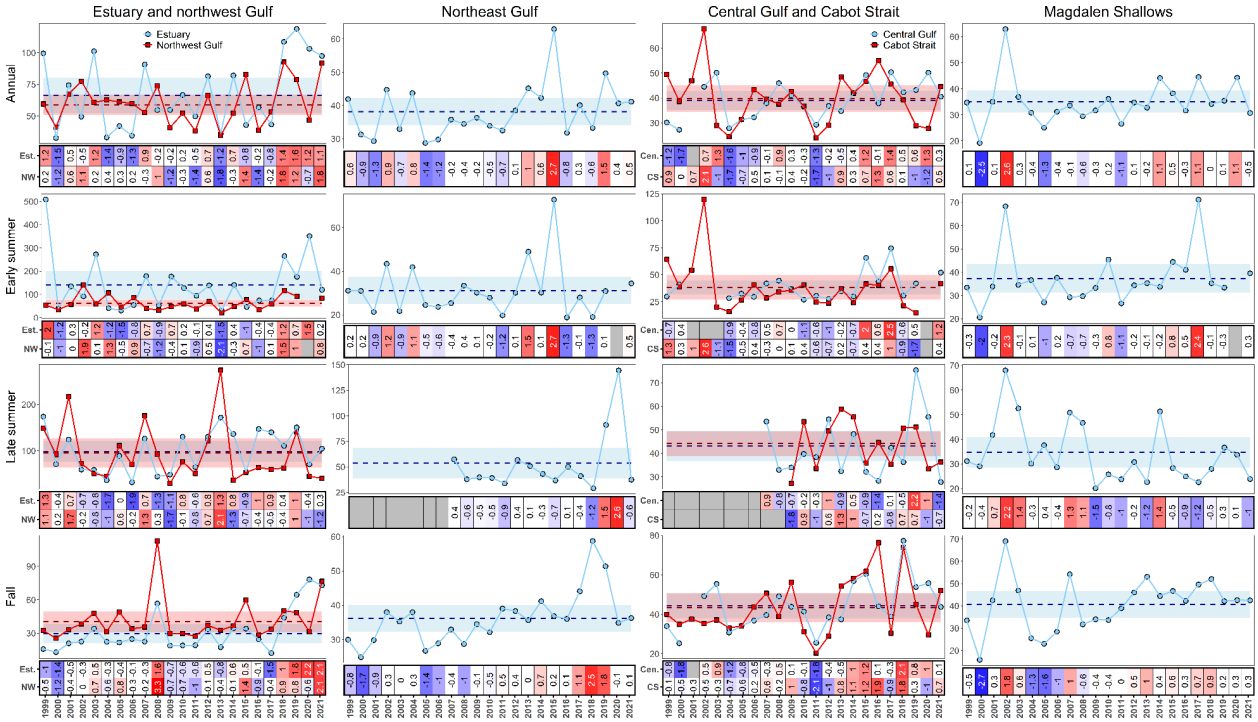

Figure 22. Time series of annual and seasonal averages (lines), and normalized annual and seasonal anomalies (scorecards) of vertically integrated chlorophyll a inventory (0–100 m; mg m^{-2}) in the Gulf regions/subregions. Means (horizontal dashed lines) and standard deviations (blue or red shading) for the climatology (1999–2019 for early summer and 1999–2020 for other seasons) are shown for each region/subregion and season. In the scorecards, blue colours indicate below-normal levels (negative anomaly), reds are above-normal levels (positive anomaly), and white represents normal levels.

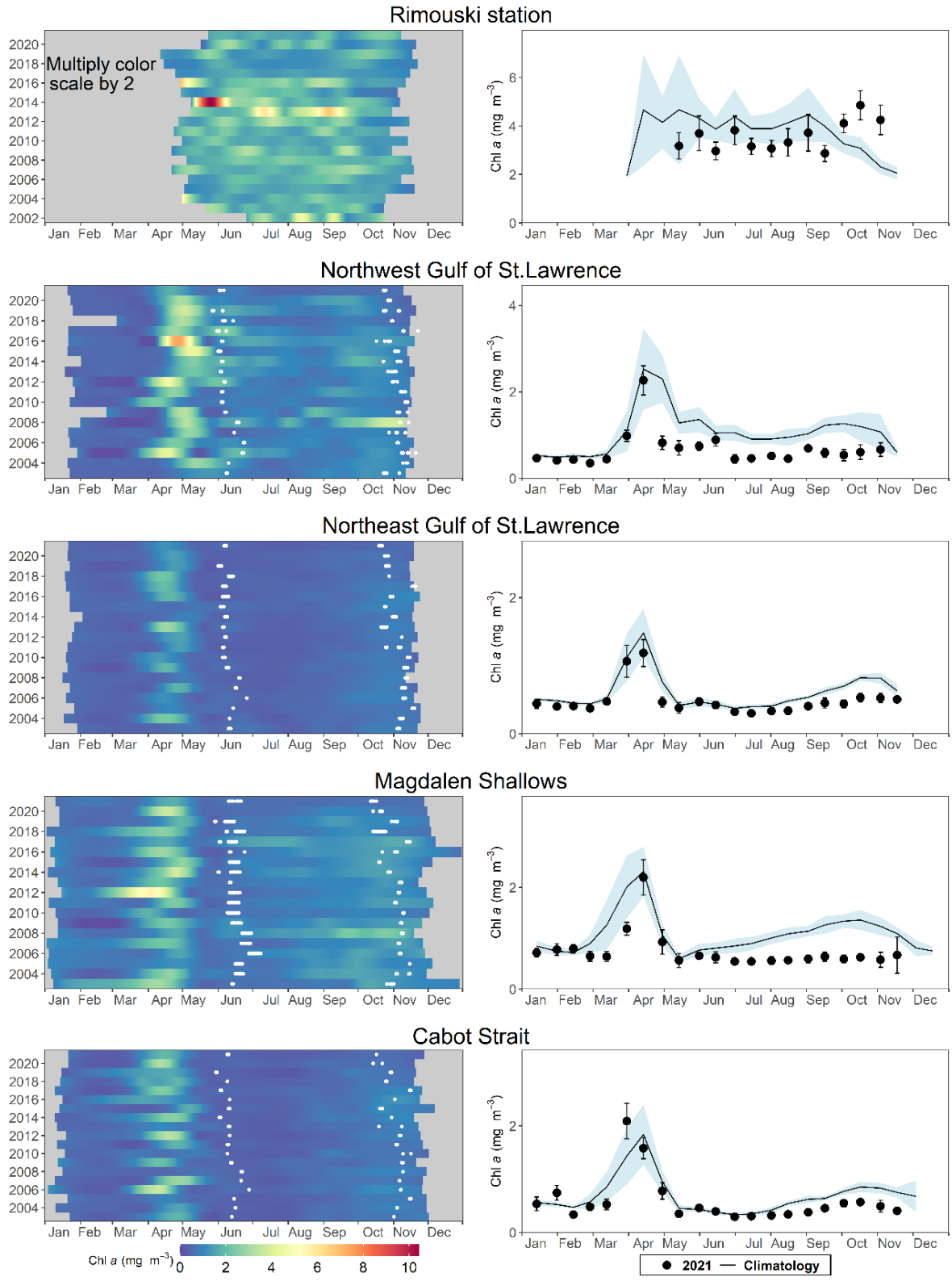

Figure 23. Left panels: LOESS-smoothed time series of daily surface chlorophyll a concentrations derived from data produced by a fluorescence sensor fixed on the Viking buoy at Rimouski station (1st row panels) and from MODIS ocean-colour data in the ocean colour boxes (see Figure 4). White dots indicate sampling times of the main AZMP surveys. Right panels: comparison of semi-monthly mean (± 0.5 SD) of surface chlorophyll a estimates in 2021 (black circles) with average (± 0.5 SD) conditions from the 2003–2020 climatology (2002–2020 for Rimouski station; solid line with blue shading) for the same ocean-colour boxes.

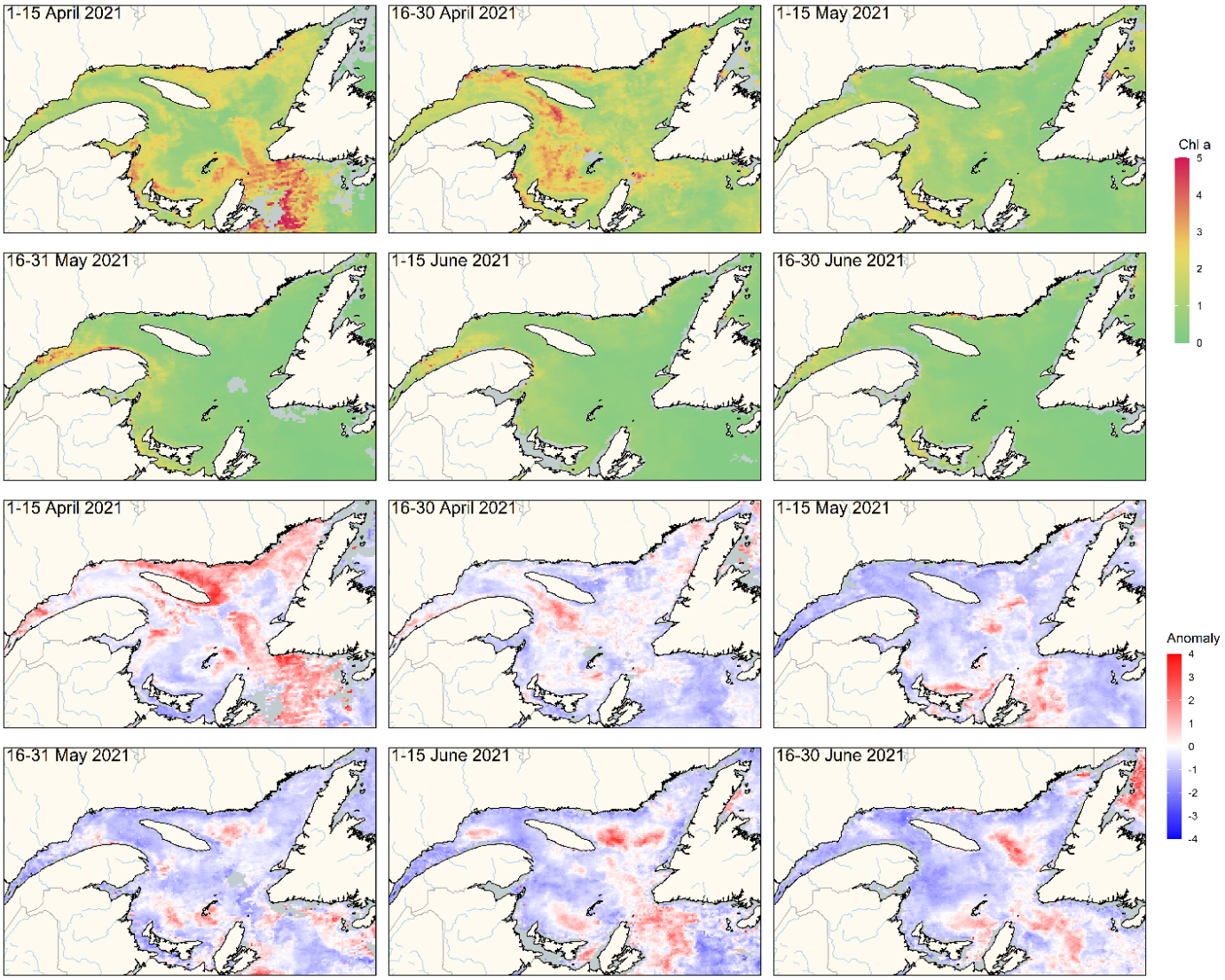

Figure 24. MODIS composite images of surface chlorophyll a (upper panels) and chlorophyll a normalized anomaly based on the 2003–2020 climatology (lower panels) in the Gulf of St. Lawrence during spring/early summer 2021.

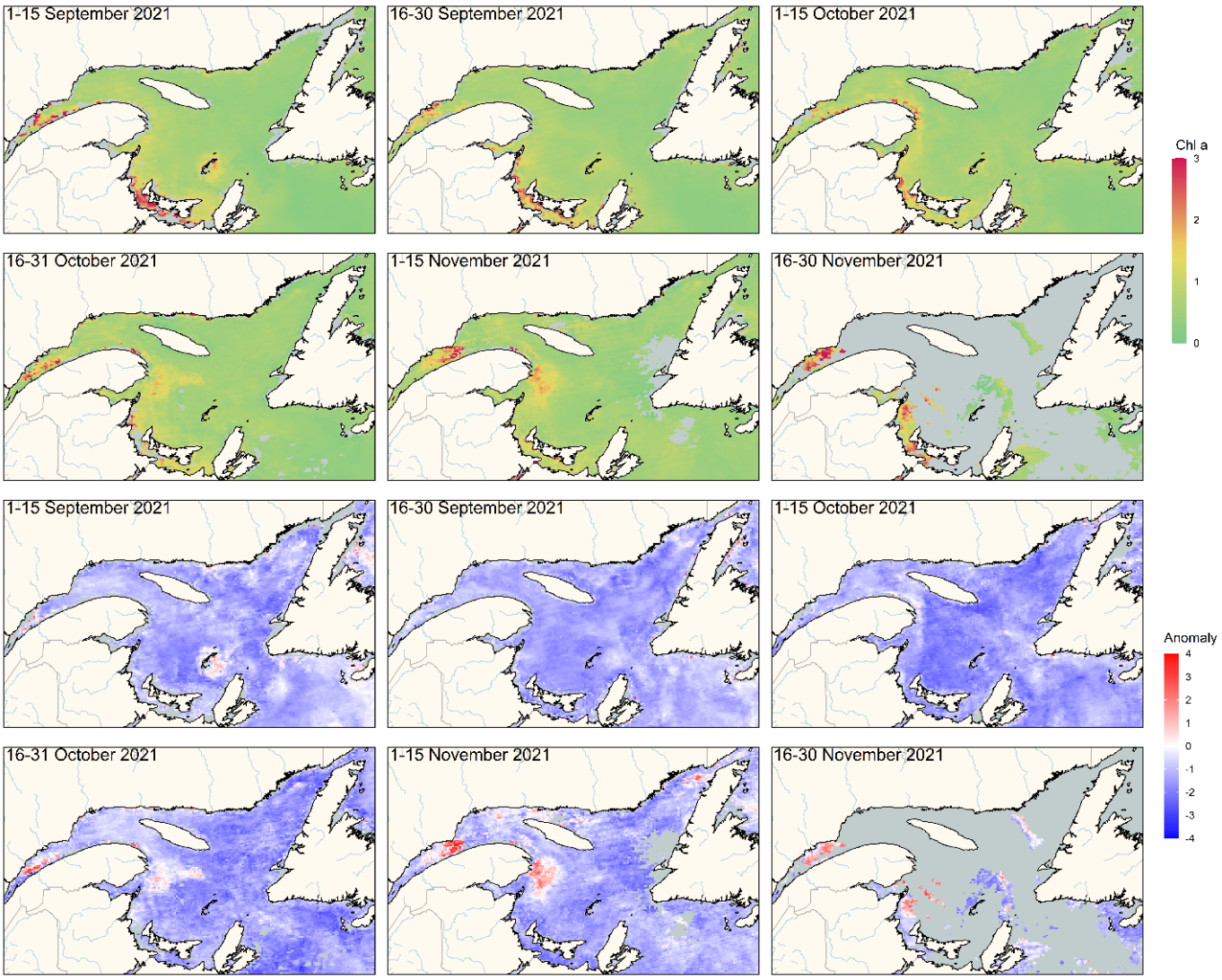

Figure 25. MODIS composite images of surface chlorophyll a (upper panels) and chlorophyll a normalized anomaly based on the 2003–2020 climatology (lower panels) in the Gulf of St. Lawrence during fall 2021.

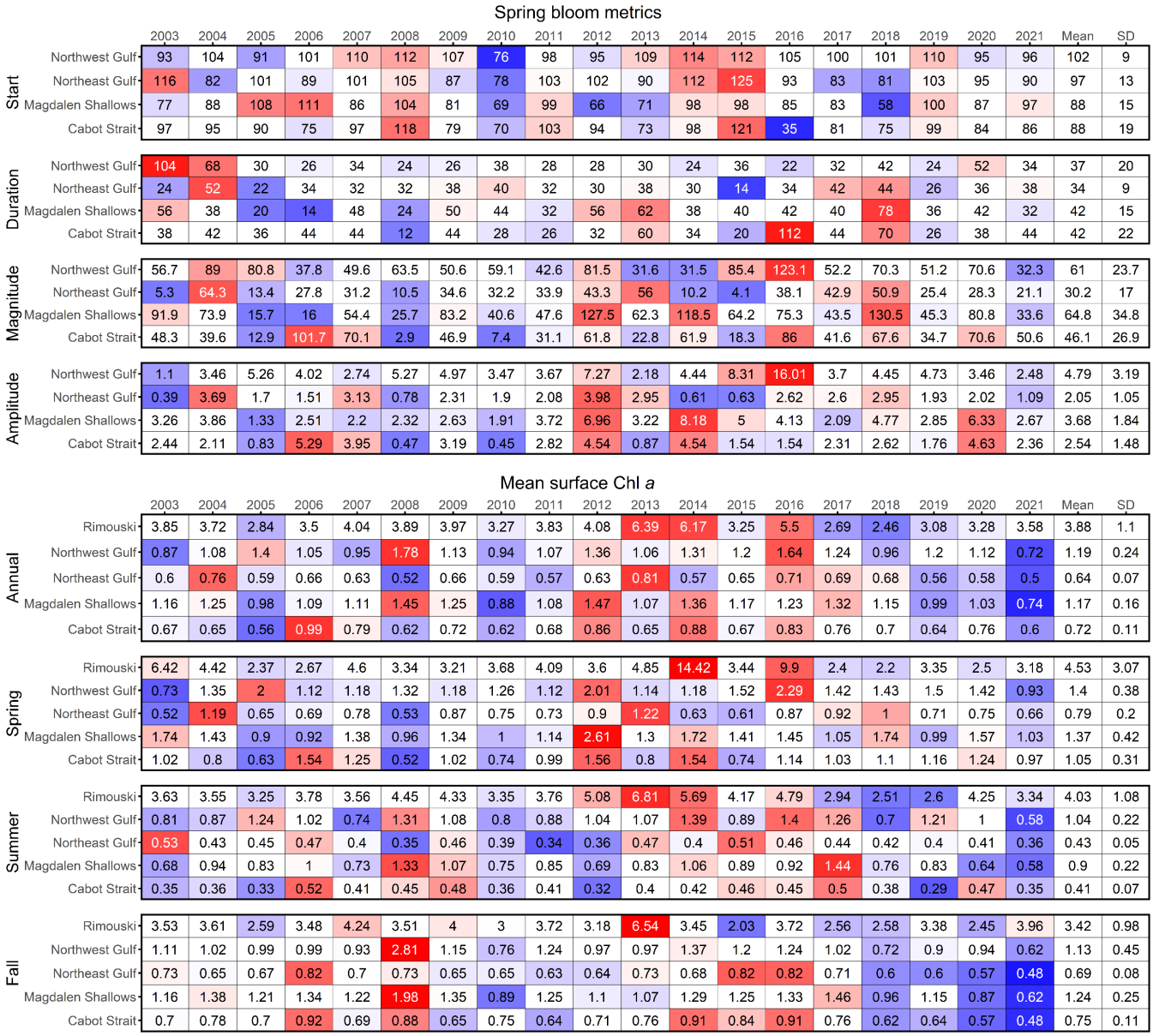

Figure 26. Time series of annual anomalies for indices of change in spring bloom metrics (upper section) and annual/seasonal mean surface chlorophyll a (lower section; mg m^{-3}) estimated from satellite ocean colour data (MODIS: 2003–present) in the Gulf of St. Lawrence ocean-colour polygons (see Figure 4) and from Viking buoy surface sensor at Rimouski station. The spring bloom indices are start (day of the year), duration (days), magnitude (mg chl m^{-2}), and amplitude (mg chl m^{-3}). Variable means and standard deviations for the 2003–2020 climatology are shown to the right of the scorecard. Blue colours indicate below-normal levels (negative anomaly), reds are above-normal levels (positive anomaly), and white represents normal levels. Spring is from March to May, summer from June to August, and fall from September to November.

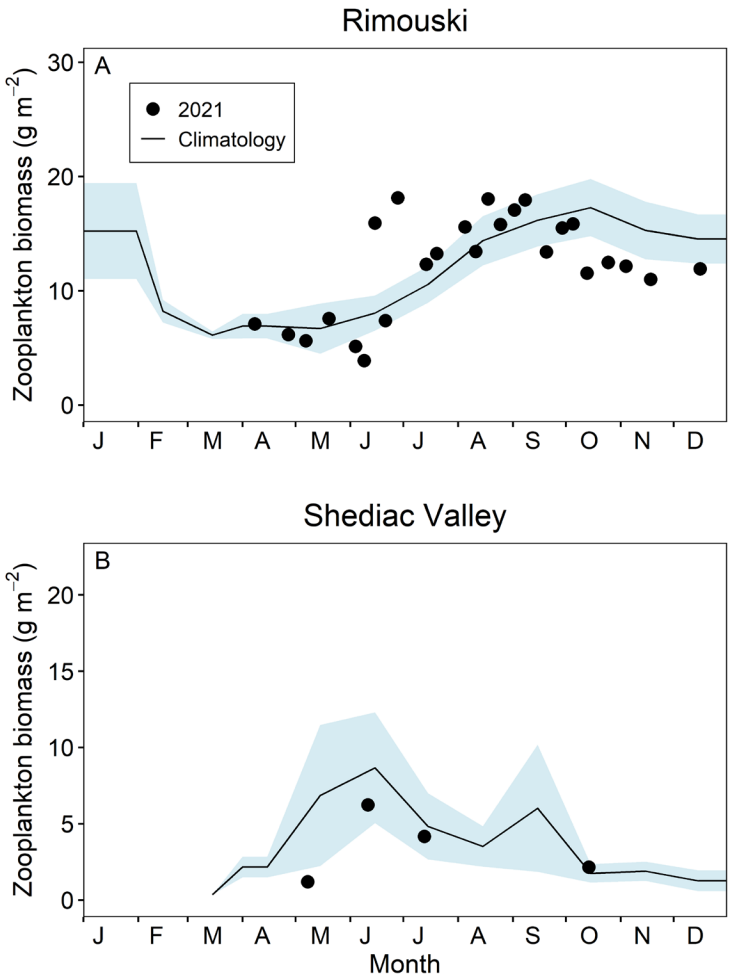

Figure 27. Comparison of total zooplankton biomass (dry weight) in 2021 (circles) with the monthly climatology from (A) Rimouski (2005–2020) and (B) Shediac Valley (1999–2020) stations (black line with blue shading). Blue shading represents ± 0.5 SD of the monthly means.

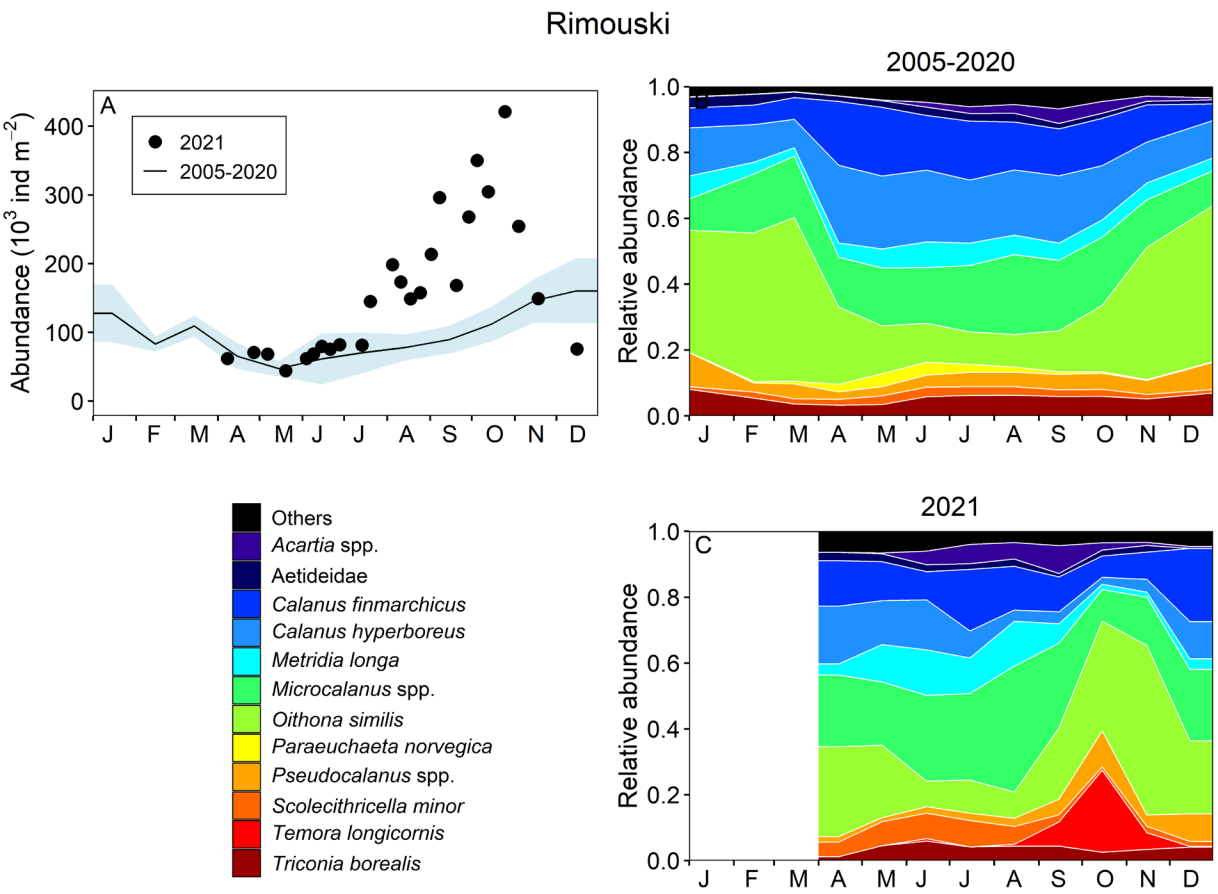

Figure 28. Seasonal variability of dominant copepods at Rimouski station. Climatology of copepod copepodite abundance (black line with blue shading indicating ± 0.5 SD) and in 2021 (circles) (A); climatology of the relative abundance of the identified copepod taxa representing 95% of total copepod abundance during the 2005–2020 period (B) and in 2021 (C).

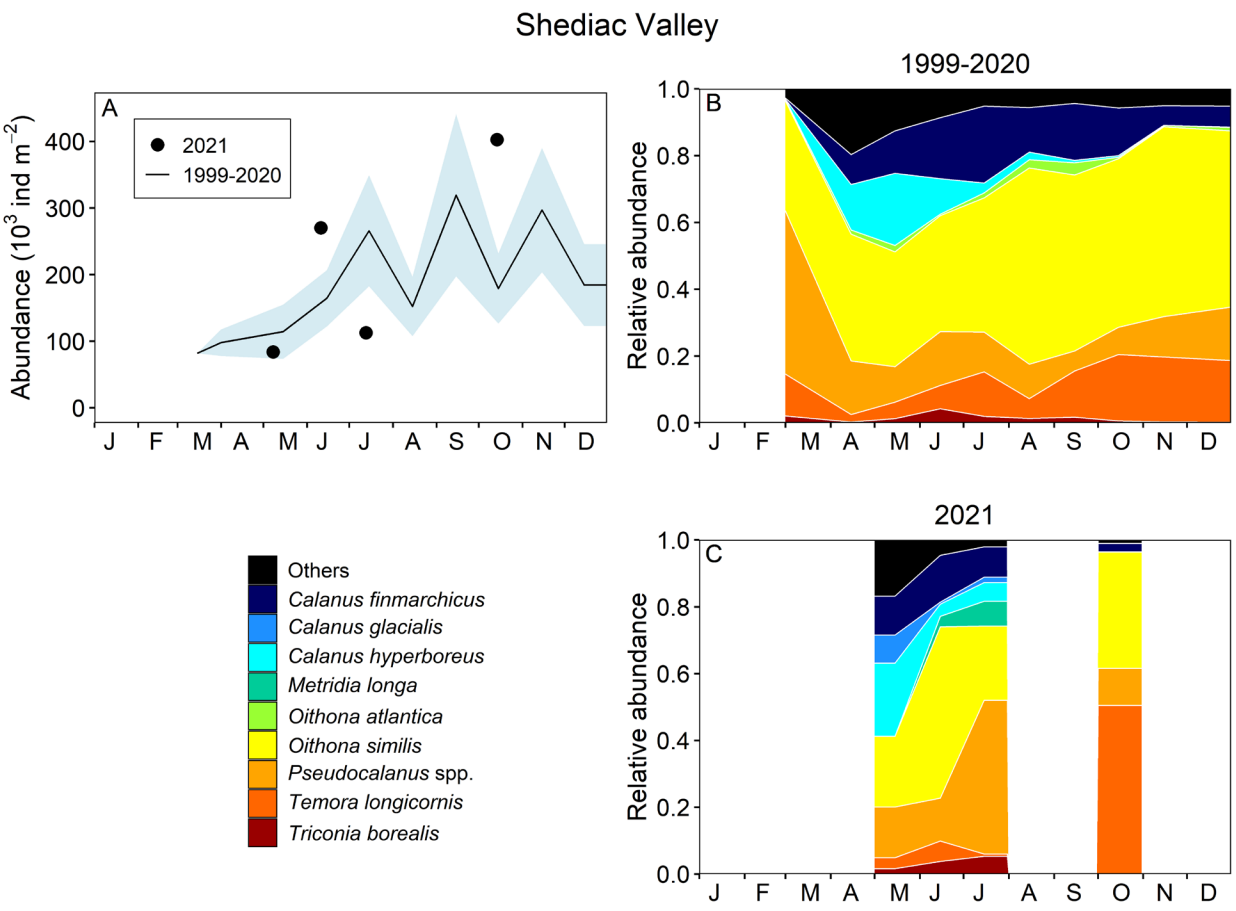

Figure 29. Seasonal variability of dominant copepods at Shediac Valley station. Climatology of copepod copepodite abundance (black line with blue shading indicating ± 0.5 SD) and 2021 (circles) (A); climatology of the relative abundance of the identified copepod taxa representing 95% of total copepod abundance during the 1999–2020 period (B) and in 2021 (C).

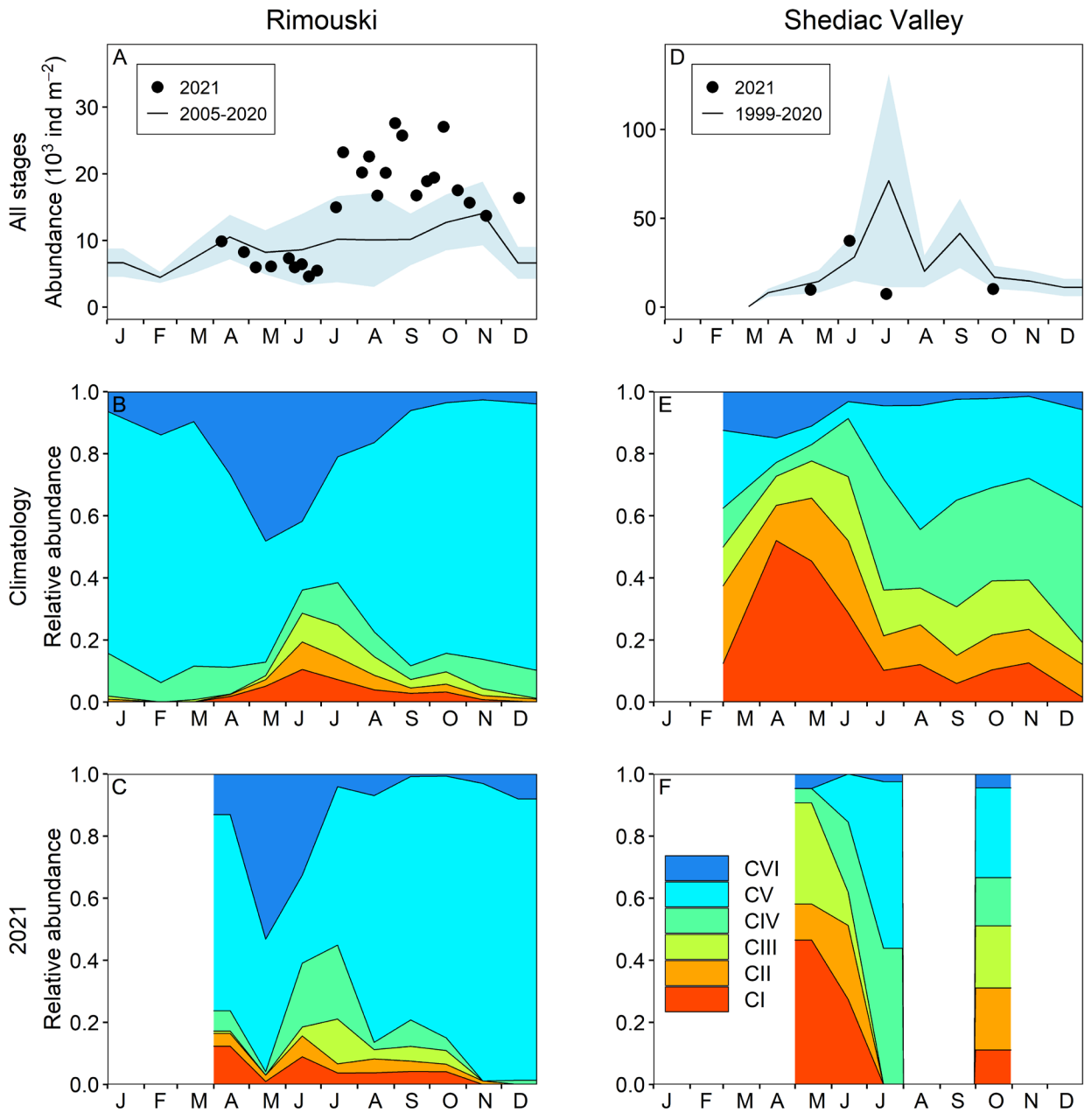

Figure 30. Seasonal variability in Calanus finmarchicus *copepodite abundance and stage distribution at Rimouski (A–C) and Shediac Valley (D–F) stations. Climatology of* C. finmarchicus *abundance (black line with blue shading indicating ± 0.5 SD) with data from 2021 (circles) (A, D). Climatology of individual copepodite stages (B, E) and data for 2021 (C, F).*

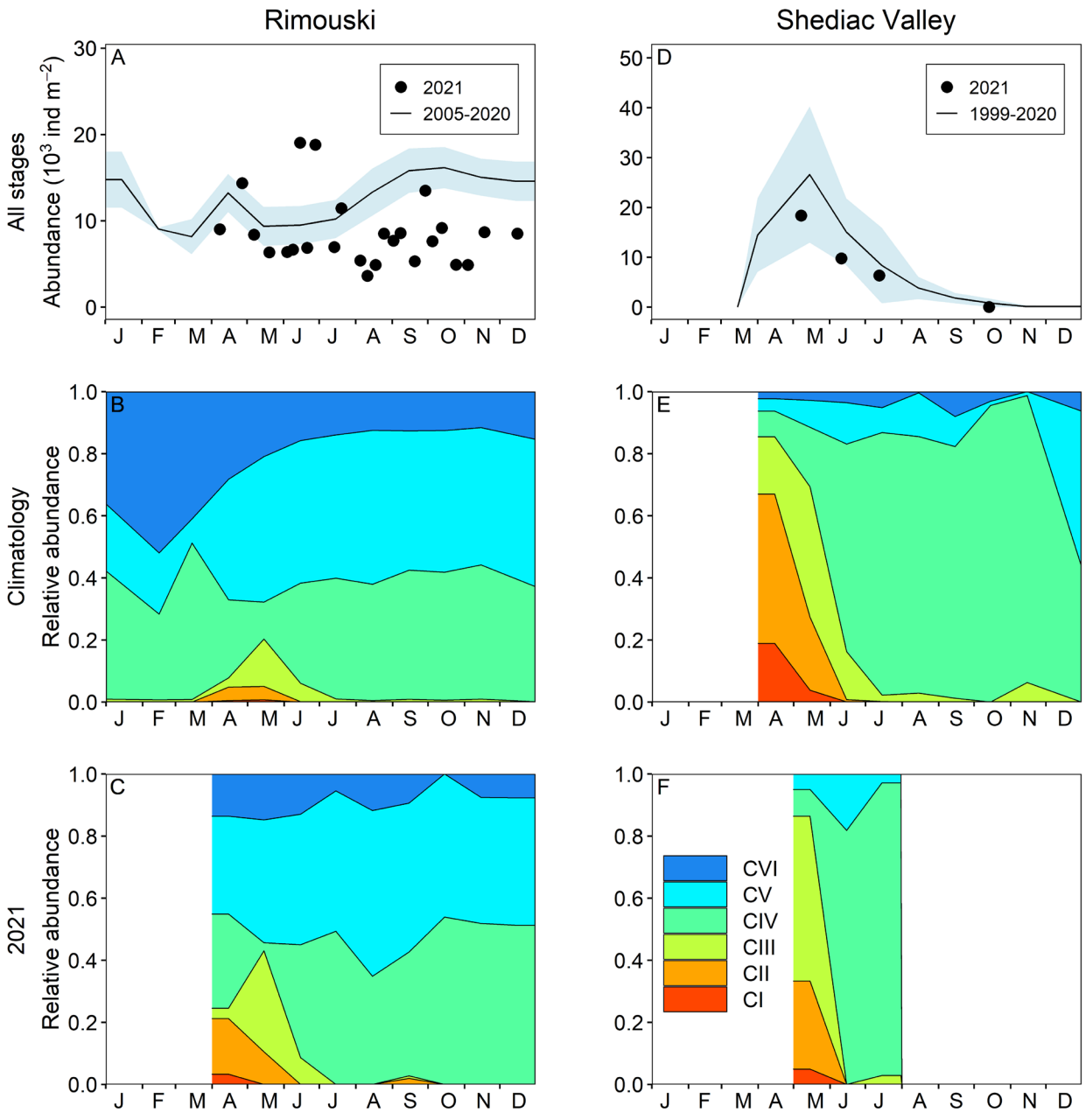

Figure 31. Seasonal variability in Calanus hyperboreus *copepodite abundance and stage distribution at Rimouski (A–C) and Shediac Valley (D–F) stations. Climatology of* C. hyperboreus *abundance (black line with blue shading indicating ± 0.5 SD) with data from 2021 (circles) (A, D). Climatology of individual copepodite stages (B, E) and data for 2021 (C, F). No* C. hyperboreus *individual was collected in the October sample at Shediac Valley.*

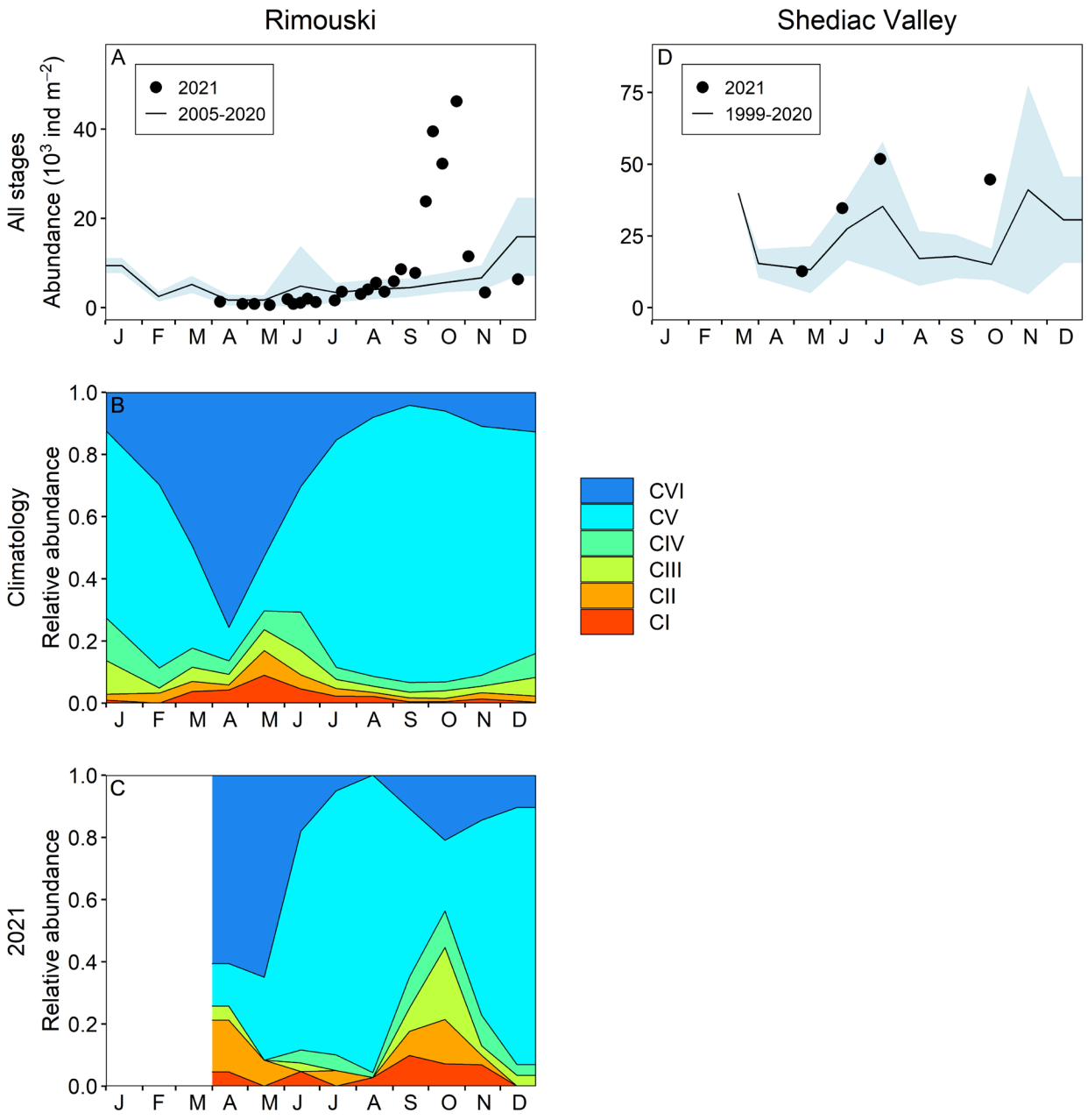

Figure 32. Seasonal variability in Pseudocalanus *spp. copepodite abundance and stage distribution at Rimouski (A–C) and Shediac Valley (D–F) stations. Climatology of* Pseudocalanus *spp. abundance (black line with blue shading indicating ± 0.5 SD) with data from 2021 (circles) (A, D). Climatology of individual copepodite stages (B, E) and data for 2021 (C, F). Stage information is not available for Shediac Valley.*

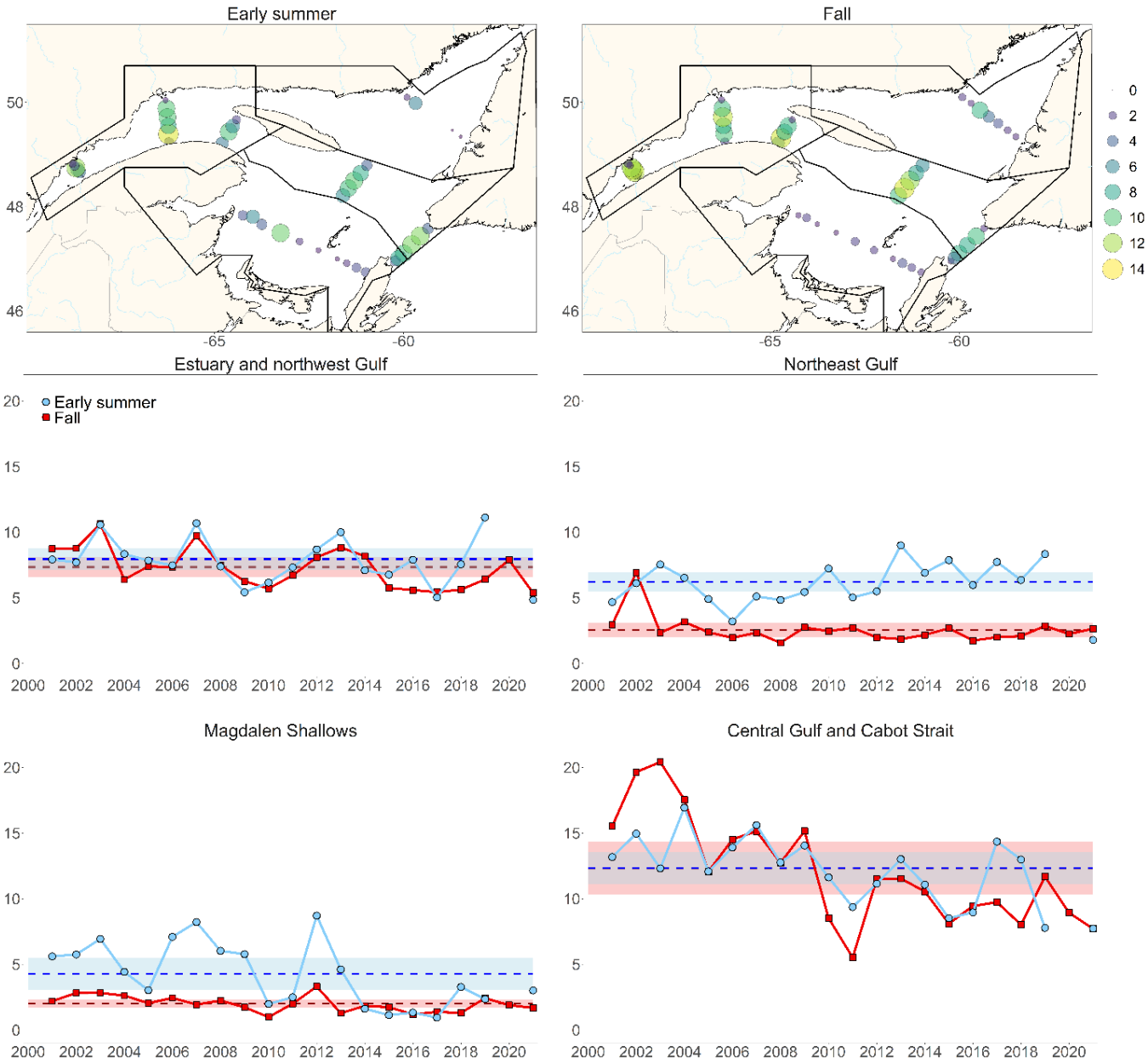

Figure 33. Zooplankton biomass (dry weight; g m^{-2}) spatial distribution during early summer and fall 2021 (upper panels) and regional seasonal time series of mean total zooplankton biomass (g m^{-2}; middle and bottom panels) calculated using GLM. Dashed blue and red lines represent the climatological (2001–2020) *averages (shading represents ± 0.5 SD) for early summer and fall, respectively.*

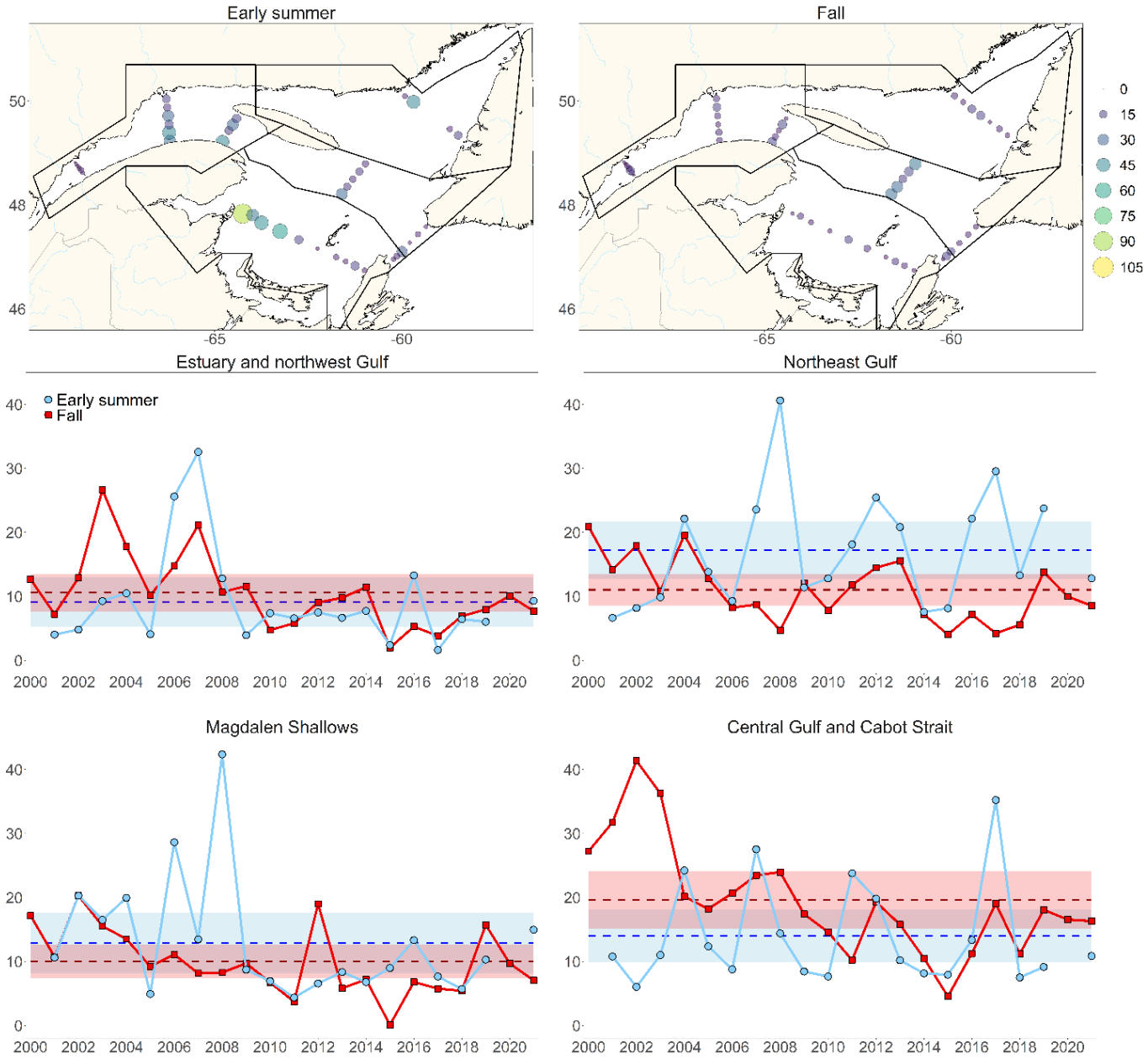

Figure 34. Calanus finmarchicus *abundance (10^3 ind m^{-2}) spatial distribution during early summer and fall 2021 (upper panels) and regional seasonal time series of mean total* C. finmarchicus *abundance (10^3 ind m^{-2}; middle and bottom panels) calculated using GLM. Dashed blue and red lines represent the climatological* (2000–2020) *averages (shading represents ± 0.5 SD) for early summer and fall, respectively*

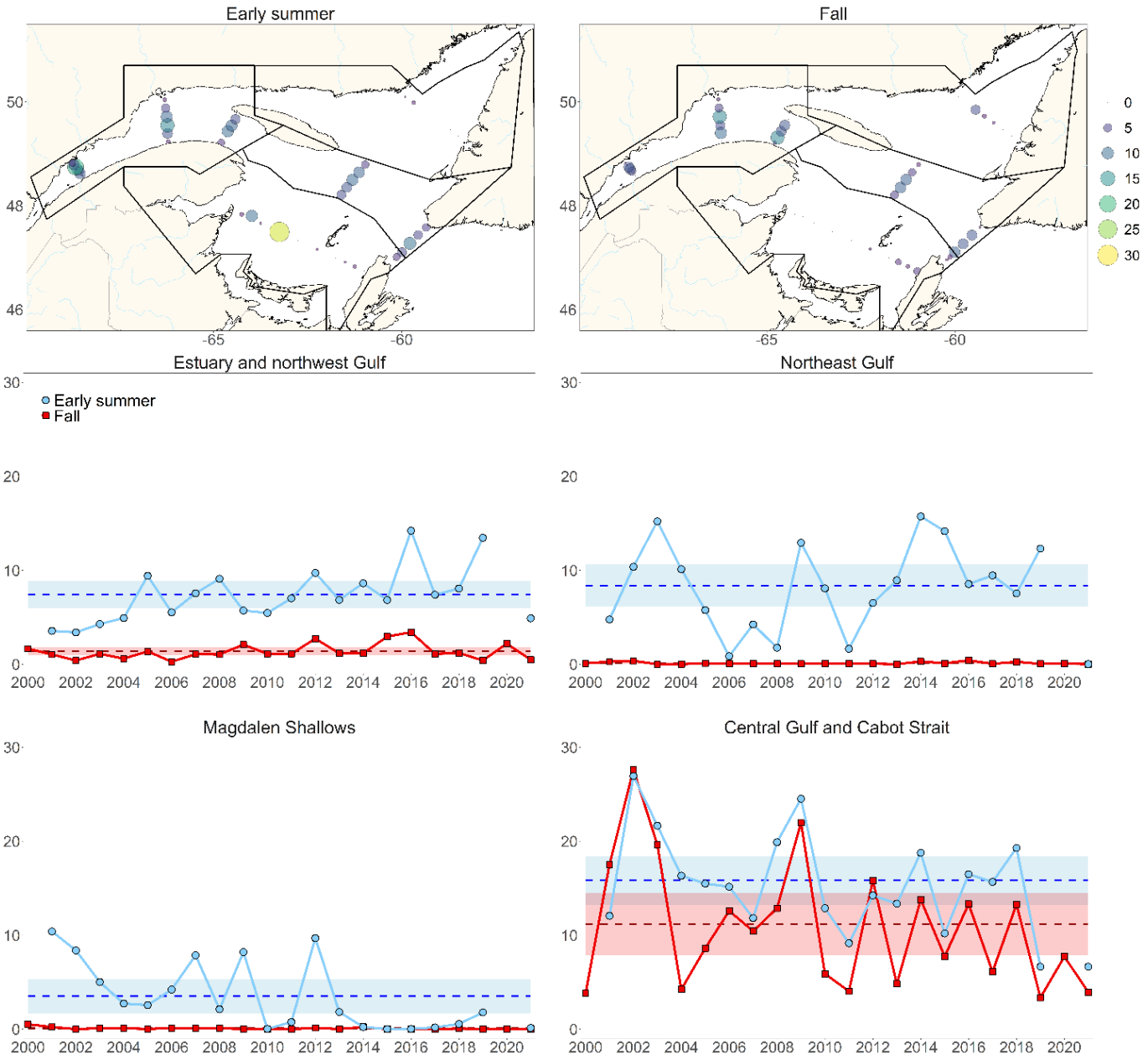

Figure 35. Calanus hyperboreus *abundance (10^3 ind m^{-2}) spatial distribution during early summer and fall 2021 (upper panels) and regional seasonal time series of mean total* C. hyperboreus *abundance (10^3 ind m^{-2}; middle and bottom panels) calculated using GLM. Dashed blue and red lines represent the climatological* (2000–2020) *averages (shading represents ± 0.5 SD) for early summer and fall, respectively.*

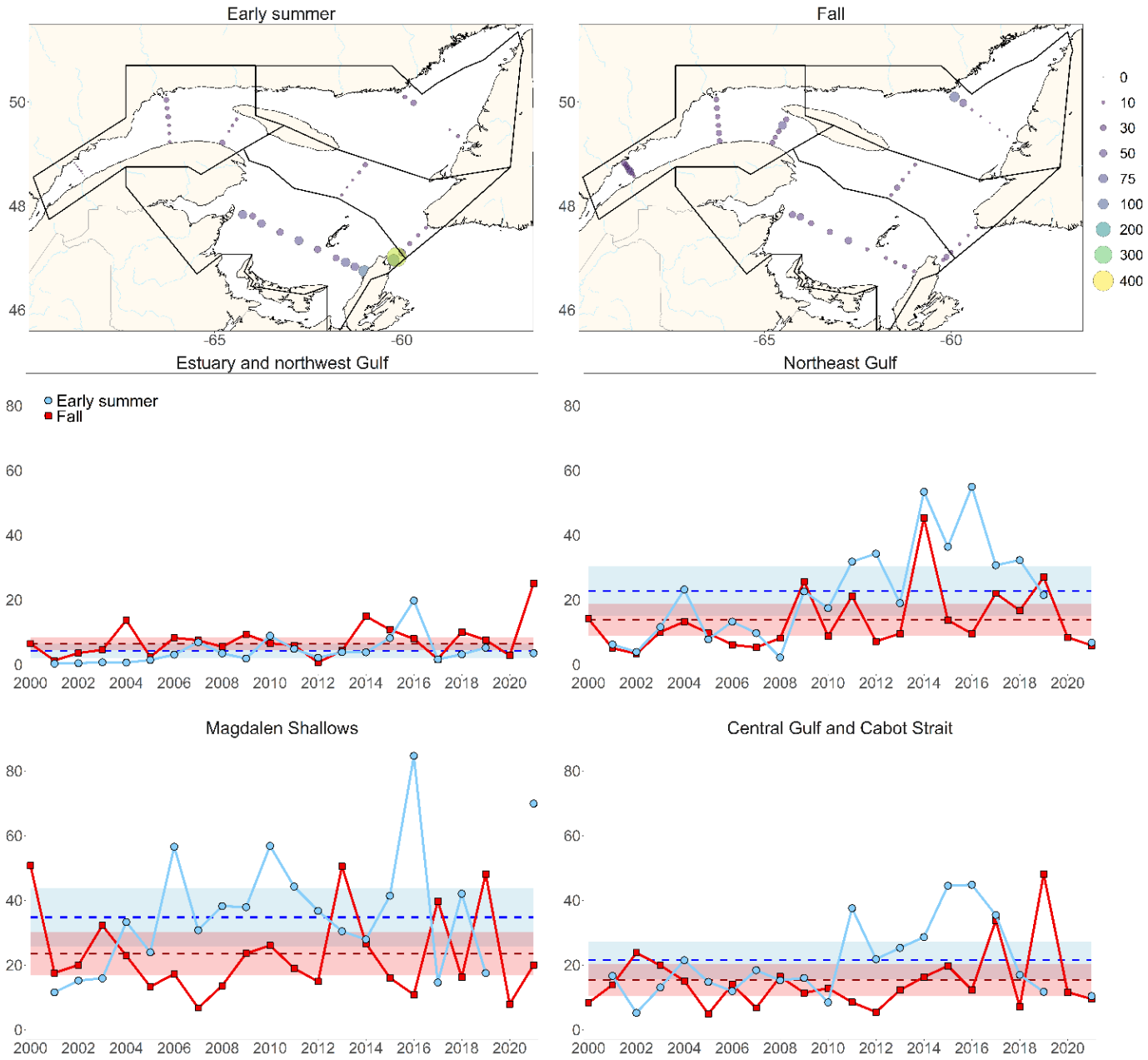

Figure 36. Pseudocalanus *spp. abundance (10^3 ind m^{-2}) spatial distribution during early summer and fall 2021 (upper panels) and regional seasonal time series of mean total* Pseudocalanus *spp. abundance (10^3 ind m^{-2}; middle and bottom panels) calculated using GLM. Dashed blue and red lines represent the climatological* (2000–2020) *averages (shading represents ± 0.5 SD) for early summer and fall, respectively.*

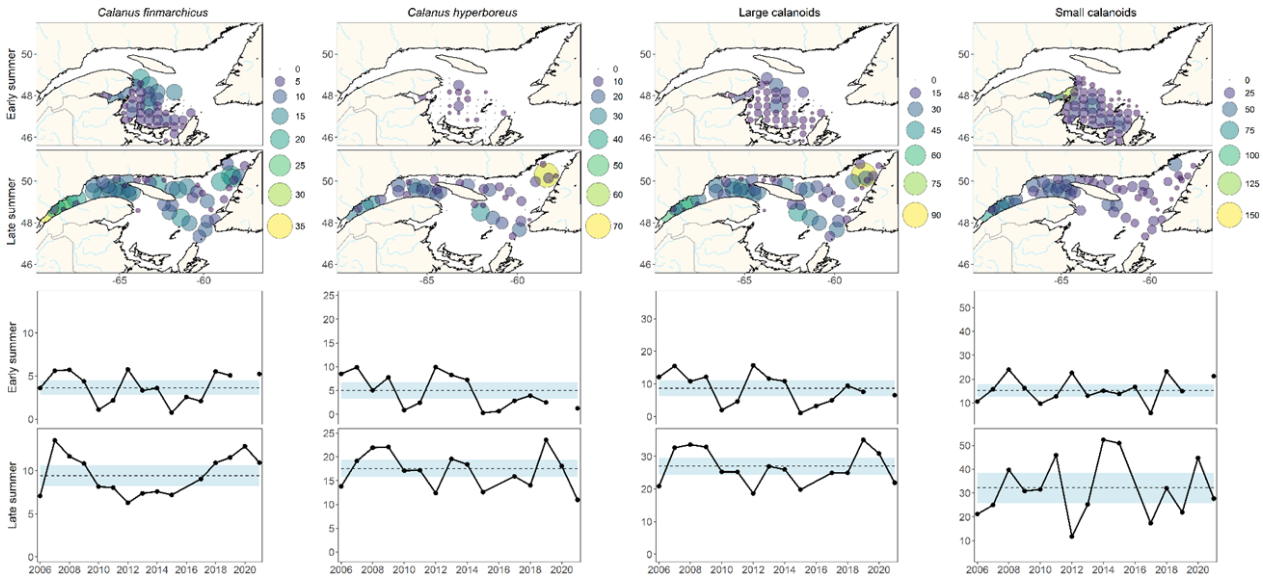

Figure 37. Abundances (10^3 ind m^{-2}) of main taxa identified through automated numerical zooplankton images analysis (ZooImage) at each sampling station during early summer in the Magdalen Shallows and late summer 2021 in the northern Gulf (upper panels). The regional seasonal time series of mean total abundances are also shown for these taxa (10^3 ind m^{-2}; bottom panels). Dashed lines represent the climatology (2006–2020) *averages (shading represents ± 0.5 SD). The abundances of* C. finmarchicus *and* C. hyperboreus *include copepodite stages CIV–CVI only. ZooImage does not distinguish between* C. finmarchicus *and* C. glacialis*, thus both species are included in the* C. finmarchicus *index. In this figure, large calanoid abundances correspond to the sum of these* C. finmarchicus *and* C. hyperboreus *indices; and small calanoid abundances correspond to the sum of the following taxa:* Temora *spp.,* Eurytemora *spp.,* Pseudocalanus *spp.,* Microcalanus *spp. and* Scolecithricella *spp.*

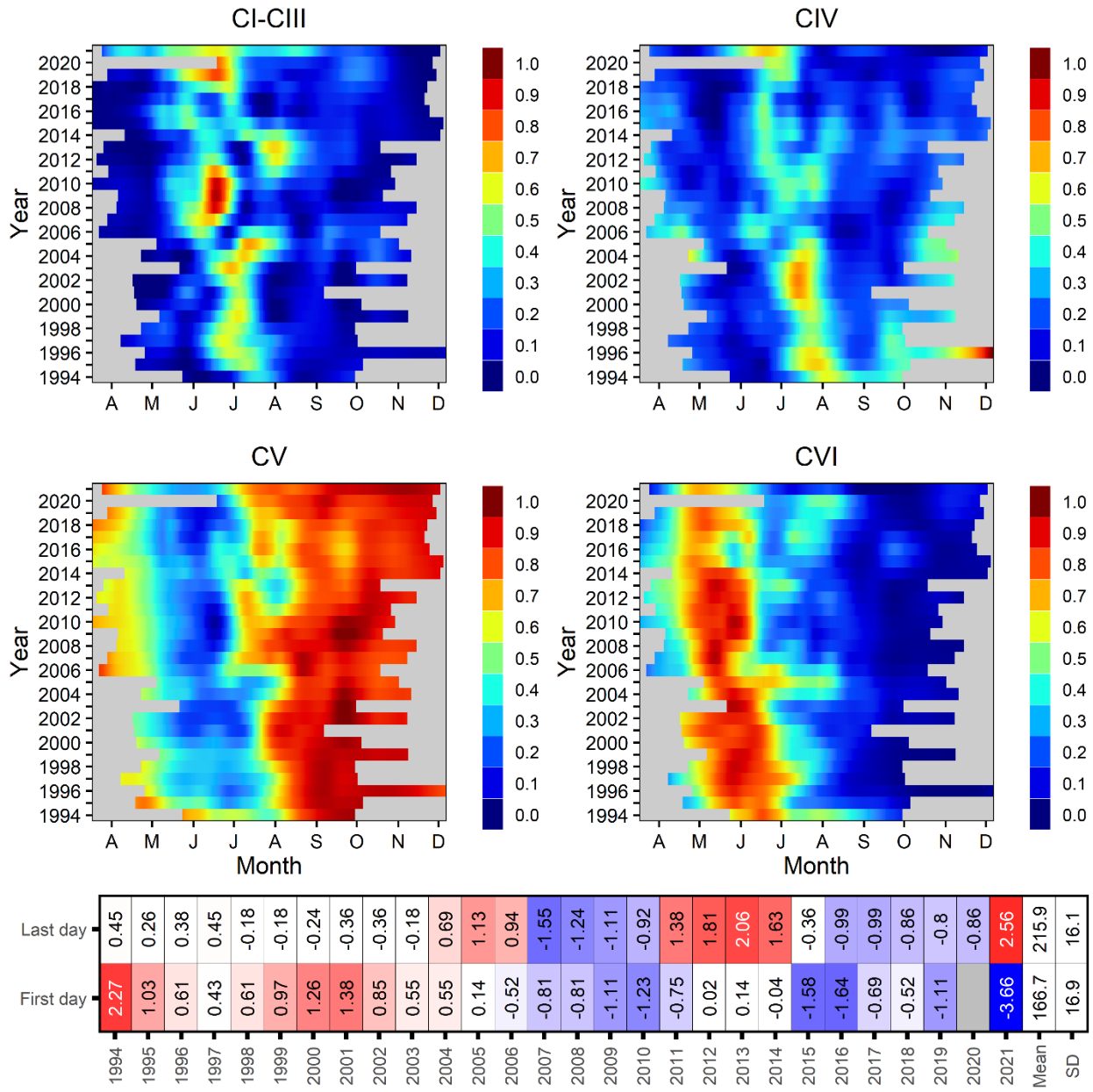

Figure 38. Time series of the seasonal cycle of total abundance for Calanus finmarchicus *copepodite stages (relative proportion; CI–CIII, CIV, CV, and CVI male + female) at Rimouski station. Proportions are normalized by their annual maximum and smoothed using a Loess regression. Bottom scorecard shows the anomaly time series (climatology 1994–2020) associated with the first and last days when the normalized proportion of CI–CIII was higher than 0.3.*

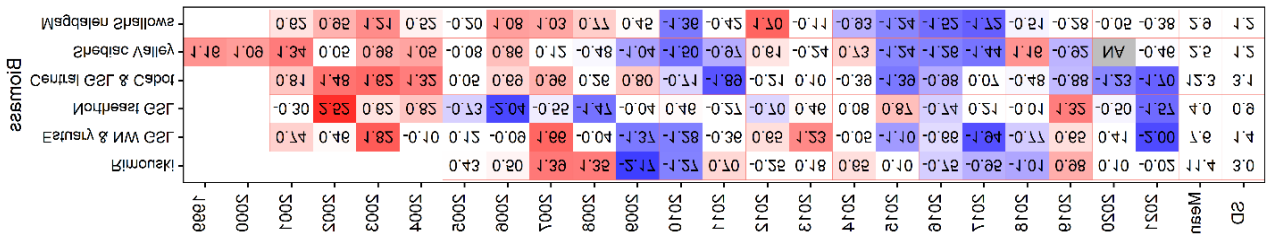

Figure 39. Time series of normalized annual anomalies of zooplankton biomass (dry weight; g m^{-2}) for the high-frequency monitoring stations and the regions of the Gulf of St. Lawrence (calculated using GLM). Variable means and standard deviations for the 2001–2020 (2005–2020 for Rimouski; 1999–2020 for Shediac Valley) climatology are shown to the right of the scorecard. Blue colours indicate below-normal levels (negative anomaly), reds are above-normal levels (positive anomaly), and white represents normal levels. GSL: Gulf of St. Lawrence.

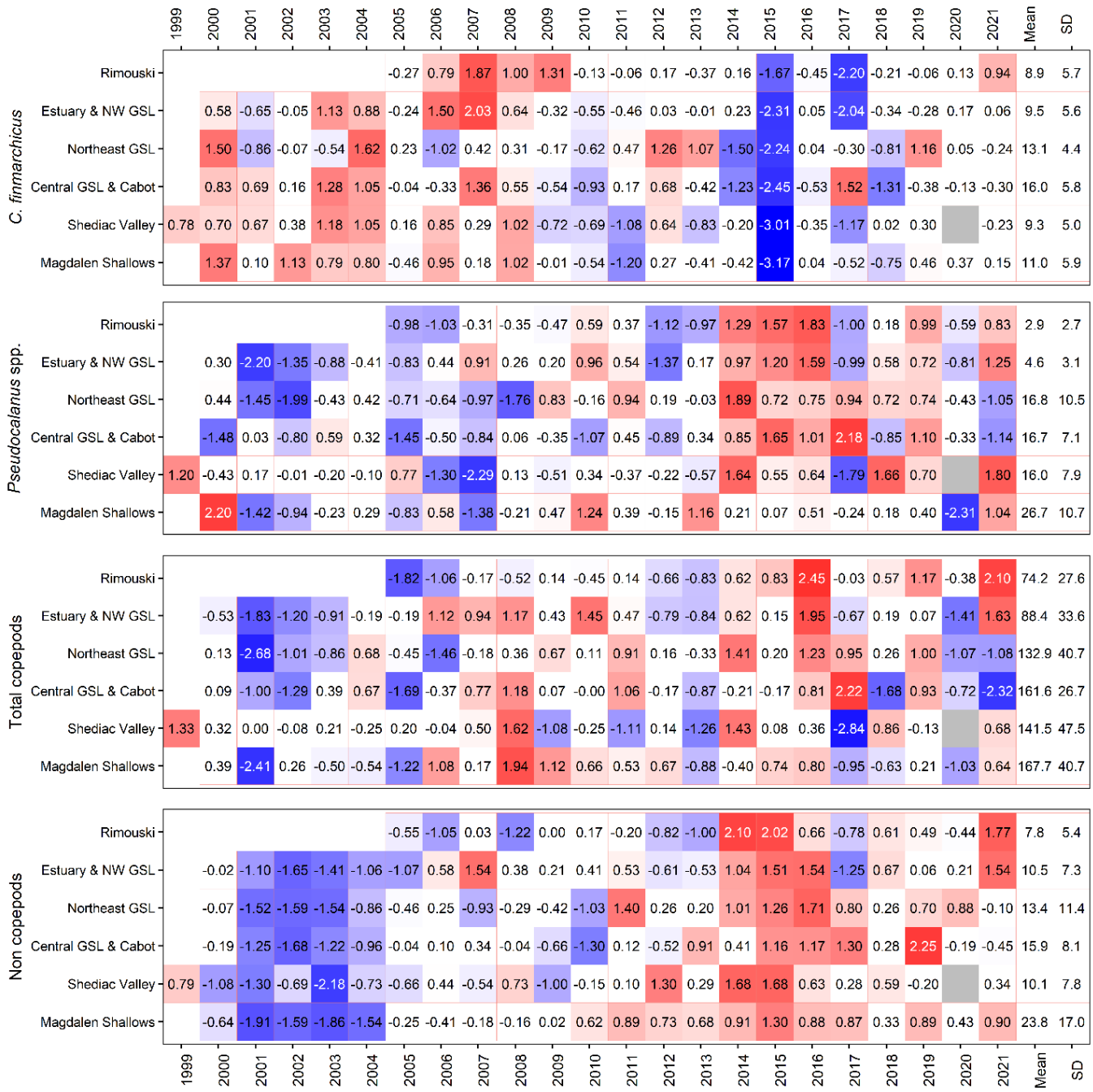

Figure 40. Time series of normalized annual anomalies for the abundance (× 10^3 ind m^{-2}) of four zooplankton categories for the high-frequency monitoring stations and regions of the Gulf of St. Lawrence (calculated using GLM). Variable means and standard deviations for the 2000–2020 (2005–2020 for Rimouski, 1999–2020 for Shediac Valley) climatology are shown to the right of the scorecard. Blue colours indicate below-normal levels (negative anomaly), reds are above-normal levels (positive anomaly), and white represents normal levels. GSL: Gulf of St. Lawrence.

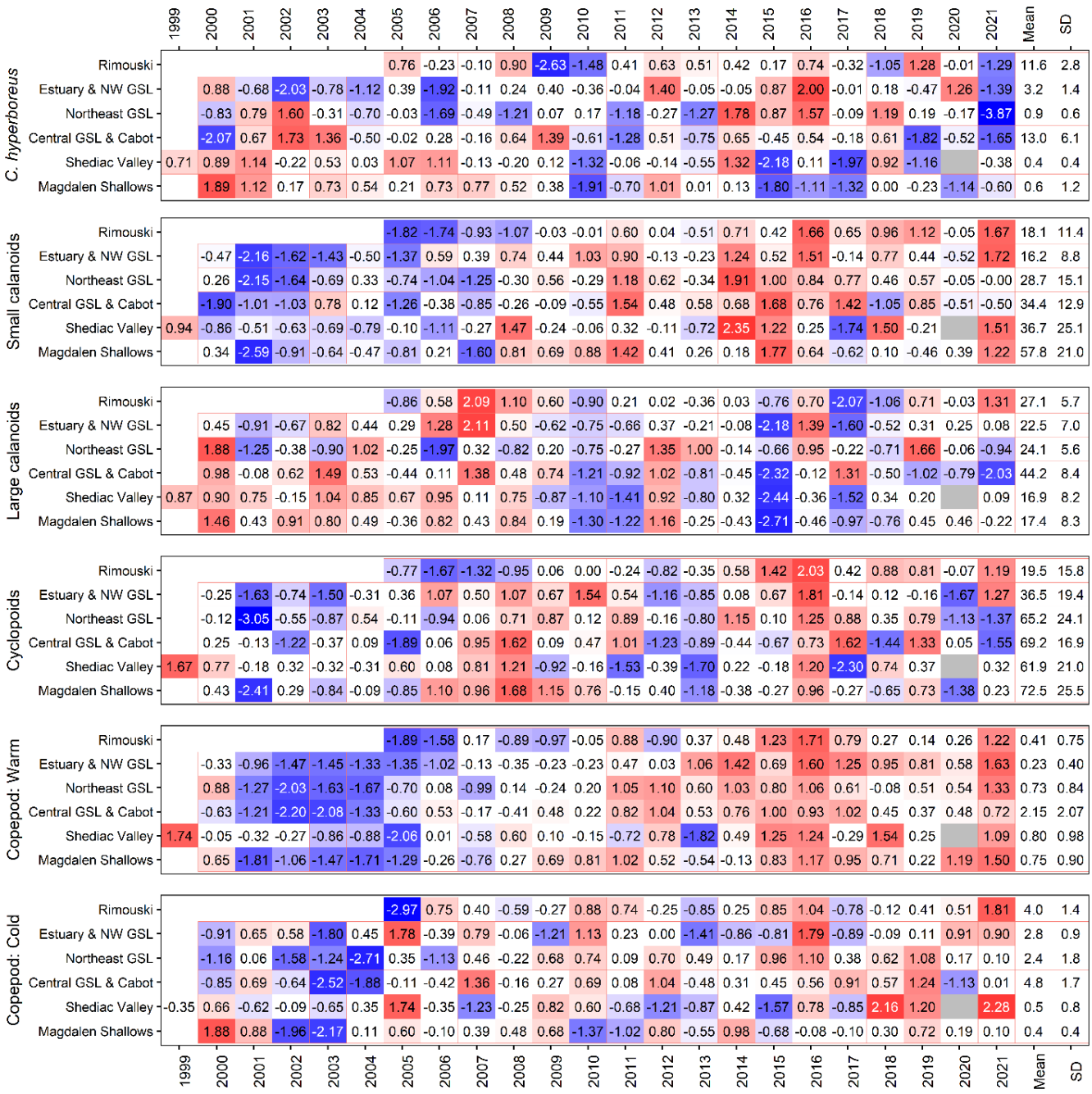

Figure 41. Time series of normalized annual anomalies for the abundance (× 10^3 ind m^{-2}) of six categories of zooplankton assemblages for the high-frequency monitoring stations and the regions of the Gulf of St. Lawrence (calculated using GLM). Variable means and standard deviations for the 2000–2020 (2005–2020 for Rimouski, 1999–2020 for Shediac Valley) climatology are shown to the right of the scorecard. Blue colours indicate below-normal levels (negative anomaly), reds are above-normal levels (positive anomaly), and white represents normal levels. A detailed list of species included in each large copepod index is presented in Appendix 2. GSL: Gulf of St. Lawrence.

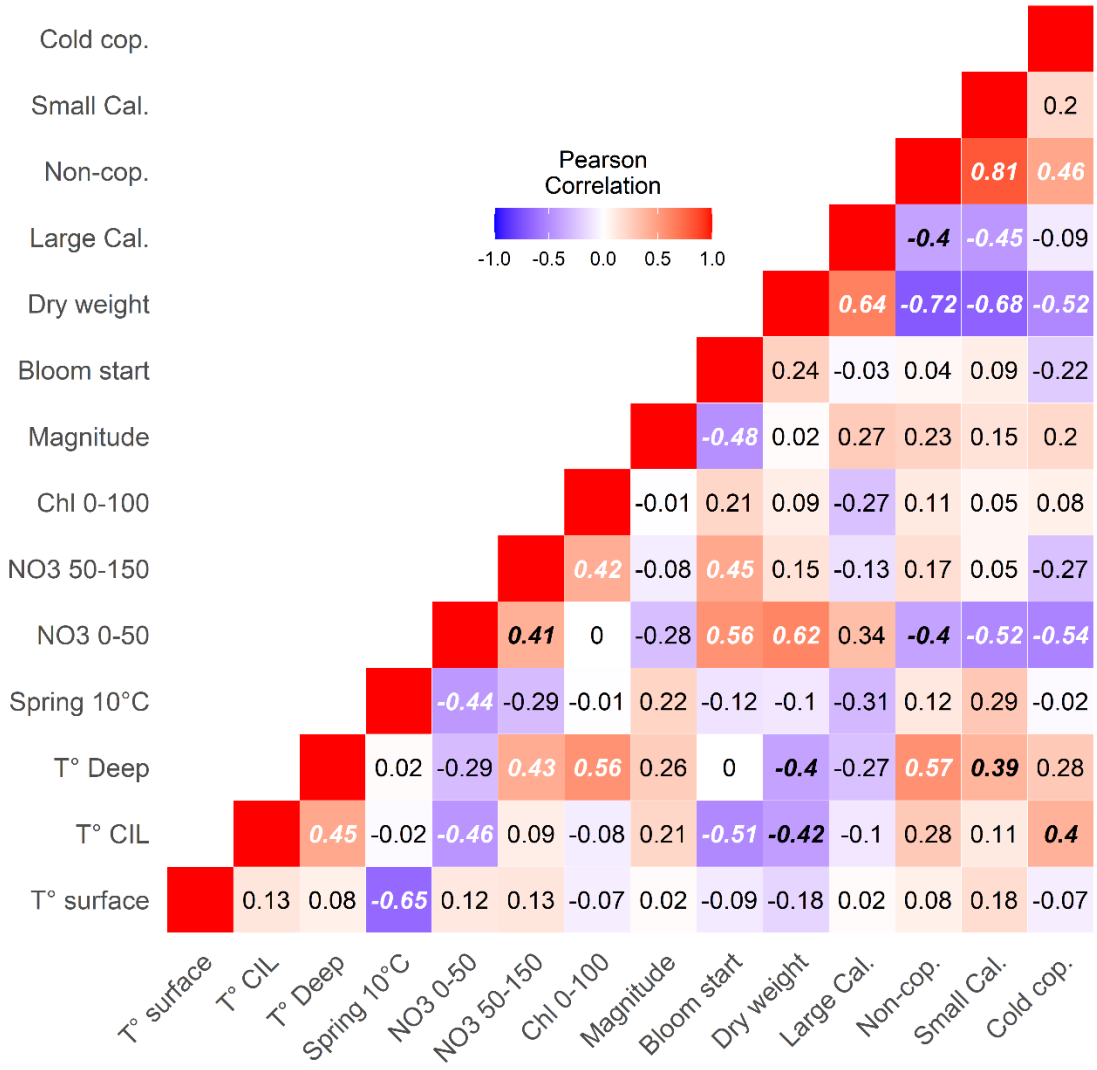

Figure 42. Correlation matrix for summed anomalies of some Gulf indices. Blue colours indicate negative correlations and reds are positive correlations. Significant correlations are indicated in black bold italic ($p < 0.1$) or in white bold italic ($p < 0.05$). CIL: cold intermediate layer. Spring 10°C is an index of spring timing based on the average Gulf temperature at the surface.

APPENDICES

Appendix 1. Detailed procedure for the intercalibration of flat-bed scanners

The flat-bed scanners for the counts and identification of zooplankton were changed in early 2022. To verify if it allows for the same classification as the previous EPSON scanners (V700, V4490 that were used for training the classifier), 9 samples from the 2019 multidisciplinary survey (200 µm) and the 29 samples from the mackerel egg survey (333 µm) of 2019 and 2018 were scanned again with the new scanner (V850). A GLM with a Tweedie error distribution was fitted with the interactions of taxa, mesh size and scanner. There were no significant difference in the abundance measured by either scanner for large calanoid (*C. finmarchicus, C. glacialis and C. hyperboreus*) and for the category including *Pseudocalanus spp., Microcalanus spp. and Scolecithricella spp.* but there were significant differences for the category that includes *Temora spp. and Eurytemora spp.* (Figure A1, Table A1). The new scanner detected half the abundance of this category compared with the previous scanners for 200 µm mesh-nets whereas it detected 2/3 of the abundance for 333 µm mesh-nets. This difference between mesh size is due to the lesser efficiency of the 333 µm to collect these small calanoids. Consequently, the fraction collected may be less likely to be misclassified as other small copepods. To provide a time series that is comparable among years, estimates of *Temora/Eurytemora* abundance from samples analyzed with the new scanner were thus multiplied by 2 and 1.5 for the multidisciplinary and mackerel egg survey respectively.

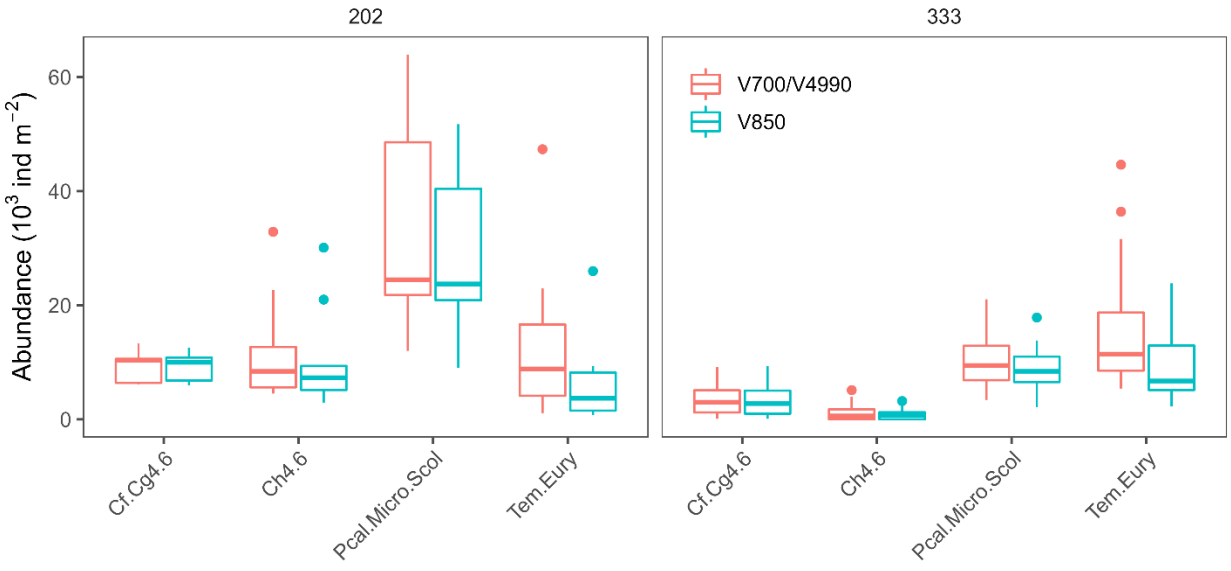

Figure A1. Boxplots of the abundance calculated by each type of scanner for the C. finmarchicus*/*C. glacialis *(Cf.Cg4.6),* C. hyperboreus *(Ch4.6),* Pseudocalanus *spp.,* Microcalanus *spp. and* Scolecithricella *spp. (Pcal.Micro.Scol) and* Temora *spp. and* Eurytemora *spp. (Tem.Eury) categories. The new scanner acquired in 2022 is in blue.*

Table A1. Least square means calculated on the response scale for each categories. Standard error (SE) and confidence intervals are reported. Significant differences are in bold.

Taxa	Scanner	Mesh size	Mean	SE	df	95% CI
Cf.Cg4.6	V700, V4490	202	9,571	1,989	288	6,357–14,409
Cf.Cg4.6	V850	202	9,302	1,948	288	6,160–14,046
Cf.Cg4.6	V700, V4490	333	3,513	526	288	2,616–4,717
Cf.Cg4.6	V850	333	3,314	504	288	2,457–4,470
Ch4.6	V700, V4490	202	12,110	2,370	288	8,238–17,800
Ch4.6	V850	202	10,351	2,109	288	6,931–15,457
Ch4.6	V700, V4490	333	1,149	229	288	776–1,702
Ch4.6	V850	333	884	189	288	581–1,346
Pcal.Micro.Scol	V700, V4490	202	33,147	5,011	288	24,617–44,633
Pcal.Micro.Scol	V850	202	30,289	4,686	288	22,338–41,070
Pcal.Micro.Scol	V700, V4490	333	10,353	1,175	288	8,281–12,945
Pcal.Micro.Scol	V850	333	8,602	1,024	288	6,806–10,873
Tem.Eury	**V700, V4490**	**202**	**13,301**	**2,541**	**288**	**9,133–19,373**
Tem.Eury	**V850**	**202**	**6,480**	**1,489**	**288**	**4,123–10,184**
Tem.Eury	**V700, V4490**	**333**	**14,924**	**1,542**	**288**	**12,178–18,290**
Tem.Eury	**V850**	**333**	**9,660**	**1,116**	**288**	**7,695–12,126**

Appendix 2. List of taxa associated with each copepod index.

Copepod index	*Taxa*
Small calanoids	*Acartia* spp.
	Aetideidae
	Centropages spp.
	Clausocalanus spp.
	Eurytemora spp.
	Microcalanus spp.
	Nannocalanus minor
	Paracalanus parvus
	Pseudocalanus spp.
	Scolecithricella spp.
	Spinocalanus spp.
	Temora spp.
	Tortanus spp.
Large calanoids	*Anomalocera* spp.
	Calanus finmarchicus
	Calanus glacialis
	Calanus hyperboreus
	Euchaeta spp.
	Metridia spp.
	Paraeuchaeta norvegica
	Pleuromamma borealis
	Pleuromamma robusta
Warm copepods	*Centropages* spp.
	Clausocalanus spp.
	Metridia lucens
	Nannocalanus minor
	Paracalanus spp.
	Pleuromamma borealis
	Pleuromamma robusta
Cyclopoids	*Oithona* spp.
	Oncaea spp.
	Triconia borealis
	Triconia conifer
	Triconia similis
Cold copepods	*Metridia longa*
	Calanus glacialis

Appendix 3. GLM results for Rimouski and Shediac Valley stations. Significance of the year and month effects as well as the adjusted R squared of the regression for nutrients and chlorophyll a are presented.

Rimouski

Index	Year (*p*)	Month (*p*)	R^2
Chlorophyll *a* (0–100m)	<0.0001	<0.0001	0.43
Nitrate (0–50m)	<0.0001	<0.0001	0.37
Nitrate (50–150m)	<0.0001	<0.0001	0.26
Nitrate (150–320m)	<0.0001	<0.0001	0.38

Shediac Valley

Index	Year (*p*)	Month (*p*)	R^2
Chlorophyll *a* (0–100m)	<0.0001	<0.0001	0.38
Nitrate (0–50m)	<0.001	<0.0001	0.33
Nitrate (50–84m)	0.7	0.001	0.06

Appendix 4. GLM results for Rimouski and Shediac Valley stations. Significance of the year and month effects as well as the adjusted R squared of the regression for phytoplankton groups are presented.

Rimouski

Index	Year (*p*)	Month (*p*)	R^2
Diatoms	<0.0001	<0.0001	0.36
Dinoflagellates	<0.0001	<0.0001	0.51
Flagellates	<0.0001	<0.0001	0.38
Ciliates	<0.0001	<0.0001	0.36
Total	0.0001	<0.0001	0.26
Diatoms/Dinoflagellates	<0.0001	<0.0001	0.31
Diatoms/Flagellates	<0.0001	<0.0001	0.23

Shediac Valley

Index	Year (*p*)	Month (*p*)	R^2
Diatoms	<0.0001	<0.001	0.35
Dinoflagellates	<0.0001	0.04	0.27
Flagellates	<0.0001	<0.0001	0.43
Ciliates	0.3	0.6	0.02
Total	<0.0001	<0.001	0.33
Diatoms/Dinoflagellates	<0.0001	<0.001	0.33
Diatoms/Flagellates	<0.0001	<0.0001	0.41

Appendix 5. GLM results for Gulf regions. Significance of the year, season, and station effects as well as the adjusted R squared of the regression for nutrients or chlorophyll a are presented.

Estuary

Index	Year (*p*)	Season (*p*)	Station(*p*)	R^2
Chlorophyll *a* (0–100m)	<0.0001	<0.0001	0.6	0.46
Nitrate (0–50m)	<0.0001	<0.0001	<0.0001	0.4
N:P (0–50m)	<0.0001	<0.0001	<0.0001	0.44
Si:N (0–50m)	<0.0001	<0.0001	0.3	0.41
Nitrate (50–150m)	<0.0001	<0.0001	<0.0001	0.23
N:P (50–150m)	<0.0001	0.7	<0.01	0.21
Si:N (50–150m)	<0.0001	<0.0001	<0.0001	0.33
Nitrate (150–btm)	<0.0001	<0.0001	<0.0001	0.89
N:P (150–btm)	<0.001	0.02	0.8	0.09
Si:N (150–btm)	<0.0001	<0.001	<0.0001	0.43

Northwest Gulf

Index	Year (*p*)	Season (*p*)	Station(*p*)	R^2
Chlorophyll *a* (0–100m)	<0.0001	<0.0001	<0.0001	0.32
Nitrate (0–50m)	<0.0001	<0.0001	<0.0001	0.53
N:P (0–50m)	<0.0001	<0.0001	<0.0001	0.46
Si:N (0–50m)	<0.0001	<0.001	<0.0001	0.24
Nitrate (50–150m)	<0.0001	<0.001	<0.0001	0.4
N:P (50–150m)	<0.0001	<0.0001	<0.0001	0.34
Si:N (50–150m)	<0.0001	<0.001	<0.0001	0.32
Nitrate (150-btm)	0.0001	<0.0001	<0.0001	0.81
N:P (150-btm)	<0.0001	0.05	<0.0001	0.31
Si:N (150-btm)	<0.0001	<0.001	<0.0001	0.42

Northeast Gulf

Index	Year (*p*)	Season (*p*)	Station(*p*)	R^2
Chlorophyll *a* (0–100m)	<0.0001	<0.0001	0.3	0.22
Nitrate (0–50m)	<0.0001	<0.0001	0.002	0.74
N:P (0–50m)	<0.0001	<0.0001	<0.001	0.75
Si:N (0–50m)	<0.0001	<0.0001	<0.0001	0.25
Nitrate (50–150m)	<0.0001	<0.0001	<0.0001	0.54
N:P (50–150m)	<0.0001	<0.0001	<0.0001	0.58
Si:N (50–150m)	<0.0001	0.2	<0.0001	0.36
Nitrate (150-btm)	<0.0001	<0.0001	<0.0001	0.92
N:P (150-btm)	<0.0001	<0.0001	<0.0001	0.58
Si:N (150-btm)	<0.0001	<0.001	<0.0001	0.54

Central Gulf

Index	Year (*p*)	Season (*p*)	Station(*p*)	R^2
Chlorophyll *a* (0–100m)	<0.0001	0.006	0.2	0.15
Nitrate (0–50m)	<0.0001	<0.0001	<0.0001	0.74
N:P (0–50m)	<0.0001	<0.0001	<0.0001	0.72
Si:N (0–50m)	<0.0001	<0.001	0.02	0.29
Nitrate (50–150m)	<0.0001	<0.0001	<0.0001	0.35
N:P (50–150m)	<0.0001	<0.0001	<0.0001	0.4
Si:N (50–150m)	<0.0001	<0.0001	<0.0001	0.46
Nitrate (150–btm)	<0.0001	<0.0001	<0.0001	0.89
N:P (150–btm)	<0.0001	<0.0001	<0.0001	0.46
Si:N (150–btm)	<0.0001	0.02	<0.0001	0.3

Cabot Strait

Index	Year (*p*)	Season (*p*)	Station(*p*)	R^2
Chlorophyll *a* (0–100m)	<0.0001	<0.001	0.3	0.22
Nitrate (0–50m)	<0.0001	<0.0001	0.08	0.7
N:P (0–50m)	<0.0001	<0.0001	0.4	0.71
Si:N (0–50m)	<0.001	0.003	0.04	0.15
Nitrate (50–150m)	<0.0001	<0.0001	<0.0001	0.42
N:P (50–150m)	<0.0001	<0.0001	<0.0001	0.45
Si:N (50–150m)	<0.0001	<0.0001	<0.0001	0.46
Nitrate (150-btm)	<0.0001	<0.0001	<0.0001	0.89
N:P (150-btm)	<0.0001	<0.0001	<0.0001	0.46
Si:N (150-btm)	<0.001	0.02	<0.0001	0.3

Magdalen Shallows

Index	Year (*p*)	Season (*p*)	Station(*p*)	R^2
Chlorophyll *a* (0–100m)	<0.0001	<0.0001	<0.0001	0.23
Nitrate (0–50m)	<0.0001	<0.0001	<0.0001	0.56
N:P (0–50m)	<0.0001	<0.0001	<0.0001	0.56
Si:N (0–50m)	<0.0001	<0.0001	<0.0001	0.34
Nitrate (50–150m)	<0.0001	<0.0001	<0.0001	0.68
N:P (50–150m)	<0.0001	<0.0001	<0.0001	0.44
Si:N (50–150m)	<0.0001	0.01	<0.0001	0.36

Appendix 6. GLM results for Rimouski and Shediac Valley stations. Significance of the year and month effects as well as the adjusted R squared of the regression for each zooplankton index are presented.

Rimouski

Index	Year (*p*)	Month (*p*)	R^2
Calanus finmarchicus	<0.0001	<0.0001	0.51
Pseudocalanus spp.	<0.0001	<0.0001	0.56
Total copepods	<0.0001	<0.0001	0.59
Non-copepods	<0.0001	<0.0001	0.44
Calanus hyperboreus	<0.0001	<0.0001	0.4
Small calanoids	<0.0001	<0.0001	0.68
Large calanoids	<0.0001	<0.0001	0.33
Cyclopoids	<0.0001	<0.0001	0.6
Copepods: Warm	<0.0001	0.8	0.48
Copepods: Cold	<0.0001	<0.0001	0.46
Dry weight	<0.0001	<0.0001	0.64

Shediac Valley

Index	Year (*p*)	Month (*p*)	R^2
Calanus finmarchicus	<0.0001	<0.0001	0.33
Pseudocalanus spp.	0.1	0.2	0.06
Total copepods	0.2	<0.0001	0.17
Non-copepods	0.001	<0.001	0.21
Calanus hyperboreus	<0.0001	<0.0001	0.67
Small calanoids	0.008	<0.0001	0.19
Large calanoids	<0.0001	<0.0001	0.35
Cyclopoids	0.3	<0.0001	0.24
Copepods: Warm	0.1	0.06	0.07
Copepods: Cold	0.04	<0.0001	0.3
Dry weight	0.0001	<0.0001	0.39

Appendix 7. GLM results for Gulf regions. Significance of the year, season, and station effects as well as the adjusted R squared of the regression for each zooplankton index are presented.

Estuary and northwest Gulf

Index	Year (*p*)	Season (*p*)	Station (*p*)	R^2
Calanus finmarchicus	<0.0001	0.001	<0.0001	0.66
Pseudocalanus spp.	<0.0001	<0.0001	<0.0001	0.55
Total copepods	<0.0001	<0.0001	<0.0001	0.76
Non-copepods	<0.0001	<0.0001	<0.0001	0.57
Calanus hyperboreus	0.01	<0.0001	<0.0001	0.6
Small calanoids	<0.0001	<0.0001	<0.0001	0.68
Large calanoids	<0.0001	0.002	<0.0001	0.77
Cyclopoids	<0.0001	<0.0001	<0.0001	0.73
Copepods: Warm	<0.0001	0.001	<0.0001	0.53
Copepods: Cold	<0.0001	<0.001	<0.0001	0.66
Dry weight	<0.0001	0.05	<0.0001	0.76

Northeast Gulf

Index	Year (*p*)	Season (*p*)	Station (*p*)	R^2
Calanus finmarchicus	0.0001	<0.0001	0.007	0.22
Pseudocalanus spp.	<0.0001	0.002	<0.0001	0.31
Total copepods	<0.0001	<0.0001	<0.001	0.39
Non copepods	<0.0001	0.008	<0.0001	0.45
Calanus hyperboreus	<0.001	<0.0001	<0.0001	0.59
Small calanoids	<0.0001	0.6	<0.0001	0.41
Large calanoids	0.009	<0.0001	<0.0001	0.45
Cyclopoids	<0.0001	<0.0001	0.1	0.5
Copepods: Warm	<0.0001	<0.0001	0.002	0.51
Copepods: Cold	<0.0001	<0.0001	<0.0001	0.43
Dry weight	<0.0001	<0.0001	<0.0001	0.68

Central Gulf and Cabot Strait

Index	Year (*p*)	Season (*p*)	Station (*p*)	R^2
Calanus finmarchicus	<0.0001	<0.001	0.007	0.26
Pseudocalanus spp.	<0.0001	<0.0001	<0.0001	0.28
Total copepods	<0.001	<0.0001	<0.001	0.18
Non-copepods	<0.0001	<0.0001	<0.0001	0.46
Calanus hyperboreus	<0.0001	<0.001	<0.0001	0.51
Small calanoids	<0.0001	0.9	<0.0001	0.31
Large calanoids	<0.0001	0.9	<0.0001	0.32
Cyclopoids	<0.0001	<0.0001	0.005	0.24
Copepods: Warm	<0.0001	<0.0001	<0.0001	0.49
Copepods: Cold	<0.001	0.3	0.3	0.09
Dry weight	<0.0001	0.5	<0.0001	0.6

Magdalen Shallows

Index	Year (*p*)	Season (*p*)	Station (*p*)	R^2
Calanus finmarchicus	<0.0001	<0.0001	<0.0001	0.32
Pseudocalanus spp.	<0.0001	<0.0001	0.6	0.12
Total copepods	<0.0001	<0.0001	<0.0001	0.21
Non-copepods	<0.0001	<0.0001	<0.0001	0.49
Calanus hyperboreus	<0.0001	<0.0001	<0.0001	0.48
Small calanoids	<0.0001	0.001	0.004	0.19
Large calanoids	<0.0001	<0.0001	<0.0001	0.5
Cyclopoids	<0.0001	<0.0001	<0.0001	0.31
Copepods: Warm	<0.0001	<0.0001	0.005	0.51
Copepods: Cold	<0.0001	<0.0001	<0.0001	0.4
Dry weight	<0.0001	<0.0001	<0.0001	0.47